ROBUST SEISMIC VULNERABILITY ASSESSMENT PROCEDURE FOR IMPROVEMENT OF BRIDGE NETWORK PERFORMANCE

by

Corey M. Beck

A Thesis

Submitted to the Faculty of Purdue University

In Partial Fulfillment of the Requirements for the degree of

Master of Science in Civil Engineering
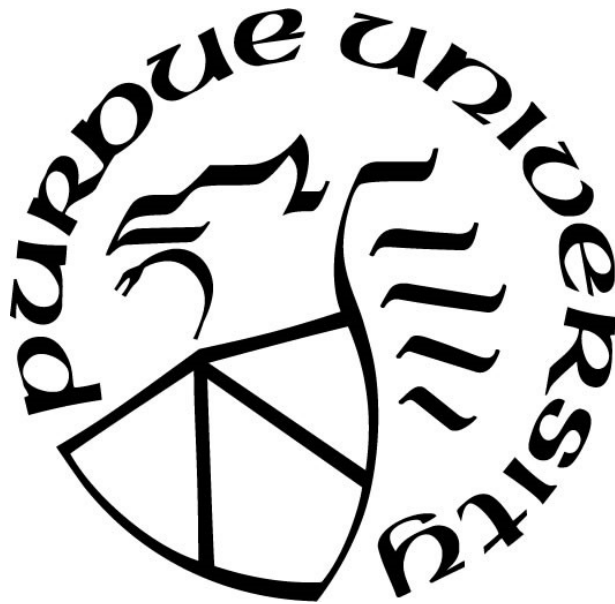
Lyles School of Civil Engineering

West Lafayette, Indiana

August 2020

THE PURDUE UNIVERSITY GRADUATE SCHOOL
STATEMENT OF COMMITTEE APPROVAL

Dr. Shirley Dyke, Co-Chair

Department of Mechanical Engineering and Lyles School of Civil Engineering

Dr. Julio Ramirez, Co-Chair

Lyles School of Civil Engineering

Dr. Luis Garcia

Distinguished Visiting Professor

Approved by:

Dr. Dulcy Abraham

To my partner, Kayla

ACKNOWLEDGMENTS

TABLE OF CONTENTS

LIST OF TABLES

LIST OF FIGURES

NOMENCLATURE

Note: To reduce the number of total variables used throughout this thesis, some variables can be applied to the analysis in both the longitudinal and transverse direction. For example, K_{sub} is used to represent the stiffness of the substructure in both the transverse and longitudinal direction.

A_b	Area of beam (in^2)
A_c	Area of column core (in^2)
A_g	Gross shear area (in^2)
A_{isol}	Cross-sectional area of isolator – for shear resistance (in^2)
A_R	Area of concrete in the railing (ft^2)
A_{rest}	Cross-sectional area of restrainers for single beam (in^2)
A_s	Area of longitudinal steel (in^2)
A_{sh}	Total cross-section area of tie reinforcement (in^2)
A_{cv}	Area of concrete in shear
A_v	Area of shear reinforcement (in)
b	Width of substructure element (in)
B_i	Bernoulli random variable
c_{isol}	Inherent viscous damping rate of isolator [($kips{\cdot}s$)/in]
C_{limit}	Limiting capacity of substructure ($kips$)
c_{pier}	Inherent viscous damping rate of pier [($kips{\cdot}s$)/in]
c_{sub}	Inherent viscous damping rate of entire substructure [($kips{\cdot}s$)/in]
$c_{N.A.}$	Depth to the Neutral Axis (in)
d_{isol}	Displacement of isolator (in)
d_y	Displacement of isolator at yield (in)
d_v	Equivalent moment arm between resulting tension and compressive forces (in)
E_c	General modulus of elasticity for given section – used in stiffness method (ksi)
E_c	Modulus of elasticity of concrete (ksi)
E_{rest}	Modulus of elasticity, restrainer material (ksi)
E_s	Modulus of elasticity for steel (ksi)
f_c	Assumed stress profile for concrete (ksi)
f_c'	Compressive strength of concrete (psi)
F_{conc}	Total force in the concrete ($kips$)
F_{isol}	Shear force of isolator ($kips$)
F_{pier}	Restoring force of each pier participating in seismic response ($kips$)
F_l	Linear force for a given time history ($kips$)
f_{nl}	Non-linear displacement modifier
F_{nl}	Non-linear force for a given time history ($kips$)
$F_R(x; y_{LS})$	Fragility function (FF)
F_{s_c}	Force in compression steel ($kips$)
F_{s_t}	Force in tension steel ($kips$)

f_y	Yield stress in reinforcement (*ksi*)
$f_{y_{rest}}$	Yield stress in restrainer (*ksi*)
F_y	Shear force of isolator at yield (*kips*)
f_s	Stress in steel reinforcement – function of depth from neutral axis (*ksi*)
G	Shear Modulus of concrete (*ksi*)
G_{isol}	Shear modulus of isolator (*ksi*)
g	Gravitational Constant (*in/s²*)
h	Depth (about the plane of bending) of substructure element (*in*)
H	Clear height of pier (*ft*)
h_b	Height of beam (*ft*)
h_c	Core dimension of tied column in the direction under consideration (*in*)
h_{isol}	Height of isolator (*in*)
I	General moment of inertia for given section – used in stiffness method (*in⁴*)
$\boldsymbol{I}$	Identity matrix
I_g	Gross moment of inertia (*in⁴*)
I_{nl}	Cracked (non-linear) moment of inertia (*in⁴*)
k	Originating stiffness matrix
K_d	Post-elastic stiffness of isolator (*kips/in*)
K_{isol}	Effective linear stiffness of single isolator (*kips/in*)
K_{isol}	Effective linear stiffness of all isolators in the system (*kips/in*)
K_{pier}	Stiffness of individual pier (*kip/in*)
K_{rest}	Stiffness of restrainers for single beam (*kips/in*)
K_{sub}	Total stiffness of substructure (*kip/in*)
K_{sys}	Stiffness of restrainer system and substructure system (*kips/in*)
K_u	Loading and unloading elastic stiffness (*kips/in*)
L	Clear spacing of beam elements (*in*)
L_{bridge}	Length of bridge (*in*)
L_{rest}	Length of activated (taut) restrainer (*in*)
l_D	Cross-sectional width of diaphragm
l_{pier}	Length of superstructure supported by each pier (*ft*)
L_p	Length of plastic hinge in substructure (*in*)
L_y	Length of yielding in substructure (*in*)
$\boldsymbol{m}$	Vector characterizing expected value of each function weight
$m(s_v)$	Posterior predictive distribution
M_{cr}	Cracking moment (*kips·ft*)
m_D	Mass of diaphragm (*kips/g*)
m_{pier}	Mass of superstructure over each pier (*kips/g*)
m_R	Mass of Railing (*kips/g*)
m_{SS}	Mass of primary structural system (*kips/g*)
m_{sub}	Mass of substructure (*kips/g*)
m_{sup}	Activated mass of superstructure (*kips/g*)
M_u	Ultimate moment (*kips·ft*)
M_y	Yield moment (*kips·ft*)
N_b	Number of beams

N_{bars}	Number of restrainer bars for a single beam
N_{bars_c}	Number of bars in compression
N_{bars_t}	Number of bars in tension
N_c	Number of columns in each bent
N_{piers}	Number of piers participating in seismic response
$N(y_{max})$	Annual frequency of exceedance function for hazard
PGA	Peak ground acceleration (*g*)
$P_B(F)$	Probability of bridge failure
$P_B(S)$	Probability of bridge success
$P_L(F)$	Probability of link failure
Q_u	Characteristic strength of isolator (*kips*)
r_{rb}	Radius of rocker bearing (*in*)
s	Spacing of shear reinforcement (*in*)
$s^2(s_v)$	Predictive uncertainty
$\boldsymbol{S}$	Vector characterizing uncertainty of each function weight
s_a	Spectral acceleration (*g*)
s_b	Spacing of beams (*ft*)
s_v	Spectral velocity (*in/s*)
t	Return period of hazard (*years*)
T	Period of structure (*s*)
t_{deck}	Thickness of the deck (*in*)
t_{steel}	Thickness of steel (*in*)
u_i	Translational degree of freedom
u_b	Relative displacement between the bottom of isolator and the ground (*in*)
$\dot{u}_b$	Relative velocity between the bottom of isolator and the ground (*in/s*)
$\ddot{u}_b$	Relative acceleration between the bottom of isolator and the ground (*in/s²*)
u_s	Relative displacement between the superstructure and the ground (*in*)
$\dot{u}_s$	Relative velocity between the superstructure and the ground (*in/s*)
$\ddot{u}_s$	Relative acceleration between the superstructure and the ground (*in/s²*)
V_{bs}	Base shear strength of pier (*kips*)
V_c	Shear strength of concrete (*kips*)
V_{cr}	Cracking shear resultant (*kips*)
V_{conn}	Shear capacity of connection (*kips*)
V_n	Shear capacity (*kips*)
$V_{n_{max}}$	Maximum allowable shear capacity for design(*kips*)
V_s	Shear strength of transverse reinforcement (*kips*)
V_y	Base shear capacity at yield (*kips*)
$\boldsymbol{w}$	Vector of weights characterizing best-fit regression function
w_b	Width of beam (*in*)
W_b	Weight of beam (*lb/lft*)
w_{rb}	Width of rocker bearing (*in*)
w_{oto}	Out-to-out width of the deck (*ft*)
W_s	Weight of steel in the railing (*lbs/lft*)
x_b	Displacement at the top of the substructure/bottom of isolator (*in*)
x_g	Ground displacement (*in*)

$\ddot{x}_g$	Ground Acceleration (in/s^2)
x_{IM}	Intensity measure
X_{max}	Maximum intensity measure from hazard curve
x_s	Displacement (*in*)
$\dot{x}_s$	Velocity (*in/s*)
$\ddot{x}_s$	Acceleration (*in/s²*)
Y	Engineering demand parameter
y_{LS}	Limit state capacity
$\boldsymbol{\alpha}$	Vector of precision for each function weight
α_c	Constant associated with the shear capacity of walls
β_C	Capacity uncertainty
β_M	Modeling uncertainty
β_T	Total uncertainty in the system
$\beta_{Y\|X}$	Demand uncertainty
Δ_A	Deflection at point A – Moment curvature theorem (*in*)
Δ_B	Deflection at point B – Moment curvature theorem (*in*)
$\Delta_{\frac{B}{A}}$	Difference in deflection between point A and B – Moment curvature theorem (*in*)
Δ_{rb}	Allowable displacement of rocker bearing (*in*)
Δ_c	Controlling linear displacement (*in*)
Δ_{cr}	Cracking displacement
Δ_l	Linear displacement (*in*)
Δ_{nl}	Nonlinear displacement (*in*)
Δ_p	Plastic displacement (*in*)
Δ_{sim}	Simulink displacement (*in*)
$\boldsymbol{\gamma}$	Hyperparameter used to represent weight precision and system noise
γ_c	Density of Concrete (*150 pcf*)
ε_c	Strain in concrete
$\varepsilon_{N.A.}$	Strain in extreme fiber for given neutral axis
ε_s	Strain in reinforcement
ε_y	Yield strain in reinforcement
ε_0	Maximum nominal concrete strain
λ	Light-weight concrete multiplier
λ_r	Aspect ratio
$\lambda_X(x)$	Probability of occurrence function for hazard
$\lambda_{Y\|X}$	Best-fit function
ρ	Reinforcement ratio of longitudinal (flexural) steel to concrete
ρ_s	Reinforcement ratio of transverse (shear) steel to concrete
θ	Substructure drift
θ_i	Rotational degree of freedom
Φ	Cumulative distribution function for standard normal distribution
$\boldsymbol{\Phi}$	Vectorized form of basis function
$\phi(s_v)$	Basis function
$\varphi(x)$	Total curvature equation
φ_{cr}	Curvature at cracking (*rad/in*)
φ_u	Curvature at ultimate moment (*rad/in*)

φ_y	Curvature at yield (*rad/in*)
$\varphi_y(x)$	Liner curvature equation
σ	Variance for given distribution
σ_n	Noise in system
ω_n	Circular natural frequency (*rad/s*)
ν	Poisson's ratio (assumed to be 0.15)
μ	Mean value for given distribution
ζ_{isol}	Viscous damping coefficient of isolator (%)
ζ_{sub}	Viscous damping coefficient of pier (%)

ABSTRACT

Ensuring the resilience of a state's transportation network is necessary to guarantee an acceptable quality of life for the people the network serves. A lack of resilience in the wake of a seismic event directly impacts the states' overall safety and economic vitality. With the recent identification of the Wabash Valley Seismic Zone (WBSV), Department of Transportations (DOTs) like Indiana's have increased awareness for the vulnerability of their bridge network. The Indiana Department of Transportation (INDOT) has been steadily working to reduce the seismic vulnerability of bridges in the state in particular in the southwest Vincennes District. In the corridor formed by I-69 built in the early 2000s the bridge design is required to consider seismic actions. However, with less recent bridges and those outside the Vincennes District being built without consideration for seismic effects, the potential for vulnerability exists. As such, the objective of this thesis is to develop a robust seismic vulnerability assessment methodology which can assess the overall vulnerability of Indiana's critical bridge network.

A representative sample of structures in Indiana's bridge inventory, which prioritized the higher seismic risk areas, covered the entire state geographically, and ensured robust superstructure details, was chosen. The sample was used to carry a deterministic seismic vulnerability assessment, applicable to all superstructure-substructure combinations. Analysis considerations, such as the calculation of critical capacity measures like moment-curvature and a pushover analysis, are leveraged to accurately account for non-linear effects like force redistribution. This effect is a result of non-simultaneous structural softening in multi-span bridges that maintain piers of varying heights and stiffnesses. These analysis components are incorporated into a dynamic analysis to allow for the more precise identification of vulnerable details in Indiana's bridge inventory.

The results of this deterministic seismic assessment procedure are also leveraged to identify trends in the structural response of the sample set. These trends are used to identify limit state thresholds for the development of fragility functions. This conditional probabilistic representation of bridge damage is coupled with the probability of earthquake occurrence to predict the performance of the structure for a given return period. This probabilistic approach alongside a Monte Carlo simulation is applied to assess the vulnerability of linked bridges along key-access corridors throughout the state. With this robust seismic vulnerability methodology, DOTs will

have the capability of identifying vulnerable corridors throughout the state allowing for the proactive prioritization of retrofits resulting in the improved seismic performance and resiliency of their transportation network.

1. INTRODUCTION

With an increased awareness of the seismic risk in central and eastern United States (CEUS), Department of Transportations (DOTs) like Indiana's are concerned with identifying structures that are expected to respond poorly to the level of seismic excitation produced by the New Madrid Seismic Zone (NMSZ) and Wabash Valley Seismic Zone (WVSZ). These deficient structures, which form critical gaps in many of the state's key access corridors, can severely impact the resiliency of Indiana's transportation system in the face of a natural disaster. This lack of resiliency directly impacts the states' overall safety, economic vitality, and recuperation rate. Thus, with this increased awareness, this project aims to develop a seismic vulnerability assessment procedure capable of proactively identifying deficient structures in key-access corridors throughout Indiana's transportation system.

With the development of a deterministic seismic vulnerability assessment procedure, the results can be leveraged to effectively identify the most vulnerable regions of the state. While the seismic assessment procedure is independently applied to each structure, the functionality of a bridge network is inherently more interdependent. For example, the entire length of a key access corridor is out of commission for the response to a natural hazard if a single structure along that critical route is significantly damaged. Thus, the seismic vulnerability assessment must be leveraged to develop fragility functions (FF). These FFs, alongside additional information such as the annual rate of earthquake occurrence, are used to probabilistically identify links of bridges throughout the transportation system which are more likely to fail in a given time period.

Only with this comprehensive approach can DOTs effectively identify the most vulnerable regions throughout the state and make informed decisions to effectively mitigate risk. With this wealth of information, DOTs can effectively prioritize retrofits that will most significantly impact the overall health and performance of their bridge network. This project, and the methodologies developed herein, can assist DOTs across the country to assess the vulnerability of their bridge networks easily and robustly.

1.1 Objective

This thesis has three primary objectives, summarized as:

- Carry out a deterministic seismic vulnerability assessment procedure applicable to bridges of varying substructure and superstructure combinations. This procedure is applied to a sample set of bridges in Indiana's bridge network to identify vulnerable substructure details and trends in the sample set's response for use in the development of fragility functions (FF).
- Develop a probabilistic methodology which addresses the inherent interdependencies within bridge networks by computing the overall probability of failure for a series of bridges using fragility functions and hazard curves.
- Identify applicable retrofits and demonstrate their capabilities for improving the seismic performance of a deficient bridge in Indiana's bridge network.

1.2 Organization

This thesis is organized into six chapters plus two appendices. Chapter 2 provides a summary of past research and literature relevant to: seismic risk in central U. S.; seismic vulnerability in central U.S.; seismic retrofits in Central Southern United States (CSUS); fragility functions; and reliability/risk assessments. A robust seismic assessment procedure applicable to all bridges in Indiana's bridge inventory is developed and demonstrated for a bridge in Indiana's bridge inventory in Chapter 3. The results and trends from this assessment procedure, alongside additional information regarding the probability of earthquake occurrence, is leveraged in Chapter 4 to probabilistically assess the overall vulnerability of a series of bridges. This probabilistic methodology allows DOTs to assess the vulnerability of entire key access corridors rather than just the independent vulnerability of individual bridges within that corridor. With the identification of vulnerabilities comes the need for strategies capable of mitigating the deficiencies. Thus, Chapter 5 demonstrates the impact seismic retrofits can have on improving the seismic performance of a deficient structure. The impact this work has, conclusions for each of the three primary objectives, and future work are summarized in Chapter 6. A summary of the bridges in the sample set used to develop the seismic assessment procedure is provided in Appendix A. Lastly, a comprehensive seismic retrofit selection procedure is provided in Appendix B.

2. LITERATURE REVIEW

2.1 Seismicity in Indiana

The seismic risk for central and eastern United States (CEUS) has largely been associated with the New Madrid Seismic Zone (NMSZ). The most notorious of the seismic events originating from NMSZ being the sequence of powerful earthquakes during the winter of 1811 and 1812 causing strong ground shaking that resulted in substantial damage to the built environment (Johnston & Schweig, 1996). While earthquakes of such magnitude have not occurred since, frequent small-to-moderate earthquakes have occurred along the Illinois and Indiana border (Hermann et al., 2008). Most of these earthquakes can be attributed to the recently-identified Wabash Valley Seismic Zone (WVSZ) along this border (Petersen et al., 2014). While many of the low-grade earthquakes originating from the WVSZ are not even felt, the identification of the zone has increased the seismic risk in the state of Indiana. This is especially true in the southwestern corner of the state, as shown in Figure 2-1.
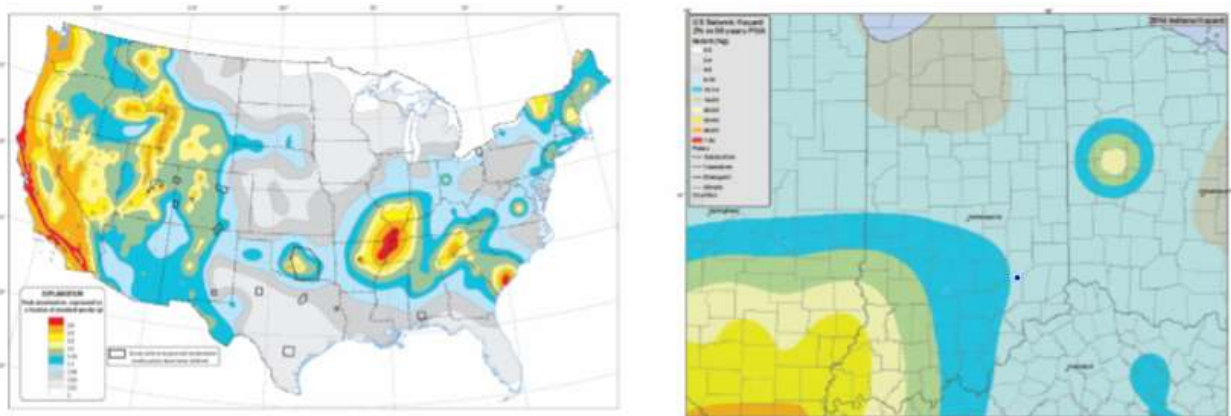
Figure 2-1. U.S. National (Left) & State (Right) Seismic Hazard Map for 2% Probability of Exceedance in 50 Years (Petersen et al., 2014).

2.2 Seismic Vulnerability in Central U.S.

Until the 1990s, most bridges and their supporting substructure throughout the central U.S. were designed primarily to resist axial failure, such as buckling, due to traffic loads. The lack of design consideration for proper seismic detailing such as adequate flexural reinforcement and

shear reinforcement has left many bridges vulnerable. Previous research conducted by Ramirez et al. (2005) focused on the development of a rapid methodology capable of assessing various levels of seismic vulnerability for bridges throughout the Vincennes District of Indiana. From this assessment, 7% of bridges were identified as having the potential for high vulnerability where the primary concern was unseating. Of these bridges, steel superstructures supported by rocker bearings, or expansion bearings, were identified as the primary concern as these bridges experienced unseating even at low peak-ground accelerations. The results from the study conducted by Ramirez et al. (2005) agree with findings reported by additional research focused on the Central Southern United States (CSUS) (Choi et al., 2004; DesRoches et al., 2004a). Choi et al. (2004) developed fragility curves to estimate the conditional probability of different damage states, as summarized in Figure 2-2, for various bridge types in moderate seismic zones.

Table 2
Description of bridge damage states (taken from HAZUS 97)

Damage states	Description
No damage (N)	No damage to a bridge
Slight/minor damage (S)	Minor cracking and spalling to the abutment, cracks in shear keys at abutments, minor spalling and cracks at hinges, minor spalling at the column (damage requires no more than cosmetic repair) or minor cracking to the deck
Moderate damage (M)	Any column experiencing moderate cracking and spalling (column structurally still sound), any connection having cracked shear keys or bent bolts, or moderate settlement of the approach
Extensive damage (E)	Any column degrading without collapse (column structurally unsafe), any connection losing some bearing support, or major settlement of the approach
Complete damage (C)	Any column collapsing and connection losing all bearing support, which may lead to imminent deck collapse

Figure 2-2. Bridge Damage States and Description (Choi et al., 2004)

This study found that steel superstructure bridges, both simply supported and continuous supported, with rocker bearings are the most vulnerable bridge type throughout the CSUS followed by prestressed concrete superstructure bridges. Reinforced concrete bridges were not considered. These vulnerabilities, specifically for steel superstructures, are confirmed by DesRoches et al., with the development of fragility functions (2004a) and demonstration of improved seismic performance using seismic isolation (2004b).

22

2.3   Seismic Retrofits in Central U.S.

For structures with vulnerable details, the seismic performance of the structure can be improved by one of two options: rebuilding the deficient structure or rehabilitating it. For most business owners, both private and public, the cost restraint associated with rebuilding all deficient structures in their inventory makes this option nearly impossible. This restraint holds true for Indiana's Department of Transportation (INDOT), as it is expected to hold true for most DOT in the country. Thus, significant research has been conducted to identify different rehabilitation strategies, referred to as retrofits, to improve the seismic performance of deficient as-built structures. These methods are deemed effective if the retrofit can reduce the seismic vulnerability and considerably costs less than the cost associated with replacing the bridge. All of the retrofits can be classified as either reducing the demand drawn to the structure (Section 2.3.1) or increasing the capacity (Section 2.3.2). A synopsis of common retrofits identified for the CSUS is shown in Figure 2-3 (Timothy, DesRoches, & Padgett, 2011). Given the similarities between CSUS and CEUS bridge vulnerabilities (presented in Section 3.5.1), it is reasonable to assume that the retrofits identified for the CSUS and others recommended by the Federal Highway Administration (FHWA) would also effectively improve the seismic performance of INDOT's bridge network.
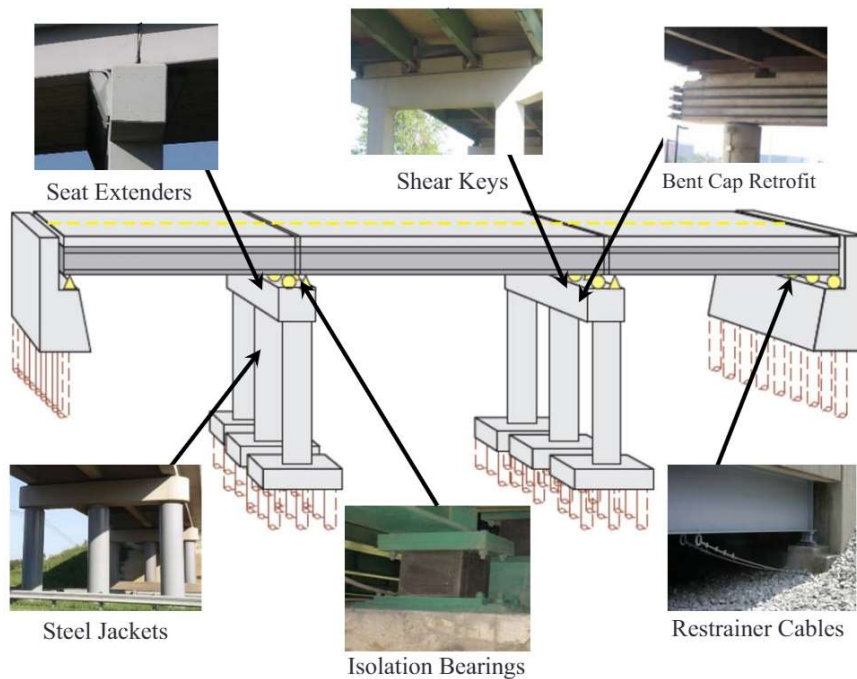
Figure 2-3. Common Retrofits in the CSUS (Timothy et al., 2011)

23

2.3.1 Reducing Demand

Retrofit methods focused on reducing demand seek to decrease or eliminate the force transferred from the bridge's superstructure to the substructure. The most effective methods for reducing demand either decouple the superstructure mass from the substructure, like seismic isolation, or ensure a more monolithic movement between the structure and the ground, like integral abutments or restrainers.

Seismic isolation incorporates an energy-dissipation mechanism responsible for reducing the displacement of the substructure, the seismic demand on the substructure, and shifting the natural frequency of the structure to a lower value. Incorporating seismic isolators is a more attractive option than other more costly retrofit alternatives focused on increasing the capacity of the substructure (Timothy et al., 2011). The FHWA retrofit manual provides guidelines for replacing bridge bearings with isolators as well as expresses the popularity and success of the retrofit measure (FHWA, 2006). Previous studies have shown that two types of isolators are particularly effective, elastomeric bearings and friction pendulum devices.

Elastomeric bearings, with or without a lead core center, normally consist of layered rubber and steel plates with steel flanges at the top and bottom to facilitate a fully fixed connection between the substructure and superstructure. Both an elastomeric bearing with and without a lead core are shown in Figure 2-4. These bearings, designed to resist axial compression, shear and rotation due to the movement of the bridge girder, provide adequate isolation primarily due to their high shear deformation capacity. With this high shear capacity comes the ability for large differential displacement resulting in decreased substructure demand and a reduction in substructure damage (Siqueira et a., 2014). Elastomeric bearings are typically applied as a retrofit to multi-span (both continuous and non-continuous) steel girder bridges supported by rocker bearings. Not only is the use of elastomeric bearings and seismic isolation applicable because these bridges been identified as the most vulnerable in Central U.S. (see Section 2.2), but the elastomeric bearing is less sensitive to corrosion than steel bearings. The replacement of rocker bearings with elastomeric bearings can also provide more reliable flexibility than rocker bearings making them a better-performing mechanism in terms of both functionality and maintenance (Choi, 2002). While standard elastomeric bearings have been shown to reduce substructure damage, they can also significantly increase the displacement of the superstructure, thus increasing the likelihood

for abutment pounding. The addition of a lead core to the elastomeric bearing has been shown to mitigate this issue (DesRoches et al., 2004b; Timothy et al., 2011).

Figure 2-4. Schematic of Elastomeric Bearing (Left); Elastomeric Bearing On-Site (Middle); Schematic of Elastomeric Bearing with Lead-Core (Right) (Ealangi, 2010; Timothy et al., 2011; Choi, 2002)

An alternative isolation mechanism to the elastomeric bearing is the friction pendulum device. Friction pendulum devices are slider bearings that use low-friction interfaces to decouple the superstructure from the substructure, as shown in Figure 2-5. The stiffness of the friction pendulum device is derived as a function of the supporting mass (in the case of bridges, the superstructure weight) and the radius of curvature. With the use of a friction pendulum device comes the potential for increased damping too although the exact value can vary significantly (5% - 20%) depending on temperature and axial stress (Calvi & Calvi, 2017). Research funded by California Department of Transportation (CalTrans) following the devastating Loma Prieta and Northridge earthquakes developed the Seismic Response Modification Device (SRMD). This testing rig allowed for full-scale testing of friction pendulum devices and the possible characterization of performance levels such as allowable displacement (Calvi & Calvi, 2017). Overall, the friction pendulum devices have been identified as a suitable design for large-scale structures in high-seismic zones, like the Benicia-Martinez structure in California. This bridge is designed for seven times the average gravitational acceleration. Additional states like North Carolina and Tennessee have implemented friction pendulum devices and additional researchers have shown the overall effectiveness of them for decreasing internal forces in substructures (Timothy et al., 2011; Gillich et al., 2013; Avossa et al., 2018).
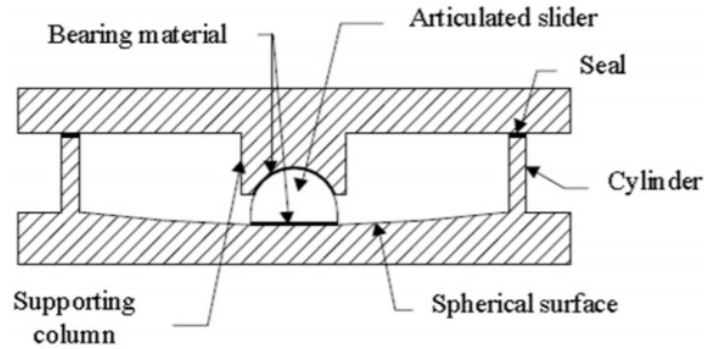
Figure 2-5. Schematic of Friction Pendulum Device (Ealangi, 2010)

Brides supported by integral abutments are not vulnerable to the expected level of seismic hazard in Indiana in the longitudinal direction (Frosch et al., 2009). The differential displacement and inertial effects typically generated during seismic excitation are negligible as the integral abutment rigidly connects the superstructure with the ground. With the elimination of the superstructure inertia, the demand in the longitudinal direction is negligible. Thus, this approach is a suitable seismic retrofit strategy. For bridges where the construction of an integral abutment is not possible, due to bridge length or skew, restrainers may instead be added to connect the abutment to the superstructure. Although this retrofit does not result in a monolithic connection like the integral abutment, when designed correctly it can significantly reduce the resulting differential displacement between the structure and adjacent ground, therefore reducing the overall seismic demand.

Two common types of restrainers, cable- and bar-type, are shown in Figure 2-6. Restrainers have been shown to effectively prevent longitudinal movement of spans at the abutment or over piers where adjacent simply-supported beams or an internal hinge are present (Timothy et al., 2011). The installation of restrainer bars is relatively inexpensive and recognized by the FHWA (2006) for its simplicity and effectiveness. Bar restrainers are less flexible but are more ductile than cable restrainers and are made of galvanized high strength steel. Typically, restrainers are designed using high-strength reinforcement such as carbon-fiber reinforcement because of the increased rigidity and yield stress.

Figure 2-6. Restrainer Cables (Left) and Restrainer Bars (Right) (Timothy et al., 2011)

2.3.2 Increasing Capacity

The capacity of each substructure is based on geometry, flexural and shear reinforcement ratio, concrete strength, and end restraining conditions. Retrofit strategies that are focused on increasing capacity serve to address one or more of these components. One typical strategy is to add exterior reinforcement in the form of a jacket. The addition of a jacket increases the reinforcement ratio therefore increasing the flexural capacity and shear strength. The jacket also enhances confinement, which provides an increase in ductility. Common jacketing techniques used in the central U.S. include steel jacketing, concrete overlays, and steel plate encasement, as shown in Figure 2-7. These retrofits are usually applied locally at the ends of the substructure member to target the plastic hinge regions, but both steel and RC jackets can be applied to the full substructure height. This approach is beneficial especially if increased shear strength along the length is desired. For vulnerable walls and hammerheads, the FHWA (2006) retrofit manual suggests the use of steel plate encasement with steel anchors to provide active confinement.

Figure 2-7. Steel Jackets (Left), RC Jacket (Middle), and Steel Plate Encasement with Steel Anchors (Right) (Timothy et al., 2011; Timothy et al., 2011; FHWA, 2006)

Typical frame bent substructures with adequate ductility can form one of two distinct collapse mechanism: weak column – strong beam or strong column – weak beam. The "weak" element referring to the member of the frame bent where the plastic hinges form first and most of the plastic hinges(s) in the mechanism form. A drawing of each collapse mechanism is provided in Section 5.6.3. These mechanisms, once formed, allow the substructure to dissipate energy. Bent caps with a low flexural reinforcement ratio are vulnerable to the less-desirable mechanism of hinge formation for frame bents: strong column – weak beam. For bridges, the formation of strong column – weak beam collapse mechanism is rather difficult to rehabilitate because the entire superstructure must be lifted so that the hinges in the bent cap can be repaired. Because of these difficulties, the desired mechanism of hinge formation is weak column – strong beam which allows plastic hinges to develop in the column before the bent cap experiences any damage. To ensure that the preferred hinge mechanism forms, both past research (Timothy et al., 2011) and the FHWA (2006) recommend increasing the strength of the bent cap via external post-tensioning or shear reinforcement, as shown in Figure 2-8.

Figure 2-8. External Post-Tensioning (left) and Shear Reinforcement (right) for Bent Cap Strengthening (Timothy et al., 2011)

2.4   Network Vulnerability

Typical seismic vulnerability assessments identify bridge-types that are independently vulnerable to the expected level of seismic hazard for the region (Choi, 2002; DesRoches et al., 2004a; Metzger, 2004; Nielson & DesRoches, 2007a; Nielson & DesRoches, 2007b). However, a bridge network is far more complex with its functionality dependent on the performance of multiple bridges within key access corridors or interchanges. Thus, the overall vulnerability of these sections must be derived as a function of each bridge's vulnerability within the corridor. To

implement this interconnected approach, certain probabilistic models for the bridge's capacity, demand, and damage must first be explored as well as previous modeling approaches for complex networks.

2.4.1 Fragility Functions

A fragility function (FF) is a probabilistic representation of a structure's likelihood to reach or exceed a certain level of damage (hereafter referred to as limit state (LS)) for a given level of hazard, represented by an intensity measure (IM). The mathematical model for an FF is shown in Equation 2-1 where the limit state is represented by y_{LS} and the intensity measure by x_{IM}.

$$F_R(x; y_{LS}) = P(Y \geq y_{LS} \mid X = x_{IM}) \qquad (2\text{-}1)$$

The engineering demand parameter (EDP) represented as Y in Equation 2-1 is a measurement used to represent the dynamic response of the structure. This parameter, as well as the threshold for each LS, should robustly capture the different levels of expected damage, either on a global or local scale. Common examples of local and global damage are better suited for buildings as these multi-degree-of-freedom (MDOF) systems lend themselves to more complex responses. For a building, global damage is represented by the overall building drift whereas local damage can be classified by inter-story drifts. The EDP can be one of many structural response parameters for which clear metrics, or thresholds, corresponding to each damage state can be identified. These parameters include displacement (Nielson & DesRoches, 2007a), drift (Gardoni et al., 2003), rotation of the plastic hinge (Shinozuka, Feng, Kim et al., 2000), or a damage index (Karim & Yamazaki, 2001; Nateghi-A & Shahsavar, 2004; Hwang & Huo, 1994). The damage index is typically an equation derived as a function of a critical element's displacement, rotation, and ductility or energy-dissipating capability.

The intensity measure, notated as x_{IM} in Equation 2-1, is responsible for characterizing the ground motion. Three classes of intensity measures exist: peak-based such as peak-ground acceleration; frequency-based such as spectral acceleration, and duration-based. Research has shown the capabilities that frequency-based intensity measures have on developing a strong correlation to structural damage (De Biasio et al., 2014). This correlation is beneficial for reducing modeling uncertainty. Additional research shows the impact spectral velocity has on reducing

epistemic uncertainty when using Bayesian inference to generate the regression function between the capacity and demand (Peña, 2019).

Many regression methods, leveraging either a deterministic or a probabilistic approach, exist for generating FF. Notable deterministic regression models include the capacity spectrum method (Shinozuka, Feng, Kim et al., 2000) and linear regression in log-space (Nateghi-A & Shahsavar, 2004; Nielson & DesRoches, 2007a; Taylor, 2007). The classic FF equation using the linear regression in log-space method is

$$F_R(x; y_{LS}) = P(Y \geq y_{LS} \mid X = x_{IM}) = 1 - \Phi\left(\frac{\ln(y_{LS}) - \lambda_{Y|X}}{\beta_T}\right), \tag{2-2}$$

where y_{LS} corresponds to the limit state capacity, $\lambda_{Y|X}$ corresponds to the best-fit function characterizing the relationship between capacity and demand in log-space, Φ represents the cumulative distribution functions for a standard normal distribution, and β_T is the total uncertainty in the system (Taylor, 2007). For a deterministic response, β_T corresponds to the summation of values commonly used to represent the uncertainty for demand ($\beta_{Y|X}$), capacity (β_C), and modeling (β_M) where the latter two correspond to 0.3 (Wen et al., 2004). Typically, $\beta_{Y|X}$ is represented with a single value calculated using a standard error formula which accounts for the spread or deviation of data from the best-fit function. As the use of FF has progressed, the methods for developing FF have also changed to better account for uncertainties in the system using probabilistic approaches. A probabilistic approach also allows for the quantification of epistemic and aleatory uncertainty. Notable probabilistic regression approaches include maximum likelihood estimation (Shinozuka, Feng, Lee et al., 2000), Gaussian Process (Gentile & Galasso, 2019), and Bayesian inference (Gardoni et al., 2003; Peña et al., 2019; Nielson & DesRoches, 2007b).

2.4.2   Reliability Estimation and Risk Assessments

The development of a reliability estimation procedure, which forms the basis for risk assessments, is first associated with the nuclear power plant industry (U.S. Nuclear Regulatory Commission, 1975). This methodology has since been leveraged to conduct risk assessments for power plants to specific hazards, such as seismic excitation (Reed, 1989). This assessment, later summarized by Huang et al. (2011), focused on developing a methodology for estimating the probability of failure for critical components of a nuclear power plant by coupling the element's

probability of damage conditioned on the occurrence of a seismic event (fragility function) with the likelihood of said event occurring (hazard curve).

Since the development of seismic risk assessment (SRA), this methodology has been modified and applied to other critical infrastructure systems such as transportation systems (Banerjee & Shinozuka, 2009; Werner et al., 2000; Padgett, DesRoches, & Nilsson, 2010) or harbors (Pitilakis et al., 2016). Werner et al. (2000) is responsible for the early development of an SRA specifically for transportation networks. This work highlighted the importance of not only single bridge performance, but also interdependencies in the highway system such as configuration and system redundancies. Like most networks, a highway system configuration can be represented as a node and link model where a link corresponds to a section of undisturbed highway and a node corresponds to the major interchanges which join these links (Banerjee & Shinozuka, 2009). In cities, a node can represent critical infrastructure like a hospital or again critical intersection between links, as shown in Figure 2-9. The spatial dispersion of these nodes, and the bridges which lie within each link, also impact the overall performance of a highway system (Werner et al., 2000).
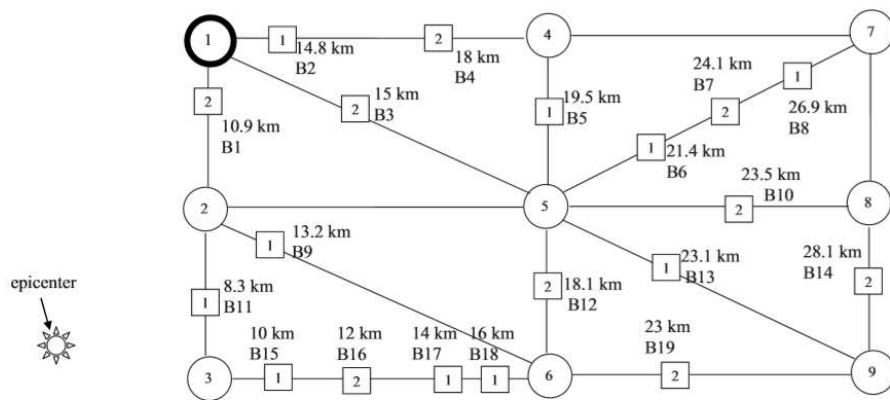
Fig. 3. Test network for bridge network reliability estimation problem. An unshaded circle represents a source node, a shaded circle represents a hospital, and squares represent bridge locations with the number indicating the type of bridge (1=single-bent overpass, 2=two-bent overpass). Distances by the bridges are the distances from the epicenter.

Figure 2-9. Sample Node and Link Model for City (Guikema & Gardoni, 2009)

The study in Figure 2-9, conducted by Guikema and Gardoni (2009), uses a Monte Carlo simulation to determine the mean probability, and corresponding 95% credible intervals, that the entire network remains connected after the occurrence of an earthquake event with different magnitude and distance properties. This probabilistic approach allows for the inclusion of uncertainty while a deterministic approach does not.

31

The results of an SRA can be combined with additional information such as a loss function to economically assess the impact of different sized hazard events. This economic loss can be categorized as either direct or indirect loss. Direct loss is considered the cost associated with potential bridge damage (Padgett et al., 2010) whereas indirect loss is a result of disturbed traffic flow resulting in increased travel times and reduced traffic flow (Werner et al., 2000). The use of a loss function to economically quantify the impact of a hazard event also allows for the effective prioritization of retrofits given the robust nature of the assessment.

2.5   Summary of Literature Review

The findings from each section of the literature review are summarized as follows:

- With the recent identification of the WBSZ, state's like Indiana have increased seismic awareness for bridge inventory which contains bridges designed without proper seismic detailing (Section 2.1)

- Similarities exist between the vulnerabilities identified in CSUS and CEUS (Section 2.2). Thus, the retrofits identified for CSUS by Timothy et al. (2011) should also be suitable for Indiana (Section 2.3).

- An FF is a probabilistic representation of a bridge's likelihood to incur a certain level of damage conditioned on the occurrence of seismic excitation. This mathematical model is capable of incorporating uncertainty associated with modeling, capacity, and demand through the use of Bayesian inference (Section 2.4.1).

- Due to the intrinsic interdependent nature of a bridge network, the use of an SRA can provide a clearer insight into the vulnerability of DOT transportation systems then a vulnerability study of single bridges in isolation (Section 2.4.2).

3. SEISMIC ASSESSMENT PROCEDURE

3.1 Introduction

This chapter discusses the bridge selection process and the seismic vulnerability assessment procedure (hereafter referred to as the seismic assessment procedure) using stochastically simulated earthquakes. The purpose of the seismic assessment is to identify vulnerable details in Indiana Department of Transportation's (INDOT) bridge network. The seismic assessment develops a 2-D finite element model to determine the dynamic response of the structure in both the transverse and longitudinal direction. This seismic assessment procedure accounts for the non-linear response, and corresponding force redistribution, of the structure up to the formation of the identified hinge mechanism, when applicable. This analysis is applied to a small, yet representative sample of structures in INDOT's bridge network and allows for the identification of trends in vulnerable details and their corresponding response parameters such as displacements and drift-based thresholds for use in Chapter 4. The seismic assessment procedure is first presented generally in Section 3.3 then applied in-detail to a prestressed concrete superstructure supported by a two-story frame bent in Section 3.4.

3.2 Bridge Selection and Earthquake Generation

The proper identification of typical vulnerable details in INDOT's infrastructure network requires the selection of a representative sample of bridges with respect to local ground motions. For many DOTs, the response of bridges along specified emergency routes are prioritized in terms of safety as the performance of these structures is more crucial in response to hazards. Therefore, representative sites along specified emergency routes, as identified in SPR-2480 (Ramirez et al., 2005), are selected. 87% of the bridges in the sample set carry or cross over an emergency route. Additional aspects to consider are the expected level of seismic hazard, availability of geotechnical information, geological and geographical diversity, type of route carried, type of route crossed, construction material, and superstructure geometry. Currently, the state of Indiana's bridge asset management database (BIAS) does not contain information regarding substructure type, thus no consideration for substructure type is possible when selecting the representative sample. 100

bridges (51 prestressed concrete, 21 reinforced concrete, and 28 steel) throughout the state of Indiana are selected for conducting a seismic assessment.

For states like Indiana, where few historical ground motions records have been recorded, the expected seismic excitations are generated using a stochastic simulation approach (Papageorgiou & Aki, 1983; Boore, 1983; Halldorsson & Papageorgiou, 2005) These stochastically simulated earthquakes consider the seismic source, attenuation, and soil condition. Consistent with the current AASHTO (2017) design specification, a return period of 1000 years (7% probability of exceedance in 75 years) is considered. For each bridge, 100 time histories are stochastically simulated using various magnitude distance bins compatible with a deaggregation analysis of United States Geological Survey (USGS) uniform hazard spectrum. Based on each magnitude-distance bin's contribution to the overall hazard, a corresponding number of time histories are generated. For bridges with adequate geotechnical information, site-specific amplification factors are used. This factor accounts for the amplification of ground motions from the seismic source to the soil-bedrock interface. As not all 100 bridges in the sample have adequate geotechnical information to generate site-specific amplification factors, generic amplification factors consistent with soil sites in the CEUS are used (Silva et al., 2000; Atkinson & Boore, 2006; Boore & Campbell, 2016). Lastly, for structures where the soil class at the site is unknown, the soil class is classified using the predicted response of the geological material (Hill, 2008).

3.2.1   Robustness of Selected Bridges

A statistical analysis of the 100 bridges is conducted to verify that the sample set reflects Indiana's bridge network for certain superstructure configurations which influence the dynamic analysis. These superstructure characteristics include max span length, total structure length, structure type, out-to-out deck width, and skew. For the 22 categories of structure types across the three main construction materials (steel, reinforced concrete, and prestressed concrete) the majority of the structure types for each construction material are present in the sample, as shown in Figure 3-1. The sample intentionally does not include culverts (structure type 19) as a buried structure does not have a face independent of the ground movement. Also, the sample contains bridges designated as RB to signify the percent of "Remaining Bridges" that did not fall into the detailed bins.

.
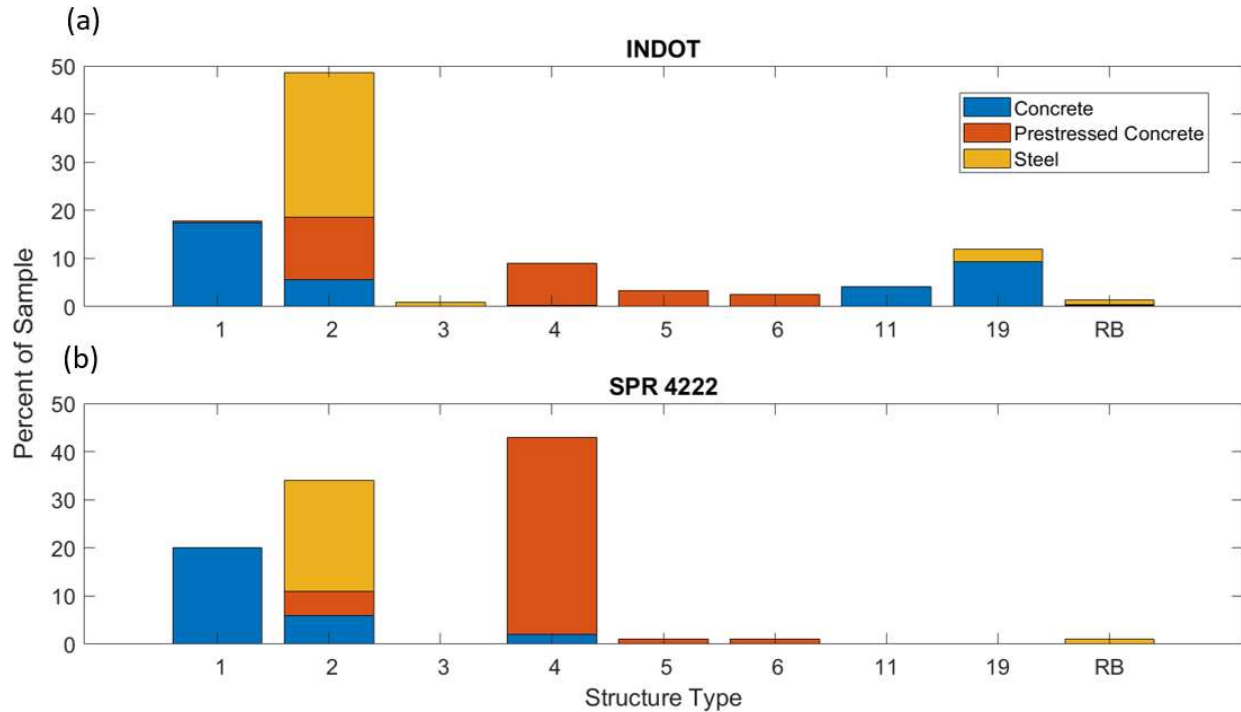
Figure 3-1. Distribution of Structure Type in (a) INDOT's Bridge Inventory and (b) Bridges in Sample Set

The remaining geometric variations in max span length, total structure length, out-to-out deck width, and skew are also found to be representative. While these characteristics are well-represented, these aspects are not shown visually as max span length, structure length, and out-to-out deck width contribute to the total mass of the deck in a straightforward manner. Skew only impacts the seismic analysis of reinforced-concrete superstructures in the transverse direction as this superstructure type is the only ones modeled as a multi-degree-of-freedom
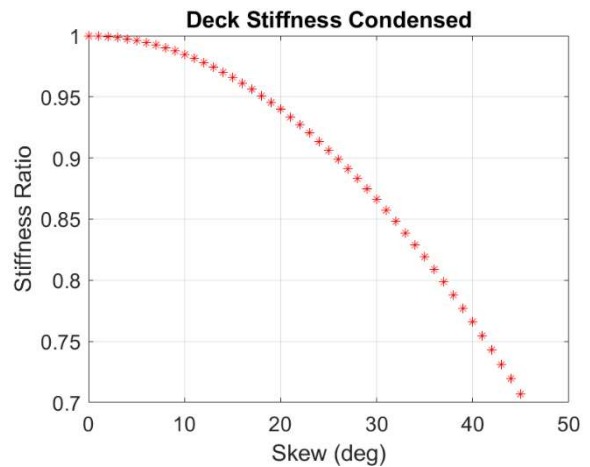
Figure 3-2. Reduction in Deck Stiffness as Function of Skew

MDOF system. A stiffness analysis, shown in Figure 3-2, shows that the effects of skew on the dynamic model is minimal for bridges with a skew less than 30 degrees. Typically, reinforced concrete superstructure bridges in Indiana's bridge network maintain a skew less than 30 degrees.

Overall, the selection is representative of the bridges in Indiana thus providing a robust sample set for the development of the seismic assessment procedure

3.3   Seismic Assessment: Methodology

The seismic assessment procedure, shown in Figure 3-3, is composed of three critical components: demand (green), capacity (purple), and vulnerability (blue). This seismic assessment procedure requires interpretation of structural drawings and an engineer's judgement to develop a representative finite element model. These models are developed using MATLAB but could also be developed in other finite-element specific programs such as SAP2000 (which will be used as validation of certain components of MATLAB results). Regardless of the software, the seismic assessment requires calculating critical capacity measures like moment-curvature and conducting a non-linear pushover analysis or non-linear time-history analysis to account for force redistribution due to non-simultaneous, non-linear behavior, when applicable. For this thesis, a non-linear pushover analysis is used. In general, a strong agreement between the results obtained using a non-linear pushover analysis versus a non-linear time history analysis have been shown for moderate-sized earthquakes like those more-frequently expected in Indiana (Shinozuka, Feng, Kim et al., 2000). The general assumptions and application for each section will first be explored, with a seismic assessment of a unique substructure type to follow.
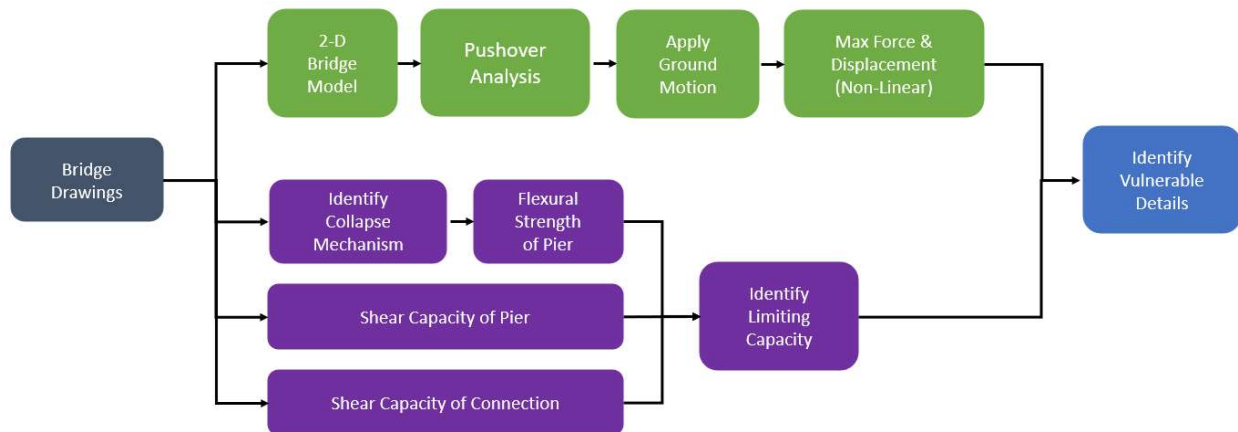
Figure 3-3. Seismic Assessment Procedure

3.3.1 Identify Mechanism of Hinge Formation

A substructure's mechanism of hinge formation (or collapse mechanism) is dependent on the structure's ability to resist moment(s) at fixed end(s). To understand the structure's potential for non-linear response, the moment-curvature relationship for cracking, yielding and ultimate moment must be calculated. This ductile mode of failure is contingent on the structure having enough shear capacity to avoid brittle failure, anchorage failure, and other potential modes of failure such as shear connection failure or unseating. The capability of the substructure to exhibit this mode of failure is based on the aspect ratio which is defined as the cross-section depth to height ratio in the plane of bending. This ratio (λ_r) determines whether the substructure is expected to have a response dominated by flexure, shear, or a combination of both. For a substructure with λ_r less than 3, the response is a combination of flexure and shear (Fares, 2018) as shown in Figure 3-4. This limit is primarily a concern for wall-type substructures in the transverse direction but can be seen across all substructure types. The research by Fares (2018), as well as experimental tests on walls (Escolano-Margarit et al., 2012) and guidance from AASHTO (2017), show that a RC substructure cannot exhibit a response dominated by flexure (> 90%) and form a plastic hinge until the aspect ratio is around 2.5 or greater. Conservatively, this threshold is taken as 3 in this procedure.
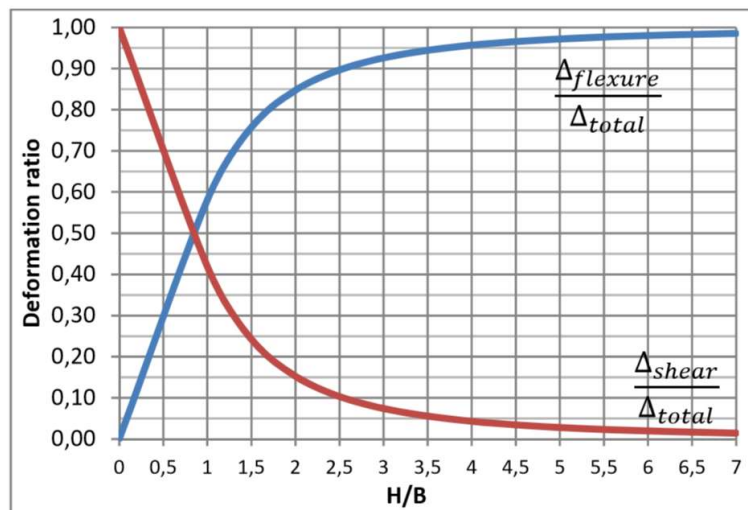
Figure 3-4. Shear & Bending Stiffness Contributions as a Function of Aspect Ratio (Fares, 2008)

The moment associated with cracking is calculated using the gross moment of inertia and a centroidal depth of half the section depth. The compressive stress of concrete follows a modified Hognestad stress-strain curve (see Section 3.4.1). The following equation for cracking moment (M_{cr}) and the corresponding curvature is

$$M_{cr} = 7.5\sqrt{f_c'} * \frac{2I_g}{h},$$

(3-1)

$$\varphi_{cr} = \frac{M_{cr}}{I_g * E_c}.$$

(3-2)

The moment associated with yielding is calculated assuming the outermost layer of longitudinal steel has just yielded. This corresponds to a yield strain of

$$\varepsilon_y = \frac{f_y}{E_s}.$$

(3-3)

The solution for the yielding moment (M_y) is achieved when the force equilibrium of the cross-section is achieved. The resulting curvature at yielding, for a neutral axis depth (c_{NA}), is

$$\varphi_y = \frac{\varepsilon_c}{c_{N.A.}}.$$

(3-4)

The ultimate moment (M_u), or the point when the substructure has fully formed the identified mechanism of hinge formation, assuming adequate confinement, is calculated assuming strain hardening of the outermost layer of longitudinal steel ($\varepsilon_s = .01$) or an extreme compression fiber strain ($\varepsilon_c = 0.003$) in the concrete has occurred. Like the yield moment, the solution is achieved when force equilibrium occurs and the resulting curvature is calculated using Equation 3-4 with a neutral axis depth that reflects the equilibrium of the cross section at the ultimate moment.

3.3.2 Shear Capacity of the Pier

The shear capacity of each substructure type is calculated in accordance with guidance outlined by AASHTO (2017). For all substructure types, regardless of λ_r, the shear force is assumed to distribute equally over the entire length of the cross-section.

3.3.3 Horizontal Shear Capacity of the Connection

The seismic assessment assumes continuity between the superstructure and substructure displacement. This assumption allows for a well-defined relationship for the restoring force drawn to each pier. The restoring force is calculated as the amount of total force drawn to each pier. In the linear range, this value is calculated using stiffness parameters. Once a pier starts to exhibit a non-linear response, this force is calculated using a pushover analysis and moment-area theorem (see Section 3.3.8 for further detail). For prestressed concrete superstructure, a diaphragm like the typical detail shown in Figure 3-5 placed between all adjacent beams over intermediate piers precipitates this continuity. For reinforced-concrete superstructures, the reinforcement bars extending from the bent cap into the superstructure facilitates this continuity. For steel superstructures, only fixed bearings are capable of ensuring continuity in the longitudinal direction whereas all bearings (fixed and expansion) allow for the pier to participate in the transverse direction. More detailed information, such as calculations for all connection types, is demonstrated by Bonthron, Beck, Lund, et al. (2020).
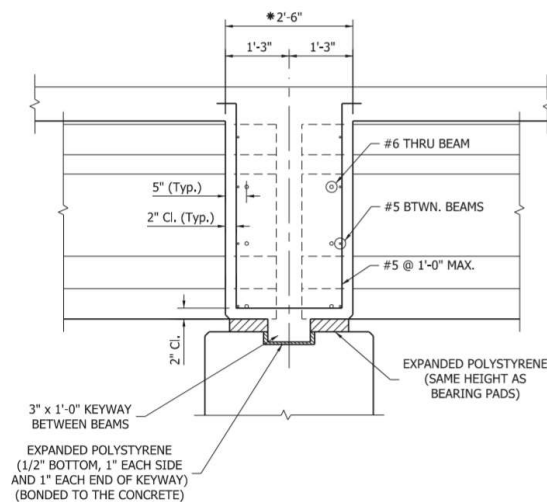
Figure 3-5. Standard Pier Diaphragm Between Beams (INDOT, 2013a)

3.3.4 Identify Limiting Capacity

The limiting capacity is identified to determine the applicable vulnerability criterion. A limit mechanism controlled by base shear is ideal as the formation of plastic hinges is a ductile mode of failure. The total collapse of these structures is dictated by a limiting rotation of the

substructure that has a low probability of exceedance. In addition to adequate confinement, this mode of failure assumes that the load capacity can be maintained considering P-delta effects introduced from the eccentricity caused by inelastic deformation. However, for bridges without adequate shear detailing or the horizontal shear connection is inadequate for transferring the restoring force, the formation of a plastic hinge will never occur. Rather, the mechanism of failure is controlled by a brittle shear failure. Additionally, it is important to note that substructures with insufficient amount of longitudinal reinforcement, e.g. sections where the cracking moment of the substructure exceeds the yield or ultimate moment, also are likely to result in a brittle failure as the steel is likely to undergo instantaneous strain hardening which could possibly result in the rupturing of the steel reinforcement (see Section 3.4.3 for further details).

3.3.5   2-D Bridge Model

A 2-D model of the structure is constructed for both the transverse and longitudinal direction separately – a typical design practice. Garcia (1998) first proposed the modeling technique used in this thesis to ascertain the dynamic response of a particular bridge type in the transverse direction. This technique, focused on modeling reinforced-concrete bridge as a MDOF system due to the rigid connection between the superstructure and substructure, has been extrapolated to model different superstructure types, different connection assumptions, and the bridge in the longitudinal direction (Metzger, 2004). For modeling purposes, the longitudinal direction is parallel with traffic flow whereas the transverse direction is perpendicular to traffic. It is important to note that the dynamic modeling technique presented emphasizes the response of the substructure. Although more complex modeling strategies such as energy-dissipation via abutment pounding could yield further insight into some specific vulnerabilities, the vulnerabilities identified and summarized in Table 3-4 are consistent with known vulnerabilities identified in other regional studies (see Section 2.2). Additionally, these vulnerabilities correspond with previously-identified vulnerability thresholds for post-earthquake evaluation in the state of Indiana (Ramirez et al., 2005). Also, because the boring depth for most geotechnical reports in Indiana is driven by the need to reach a certain bearing capacity, rather than achieving a soil profile which allows for the evaluation of liquefaction potential, this modeling component cannot be accounted for in this vulnerability assessment. If adequate soil profiles are achieved (see Section 6.1.1 for requirements), then liquefaction potential should be considered for all bridges.

The 2-D bridge model is composed of three critical components: stiffness, mass, and damping. Information required to calculate the stiffness of each pier includes unsupported height, cross-section dimensions, material properties, and the degree of fixity both at the base of the substructure and between the substructure and superstructure. Traditionally, for most prestressed concrete bridges, the former is fixed, and the latter is semi-fixed. The semi-fixed degree of fixity corresponds to a leading stiffness coefficient of 6, which is further explain in the case study presented, and the recommended value defined by INDOT (2013b). For steel bridges, the former is fixed, and the latter is free. The substructures throughout the state of Indiana fall into four distinct categories: frame bents, walls, hammerhead walls, and other. The equations for calculating the stiffness of the first three, considered to be *typical substructure types*, is presented by Bonthron et al. (2020). An approach for calculating stiffness of a substructure labeled other is presented in Section 3.4.6.

Unlike RC superstructures, the lateral stiffness of prestressed concrete and steel superstructures in the transverse direction derives solely from the stiffness of the substructure as the connection between the superstructure and substructure is incapable of transferring a moment. However, both prestressed concrete and steel superstructures are assumed to be sufficiently rigid such that the intermediate piers act as springs in parallel, but not so rigid as to inhibit the inertial effects of the mass. Thus, prestressed concrete and steel superstructure bridges are modeled as a single-degree-of-freedom (SDOF) system with a singular displacement in the transverse direction. All bridges are modeled as single-degree-of-freedom (SDOF) systems in the longitudinal direction.

The mass of the bridge is calculated using the superstructure geometry, barrier dimensions from INDOT Standard Drawings (2012b), concrete diaphragms, and the material properties of concrete and steel. In the transverse direction, the mass that participates in the response of the structure is calculated using a lumped mass model technique where the total mass attributed to each pier corresponds to the tributary length supported by each pier. In the longitudinal direction, the entire mass of the superstructure is considered.

Less certain to the dynamic model than the mass and stiffness is the damping. While damping is inherent to all structural systems, it is difficult to predict outright and varies non-linearly as a result of structural softening. For this assessment, an equivalent linear viscous damping coefficient (ζ_{sub}) of 5% is used.

Using a modal damping technique, the inherent viscous damping rate of the substructure is

$$c_{sub} = 2\zeta_{sub}\sqrt{K_{sub}m_{sup}} \qquad (3\text{-}5)$$

With all three critical dynamic components calculated, the equation-of-motions for the bridge subjected to ground motion is written as

$$m_{sup}\ddot{x}_s + c_{sub}\dot{x}_s + K_{sub}x_s = -m_{sup}\ddot{x}_g. \qquad (3\text{-}6)$$

Alternatively, Equation (5-3) can be written, using the circular natural frequency (ω_n) as

$$\ddot{x}_s + 2\zeta_{sub}\omega_n\dot{x}_s + \omega_n^2 x_s = -\ddot{x}_g \qquad (3\text{-}7)$$

where the circular natural frequency and period is calculated as

$$\omega_n = \sqrt{\frac{K_{sub}}{m_{sup}}}, \qquad (3\text{-}8)$$

$$T = \frac{2\pi}{\omega_n}. \qquad (3\text{-}9)$$

3.3.6 Non-Linear Pushover Analysis (NLPA)

For bridges with multiple piers, specifically ones that experience a change in ground profile along the length of the bridge which result in different pier heights and stiffnesses, a displacement-controlled pushover analysis is necessary. Due to significant variations in restoring capacity, individual piers may exhibit non-simultaneous, non-linear response. This response is a phenomenon related to structural softening caused by the yielding of longitudinal steel and increase in concrete cracking once the yield moment capacity of the identified mechanism of hinge formation for the substructure is exceeded. The NLPA allows for a better understanding and quantification of the expected redistribution of lateral forces as a result of structural softening.

To perform a NLPA, a singular displacement is incrementally applied to the structure. The displacements range from the displacement corresponding to the first yield of the longitudinal steel for the controlling pier to the full development of the identified mechanism for hinge formation.

Using the linear stiffnesses, the displacement corresponding to the first yield of the controlling pier (e.g. the displacement causing the first pier to start exhibiting non-linear behavior) is calculated as

$$\Delta_c = \min\left(\frac{(V_y * K_{pier})_i}{\sum_{j=1}^n K_{pier\,j}}\right). \tag{3-10}$$

The displacement is increased at a rate of .01 inch until all piers have developed the identified mechanism of hinge formation. At each increment, the force drawn to the pier is dictated by the controlling assumption that all piers will equally displace. Using the moment-area theorem, the force that results due to the displacement is calculated. The percent of the total force drawn to each pier (force ratio) is also calculated. It is important to note that this analysis requires the piers to exhibit a ductile mode of failure (plastic hinges) therefore, it is not conducted for bridges with a substructure that is expected to experience a brittle mechanism of failure as the failure is sudden and no redistribution is expected.

SAP 2000 17, a finite-element program, is used to verify the NLPA. A finite element model of a two-span, continuous steel bridge with circular reinforced-concrete frame bents (NBI 33280) is developed to verify the pushover analysis. Using the same assumptions and moment-curvature response as the MATLAB model, a NLPA in the longitudinal direction is conducted. The results of the model, which show a very similar non-linear redistribution between the two models, is shown in Figure 3-6.
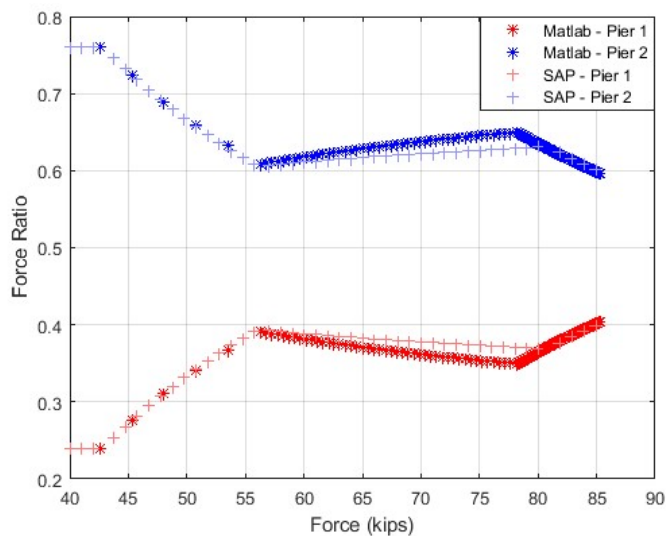
Figure 3-6. Validation of MATLAB Pushover Analysis Using SAP2000

3.3.7 Apply Ground Motion

The seismic assessment procedure uses stochastically simulated earthquakes specific to the location of each bridge and developed using a deaggregation technique consistent with the U.S. Geological Survey. The time histories are generated for a 7% probability of exceedance in 75 years. A time-domain analysis using a 4th order Runge-Kutta integration scheme, defined as ODE4 within MATLAB, is used to determine the displacement-response of the structure.

3.3.8 Maximum Force & Displacement

The displacement of each pier is calculated using the second moment-area theorem. The fundamental theorem states that the vertical distance between a reference tangent line at point B and a displacement at point A is equal to the moment of the area beneath the curvature diagram between the two points with the moment calculated about the point corresponding to the reference tangent line (B). This approach utilizes the moment-curvature relationship previously calculated for capacity. For a frame bent where the base is fixed (Point A) and the point of inflection occurring at half the unsupported height (Point B), as shown in Figure 3-7, the displacement using moment area theorem is calculated as

Figure 3-7. Moment-curvature Diagram for Frame Bents

$$\Delta_{\frac{B}{A}} = \Delta_B - \Delta_A = \Delta_B = \int_0^{\frac{H}{2}} \varphi(x) * \left(\frac{H}{2} - x\right) dx \tag{3-11}$$

where $\Delta_A = 0$ for fixed-end deflections. With the idea of moment-area theorem introduced, Equation (3-11) can be refined into linear and plastic components as shown in Figure 3-7 where the total non-linear displacement is the sum of the two components.

The two displacement components are taken as

$$\Delta_p = \int_0^{L_y} \left(\varphi(x) - \varphi_y(x)\right) * \left(\frac{H}{2} - x\right) dx, \qquad (3\text{-}12)$$

$$\Delta_l = \frac{\dfrac{2M_y}{H}}{K_{pier}} = \frac{V_y}{K_{pier}}. \qquad (3\text{-}13)$$

Equation (3-14) is rewritten as

$$\Delta_{\frac{B}{A}} = \Delta_{nl} = \Delta_l + \Delta_p. \qquad (3\text{-}14)$$

The seismic assessment procedure assumes the total force drawn to the structure remains the same for both a linear and nonlinear approach. This assumption is supported by using linear modifiers to estimate the substructure's non-linear moment of inertia and displacement, such as

$$I_{nl} = 0.7 I_g, \qquad (3\text{-}15)$$

$$\Delta_{nl} = \sqrt{2}\Delta_l. \qquad (3\text{-}16)$$

Therefore, the non-linear force drawn to the structure is approximated to the linear force as

$$F_{nl} = (K\Delta)_{nl} = 0.7 K_l * \sqrt{2}\Delta_l = (K\Delta)_l = F_l. \qquad (3\text{-}17)$$

Using the total force from the time-domain analysis of the linear model, the forces are redistributed (when applicable) using the results from the NLPA. From the NLPA, the redistribution ratio and displacement are known for all loads that precipitate non-linear response. The same SAP2000 model is used to evaluate the MATLAB results for total force versus bridge displacement shown in Figure 3-8.
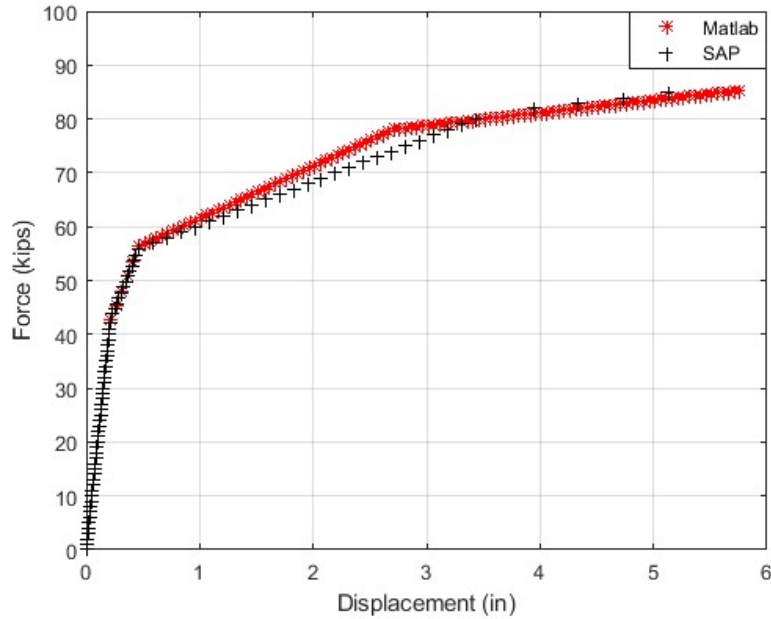
Figure 3-8. Force vs. Bridge Displacement Comparison and Validation

3.3.9   Identify Vulnerable Detail

Based on the response of the structure to the suite of ground motions, vulnerable details characteristic to INDOT's bridge network can be identified.

3.4   Seismic Assessment: Application to Case Study

The general methodology presented in Section 3.3 is applied to a sample bridge with a substructure categorized as *other*. The purpose of this section is to show additional adaptations that may be required to successfully implement the procedure. While the overall seismic assessment procedure is considered robust enough to be used in assessing the vulnerability of every bridge in INDOT's bridge network, certain adaptations may be necessary for certain steps. For example, as is necessary for this case study, the approach and assumptions for calculating the stiffness of the substructure must be adapted. While the approach still uses the stiffness method, additional rotational and translational degrees of freedom must be considered.

3.4.1 Prestressed Concrete Bridge with Two-Story Rectangular Frame Bent

Structure Number 050-15-00210 BEBL (NBI 18790) is a five-span prestressed concrete bridge located in Dearborn County of the Seymour District. Originally constructed in 1938, the bridge has had two rehabilitations. In 1976, the bridge underwent general rehabilitation and in 2016, the superstructure was replaced (steel to prestressed concrete) and both the superstructure and substructure were widened. With this rehab, an additional column was added to each pier. The superstructure is composed of seven Bulb-Tee 66 X 60 Beams with an 8-inch (20.3 cm) reinforced-concrete deck. The bridge is skewed at 20-degrees, has span lengths of approximately 82'-2", 105'-7.5", 113'-9", 105'-7.5", and 81'-3", and is 72'-2" wide.
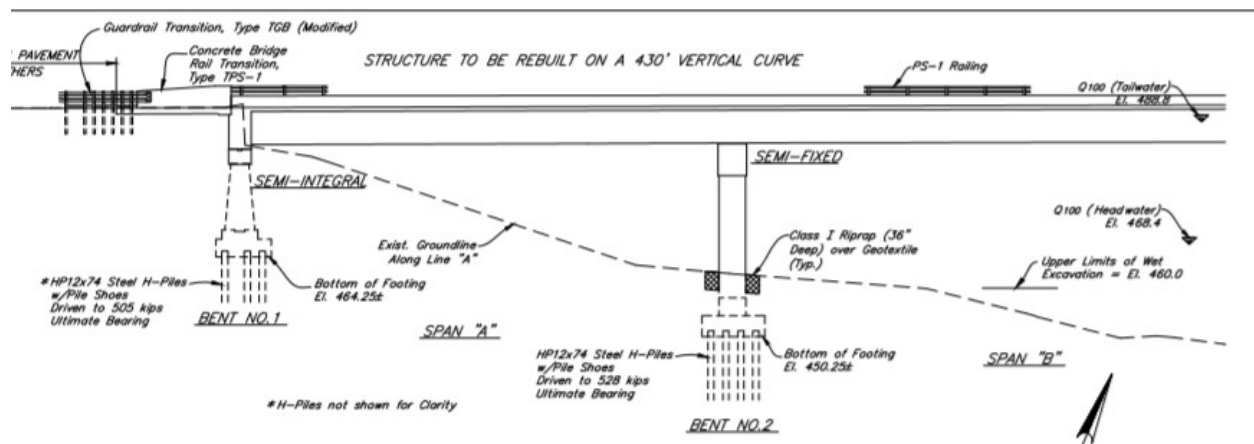
Figure 3-9. Elevation View of the Bridge - Span 1 and 2 (NBI 18790) (2014)
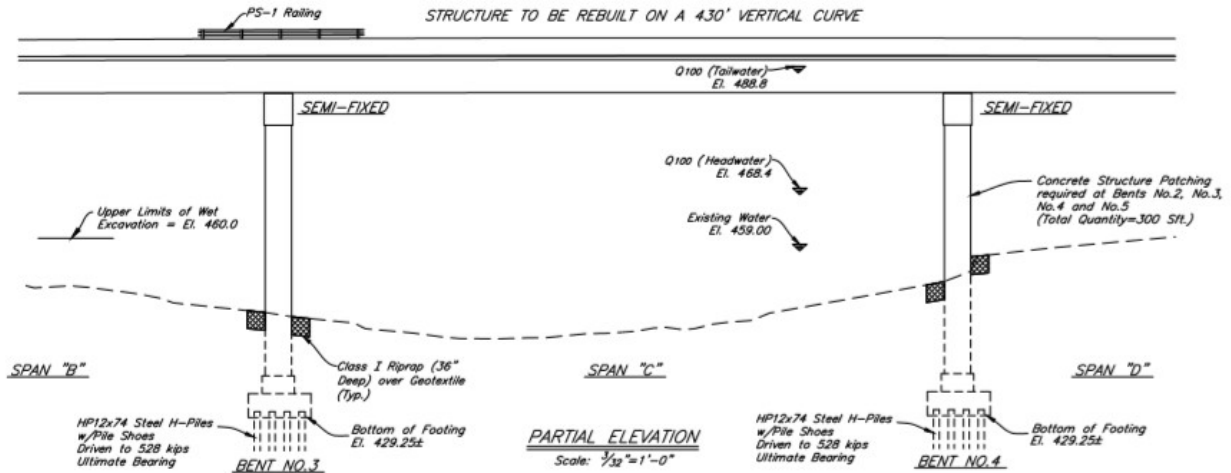
Figure 3-10. Elevation View of the Bridge - Span 2, 3 and 4 (NBI 18790) (2014)
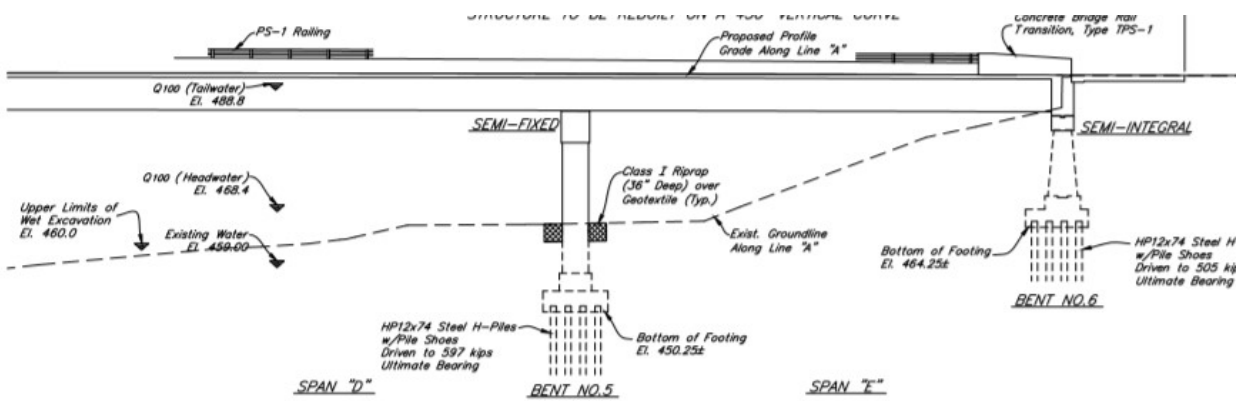
Figure 3-11. Elevation View of the Bridge - Span 4 and 5 (NBI 18790) (2014)
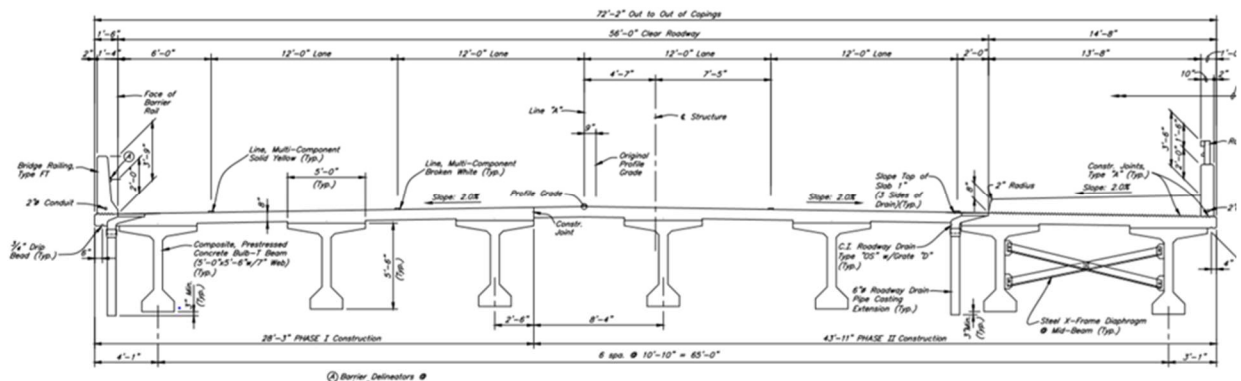
Figure 3-12. Typical Section of the Bridge (NBI 18790) (2014)

The bridge is supported by two integral-type abutments and four interior rectangular column frame-bent piers, as shown in Figure 3-13 through Figure 3-14. From left to right, the piers are classified as one-story, two-story, two-story, and one-story frame bents. Due to the presence of semi-integral abutments, the bridge will not be vulnerable to seismic hazards in the longitudinal direction of motion as the inertial effects of the mass are negligible (Frosch et al., 2009).

Piers 2 and 5 are composed of four, 48"x48" rectangular-type reinforced-concrete (RC) columns and a 54"x54" RC bent cap. The columns have a clear height of 21'-0" and a clear span of 21'-0", except for the outermost column, which has a clear span of 7'-1/2". Piers 3 and 4 is a two-story frame bent. The bottom story is composed of four, 54"x54" rectangular-type RC columns whereas the top story is composed of four, 48"x48" rectangular-type RC columns and a 54"x54" bent cap. The bottom-story columns have a conservative modeling height of 23'-6" and a clear span of 20'-6", except for the outermost column, which has a clear span of 7'. Naturally, the spacing of the top columns remains the same as the bottom. The modeling height of the top columns is taken as 18'-3". The modeling height is defined by the change in cross-sectional area of the column.
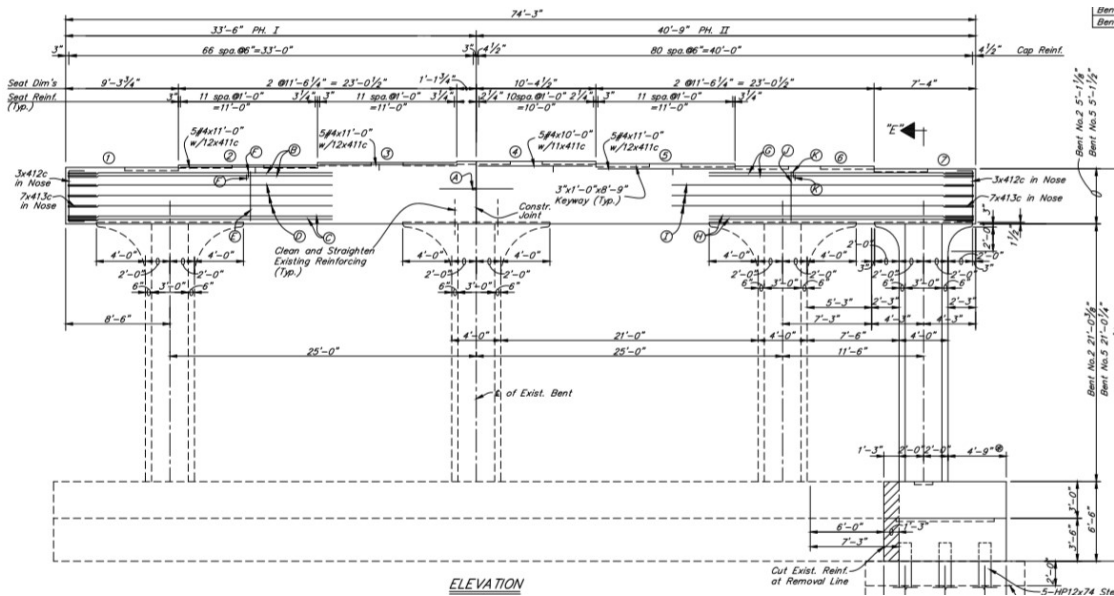
Figure 3-13. Transverse Elevation of Interior Pier 2 (NBI 18790) (2014)
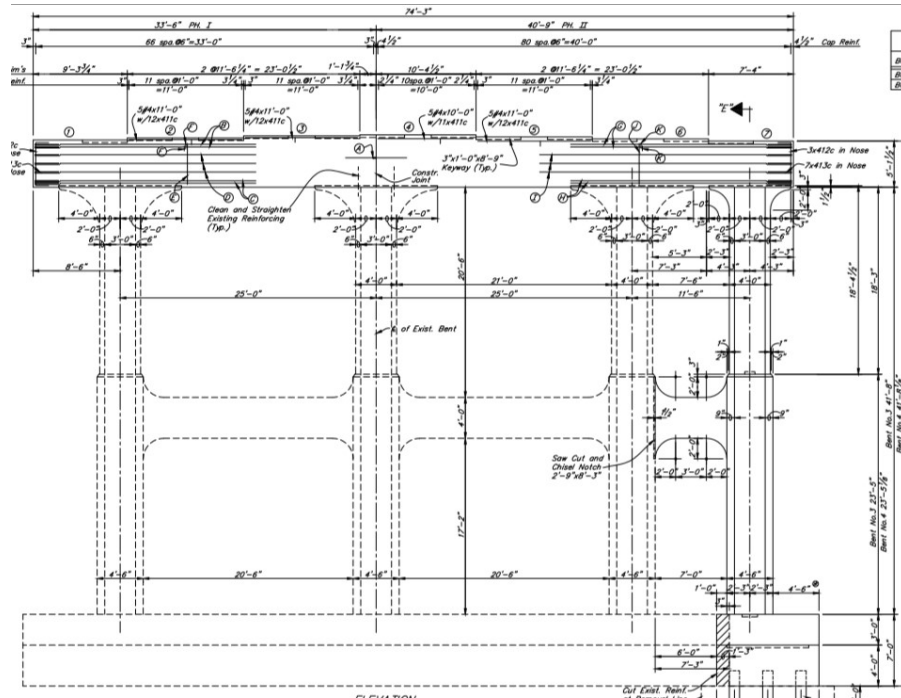
Figure 3-14. Transverse Elevation of Interior Pier 3 (NBI 18790) (2014)

3.4.2 Identify Mechanism of Hinge Formation (NBI 18790)

A limit analysis is used to identify the controlling mechanism of hinge formation of the frame bents. For Piers 2 and 5, the conventional collapse mechanisms (weak column – strong beam and strong column – weak beam) are considered. For Piers 3 and 4, three different collapse mechanisms are considered: formation of two plastic hinges in the first-story columns (mechanism of hinge formation no. 1), formation of a plastic hinge in the column at the base and bent cap and two hinges in each intermediate beam (mechanism of hinge formation no. 2), and the formation of a plastic hinge in the column at the base and two plastic hinges in each intermediate beam and bent cap (mechanism of hinge formation no. 3). The mechanism of hinge formation for Piers 3 and 4 are shown in Figure 3-15, Figure 3-16, and Figure 3-17 respectively.

50
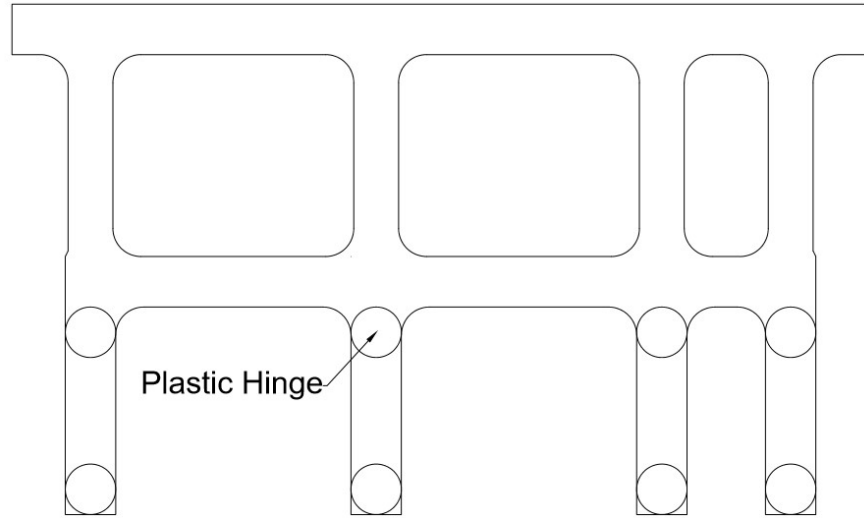
Figure 3-15. Mechanism of Hinge Formation No. 1
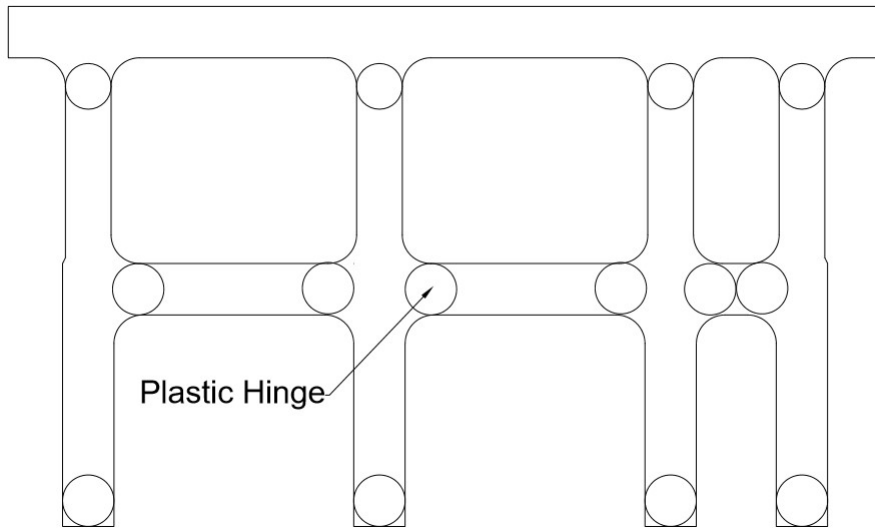
Figure 3-16. Mechanism of Hinge Formation No. 2
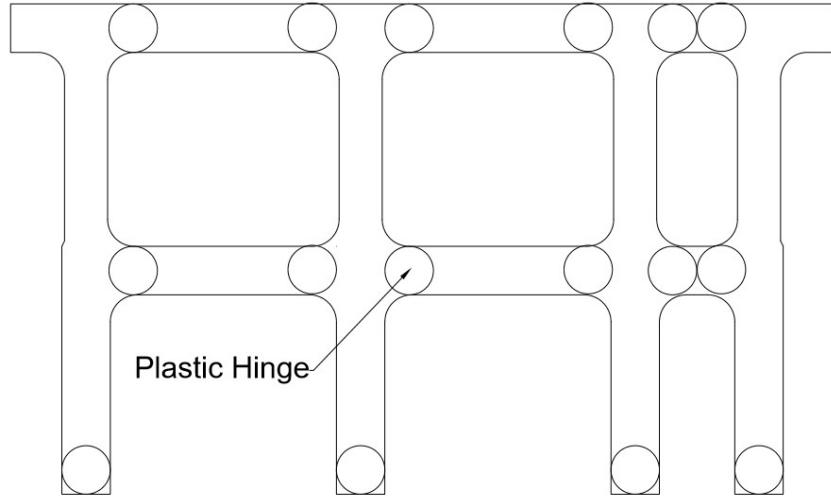
Figure 3-17. Mechanism of Hinge Formation No. 3

The reinforcement layouts are grouped based on design similarities and are defined as: the columns in Pier 2, Pier 5, and the top story of Piers 3 and 4 (column type 1), the columns in the bottom story of Piers 3 and 4 (column type 2), the bent caps of all piers (beam type 1), and the intermediate beams for Piers 3 and 4. All details are shown in Figure 3-18 and Figure 3-19. Detailed calculations are provided for Beam Type 2 to show the validity of the moment-curvature methodology.
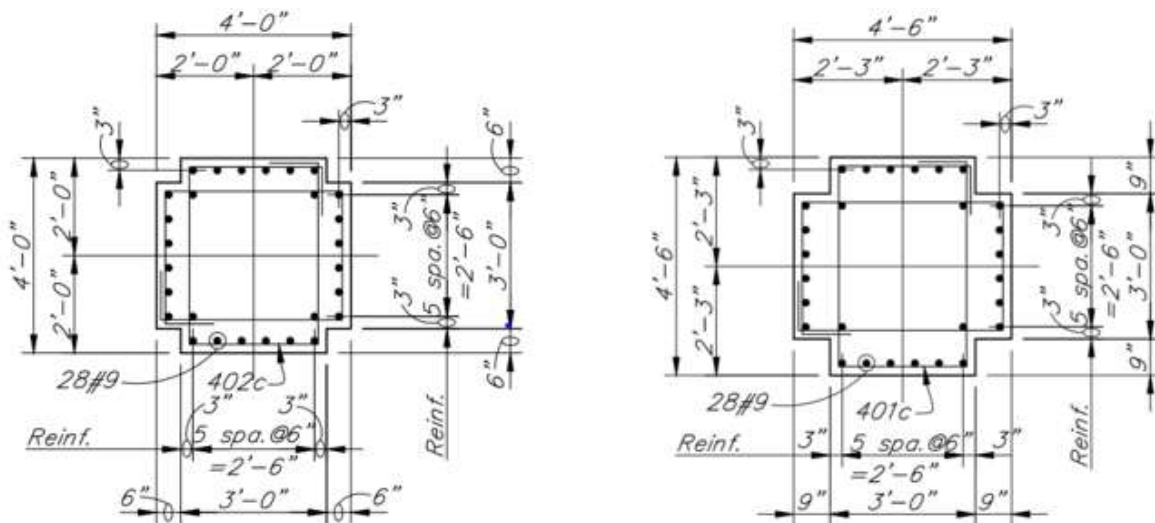
Figure 3-18. Cross-Section Column Type 1 (Left) and Column Type 2 (Right) (NBI 18790) (2014)

52
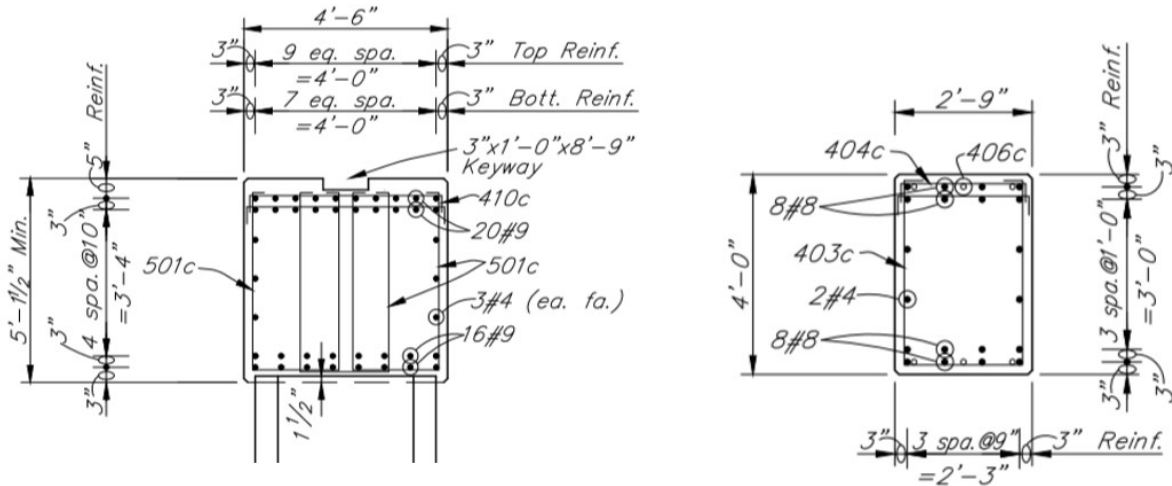
Figure 3-19. Cross-Section Beam Type 1 (Left) and Beam Type 2 (Right) (NBI 18790) (2014)

The moment associated with cracking is calculated using the gross moment of inertia and a centroidal axis of half the cross-section depth. The gross moment of inertia is

$$I_g = \frac{bh^3}{12} = \frac{33\ in * (48\ in)^3}{12} = 304128\ in^4. \tag{3-18}$$

Using Equation 3-1 the cracking moment is computed as

$$M_{cr} = 7.5\sqrt{3500\ psi} * \frac{2 * 304128\ in^4}{48\ in} = 468.5\ kip * ft. \tag{3-19}$$

Assuming plane sections remain plane and the strain varies linearly along the cross-section depth, the curvature associated with the cracking moment is calculated using Equation 3-2 as

$$\varphi_{cr} = \frac{468.5\ kip * ft}{304128\ in^4 * 3410\ ksi} = 5.42 * 10^{-6} \frac{rad}{in}. \tag{3-20}$$

The yielding moment is calculated assuming the outermost layer of longitudinal steel has just yielded. For a neutral axis value (c_{NA}) of 11.75 inch, force equilibrium is achieved.

Taking the maximum nominal concrete strain as

$$\varepsilon_o = \frac{2f_c'}{E_c}, \tag{3-21}$$

the assumed stress profile, using a Hognestad confined concrete model, is

$$f_c = \begin{pmatrix} f_c * (2\frac{\varepsilon_c}{\varepsilon_o} - \left(\frac{\varepsilon_c}{\varepsilon_o}\right)^2 & \varepsilon_c \leq \varepsilon_o \\ f_c\left(1 - \frac{0.15(\varepsilon_c - \varepsilon_o)}{.003 - \varepsilon_o}\right) & \varepsilon_c > \varepsilon_o \end{pmatrix}. \tag{3-22}$$

Using numerical integration (e.g. Simpson's rule), the compressive concrete force is

$$F_{conc} = \int_0^{\varepsilon_{NA} = .00049} b * f(x)dx = 217.8 \; kips. \tag{3-23}$$

Using the yield strain of steel ($\varepsilon_y = \frac{f_y}{E_s} = \frac{40 \; ksi}{29000 \; ksi}$) and a linear-varying strain profile along the cross-section, the stress for each layer of steel is calculated as

$$f_s = \begin{pmatrix} f_y * \left(\frac{\varepsilon_s}{\varepsilon_y}\right) & \varepsilon_s \leq \varepsilon_y \\ f_y & \varepsilon_s > \varepsilon_y \end{pmatrix}. \tag{3-24}$$

The total compressive and tensile force of the steel is calculated by summing the force in each layer of steel. The strain in each layer is calculated based off the distance from the neutral axis and the force is calculated for compressive and tension, respectively, as

$$F_{s_c} = \sum_{i=1}^{N_{bars_c}} f_{s_i}(x) * A_{s_i} = 36.3 \; kips, \tag{3-25}$$

$$F_{s_t} = \sum_{i=1}^{N_{bars_t}} f_{s_i}(x) * A_{s_i} = 253.2 \; kips. \tag{3-26}$$

Summing all the forces, the equilibrium of the section is confirmed to a reasonable threshold of 5 kips. The total force-equilibrium is taken as

$$F_{conc} + F_{s_c} + F_{s_t} = 217.8 \; kips + 36.3 \; kips - 253.2 \; kips = 0.9 \; kips. \tag{3-27}$$

The yield moment is calculated about the neutral axis as

$$M_y = 769.7 \; kip * ft \tag{3-28}$$

and the resulting curvature is

$$\varphi_y = 4.1 * 10^{-5} \frac{rad}{in}. \tag{3-29}$$

The same approach for calculating the moment-curvature at yield is applied to the beam section to determine the ultimate moment. The solution occurs when either strain hardening occurs in the outermost layer of longitudinal steel, or the strain of the extreme compressive fiber of the concrete reaches 0.003. For this cross-section, as is typical for most substructures in the sample set, the strain hardening of the outermost layer of longitudinal steel controls. The resulting ultimate moment for a neutral axis depth of 6.1 inch and a concrete strain of 0.0016 is

$$M_u = 903.8 \; kip * ft. \tag{3-30}$$

The corresponding curvature is

$$\varphi_u = 2.6 * 10^{-4} \frac{rad}{in}. \tag{3-31}$$

Figure 3-20 shows the resulting moment-curvature plot for beam element type 2.
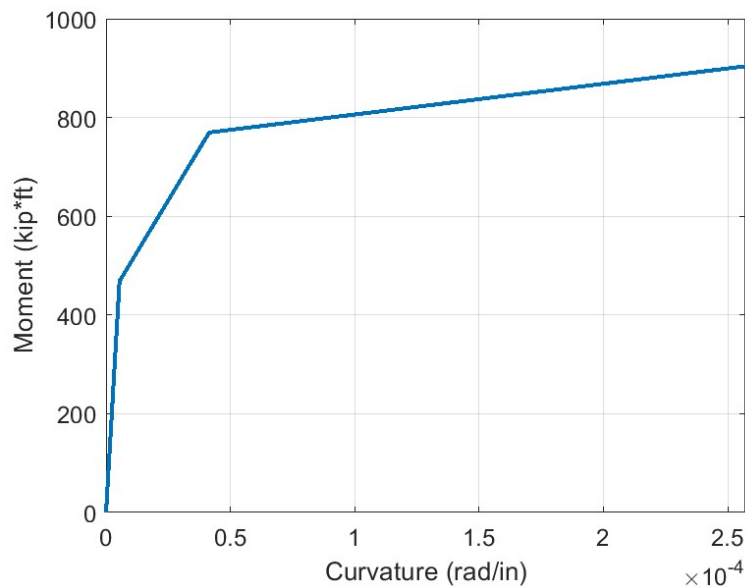
Figure 3-20. Moment-Curvature Diagram for Beam Element Type 2 (NBI 18790)

Table 3-1 shows the moment-curvature results for all column and beam elements.

Table 3-1. Column and Beam Moment-Curvature Results

	Column Type 1		Column Type 2		Beam Type 1		Beam Type 2	
	Moment $(kips \cdot ft)$	φ (rad/in)	Moment $(kips \cdot ft)$	φ (rad/in)	Moment $(kips \cdot ft)$	φ (rad/in)	Moment $(kips \cdot ft)$	φ (rad/in)
Cracking	401.5	5.4E-06	571.6	4.8E-06	1198	4.3E-06	468.6	5.4E-06
Yield	1429.3	4.6E-05	1584.1	3.9E-05	2735.4	4.1E-05	769.7	4.2E-05
Ultimate	2063.9	2.8E-04	2365.4	2.4E-04	3398.2	2.4E-04	903.8	2.5E-04

Using the ultimate moment capacity and the number of hinges based on each mechanism of hinge formation, the base shear is calculated. The base shear is the lateral force required to be transferred from the superstructure to the substructure to cause the development of the identified mechanism of hinge formation. The mechanism of hinge formation corresponding to the minimum base shear value is considered the controlling mechanism as this mechanism requires the minimum amount of energy to form the collapse mechanism. The base shear capacity for mechanism of hinge formation no. 1, shown in Figure 3-15, is

$$V_{bs,1} = \frac{2\frac{hinge}{col} * 2361.8\ kip * ft}{23.5\ ft} * 4\frac{col}{pier} = 805\ kips. \quad (3\text{-}32)$$

The base shear capacity for mechanism of hinge formation no. 2, shown in Figure 3-16, is

$$V_{bs,2} = \frac{(2361.8 + 2061.6)\frac{kip * ft}{col} * 4\frac{col}{pier}}{0.5 * (23.5 + 18.5)ft} + \frac{2\frac{hinge}{beam} * 902\ kip * ft * 3\frac{beams}{pier}}{\left(\frac{1}{3}\right) * (2 * 20.5\ ft + 7\ ft)}$$
$$= 1180\ kips. \quad (3\text{-}33)$$

The base shear capacity for mechanism of hinge formation no. 3, shown in Figure 3-17, is

$$V_{bs,3} = \frac{2361.8\frac{kip * ft}{col} * 4\frac{col}{pier}}{23.5ft} + \frac{2\frac{hinge}{beam} * (902 + 3394.9)\frac{kip * ft}{col} * 3\frac{beams}{pier}}{\left(\frac{1}{3}\right) * (2 * 20.5\ ft + 7\ ft)}$$
$$= 2013\ kips. \quad (3\text{-}34)$$

Mechanism of hinge formation no. 1 is identified as the controlling mechanism as it requires the least amount of energy to form. This mechanism, identified as weak column – strong beam, corresponds to a base shear capacity of 805 kips. The controlling mechanism of hinge

56

formation for Piers 2 and Pier 5 is also identified as weak column – strong beam and have a corresponding base shear capacity of 784 kips and 1362 kips, respectively. The difference in capacity is attributed to the difference in each pier's height.

3.4.3 Shear Capacity of the Pier (NBI 18790)

The shear capacity at the identified critical section(s) is calculated in accordance with AASHTO (2017) Section 5.8.3.3. The shear capacity is taken as

$$V_n = V_c + V_s \tag{3-35}$$

where V_c and V_s are calculated as

$$V_c = 0.0316 * 2\sqrt{f_c'} b d_v \tag{3-36}$$

$$V_s = \frac{A_v f_y d_v}{s}. \tag{3-37}$$

The shear capacity is bounded by a maximum value taken as

$$V_{n_{max}} = 0.25 f_c' b d_v. \tag{3-38}$$

With an identified collapse mechanism of weak column – strong beam, the critical section of the pier is the base and top of the first-story column. With a uniform shear spacing, the capacity of both sections is the same as shown in Figure 3-21.
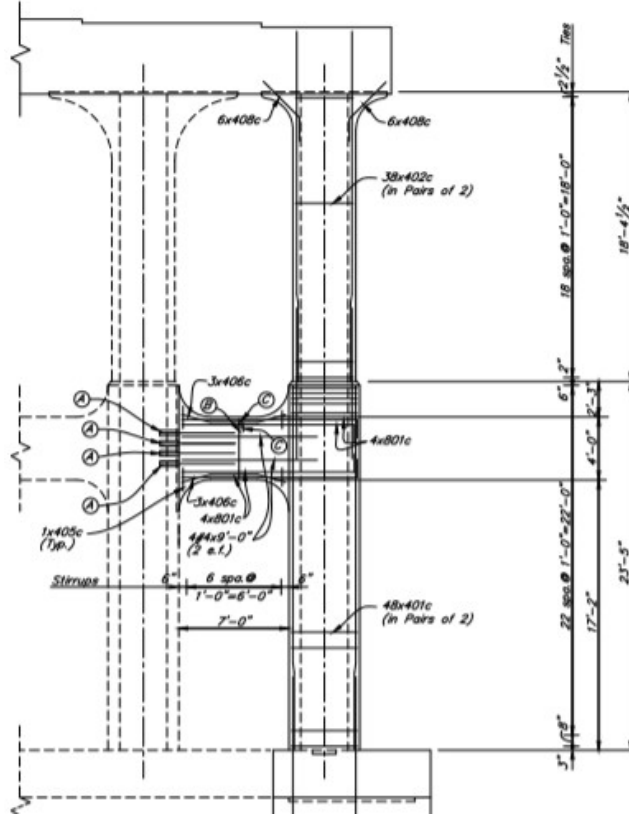
Figure 3-21. Shear Detailing of Column for Pier 3 (NBI 18790) (2014)

The shear strength of the concrete in one column is

$$V_c = 0.0316 * 2\sqrt{f_c'}bd_v = 0.0316 * 2\sqrt{3.5\ ksi} * 54\ in * 36\ in = 230\ kips. \qquad (3\text{-}39)$$

The shear strength of the steel in one column is

$$V_s = \frac{A_v f_y d_v}{s} = \frac{0.8\ in^2 * 40\ ksi * 36\ in}{12\ in} = 96\ kips. \qquad (3\text{-}40)$$

The maximum value for the shear strength of a single column is

$$V_{n_{max}} = 0.25 f_c'bd_v = 0.25 * 3.5ksi * 54\ in * 36\ in = 1705\ kips. \qquad (3\text{-}41)$$

With the shear strength of each column component well below the upper bound, the shear strength of a single column is

$$V_n = V_c + V_s = 230\ kips + 96\ kips = 326\ kips. \qquad (3\text{-}42)$$

The shear strength of the pier is

$$V_n = N_c * V_n = 4\frac{cols}{pier} * 326\frac{kips}{col} = 1304\ kips. \tag{3-43}$$

3.4.4 Shear Capacity of the Connection (NBI 18790)

The validity of the modeling approach relies on the transfer of force from the superstructure to substructure. For prestressed concrete bridges, this transfer is precipitated by the lateral diaphragms placed over each interior pier. With this detail, the piers can restore the bridge mass to its original position, when the structure is excited. Using the detail shown in Figure 3-24 the shear capacity of the connection is taken as the direct shear capacity of the concrete key. This section is modeled like corbels using equations from AASHTO 5.13.2.4.2. The shear capacity of the connection is taken as

$$V_{conn} = 0.2f_c'A_{cv}(N_b - 1) = 0.4 * 3.5ksi * (130\ in - 60\ in) * 12\ in * 6 = 4032\ kips. \tag{3-44}$$

3.4.5 Identify Limiting Capacity (NBI 18790)

The limiting capacity is identified as the minimum of the capacity associated with the controlling mechanism of hinge formation, shear capacity of the pier, and shear capacity of the connection. The limiting capacity is the same for all four piers – the formation of a weak column – strong beam collapse mechanism in the first-story columns. The controlling capacity for Piers 2, 3, 4, and 5, respectively, is

$$C_{limit} = [784 \quad 805 \quad 805 \quad 1132]\ kips. \tag{3-45}$$

3.4.6 2-D Bridge Model (NBI 18790)

The stiffness is derived solely from the substructure stiffness. As mentioned in Section 3.3.5, the deck is assumed to be sufficiently rigid to allow the intermediate piers to act as springs in parallel. All four piers are modeled using the stiffness method. Each pier is modeled as a planar moment resisting frame with rotational degree of freedoms (DOF) allowed at the connection of every column and beam element and a singular translation DOF allowed at every beam tier. A diagram of the degrees of freedom for Piers 3 and 4 is shown in Figure 3-22.
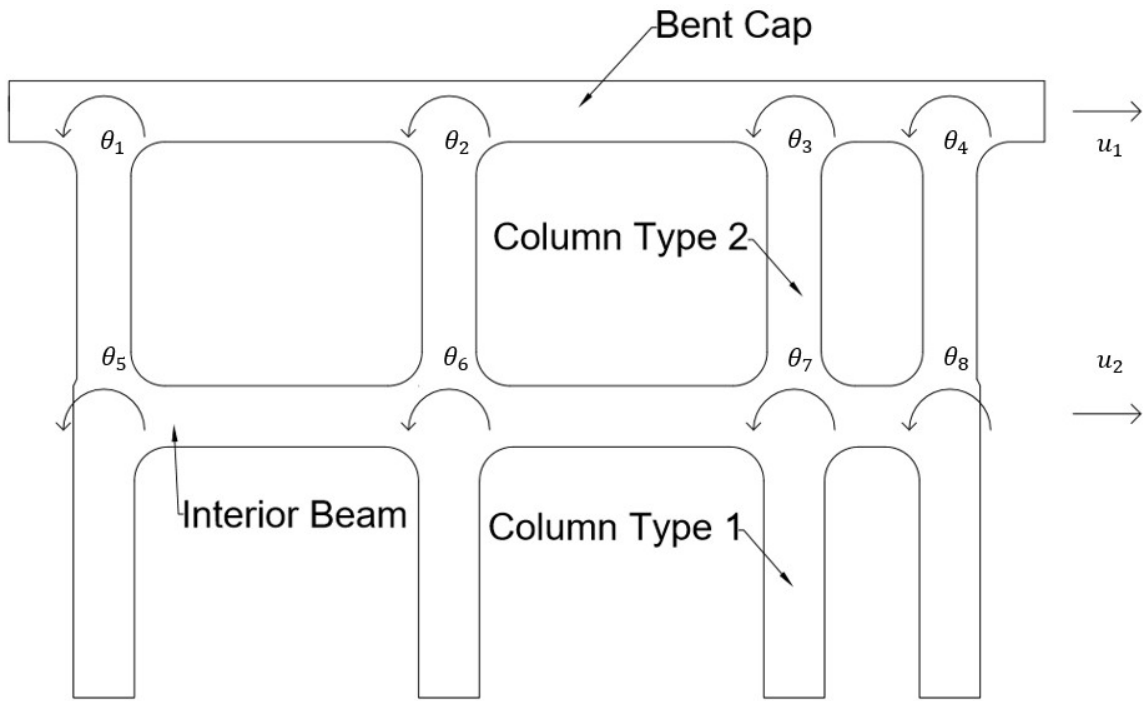
Figure 3-22. Transverse Elevation of Interior Pier with Degrees of Freedom Shown

The stiffness matrix for each bent is assembled using the stiffness method where Equation (3-46) shows the originating matrix.

$$k = \frac{EI}{L^3} \begin{bmatrix} u_i & \theta_i & u_j & \theta_j & \cdot \\ 12 & 6L & -12 & 6L & u_i \\ 6L & 4L^2 & -6L & 2L^2 & \theta_i \\ -12 & -6L & 12 & -6L & u_j \\ 6L & 2L^2 & -6L & 4L^2 & \theta_j \end{bmatrix} \tag{3-46}$$

The global stiffness matrix for the pier shown in Figure 3-22 is shown in Table 3-3. The following subscript notation, summarized below, are added to the typical notation for representing the height (H) of column elements and clear spacing (L) of beam elements in

Table 3-2. Subscripts for Table 3-3

Column Subscript	Representation	Beam subscript	Representation
1	Top Story Columns	r	Added beams from Rehabilitation
2	Bottom Story Columns	e	Existing Beam

Table 3-3. Transverse Stiffness Matrix Corresponding to the Pier in Figure 3-22

	u_1	u_2	θ_1	θ_2	θ_3	θ_4	θ_5	θ_6	θ_7	θ_8
u_1	$4\left(\frac{12EI}{H_1^3}\right)$	$-4\left(\frac{12EI}{H_1^3}\right)$	$-\frac{6EI}{H_1^3}$	$-\frac{6EI}{H_1^3}$	$-\frac{6EI}{H_1^3}$	$-\frac{6EI}{H_1^3}$	$-\frac{6EI}{H_1^3}$	$-\frac{6EI}{H_1^3}$	$-\frac{6EI}{H_1^3}$	$-\frac{6EI}{H_1^3}$
u_2	$-4\left(\frac{12EI}{H_1^3}\right)$	$4[\left(\frac{12EI}{H_1^3}\right)+\left(\frac{12EI}{H_2^3}\right)]$	$\frac{6EI}{H_1^3}$	$\frac{6EI}{H_1^3}$	$\frac{6EI}{H_1^3}$	$\frac{6EI}{H_1^3}$	$\frac{6EI}{H_1^3}+\frac{6EI}{H_2^3}$	$\frac{6EI}{H_1^3}+\frac{6EI}{H_2^3}$	$\frac{6EI}{H_1^3}+\frac{6EI}{H_2^3}$	$\frac{6EI}{H_1^3}+\frac{6EI}{H_2^3}$
θ_1	$-\frac{6EI}{H_1^3}$	$\frac{6EI}{H_1^3}$	$4(\frac{EI}{H_1}+\frac{EI}{L_e})$	$\frac{2EI}{L_e}$			$\frac{2EI}{H_1}$			
θ_2	$-\frac{6EI}{H_1^3}$	$\frac{6EI}{H_1^3}$	$\frac{2EI}{L_e}$	$4(\frac{EI}{H_1}+2\frac{EI}{L_e})$	$\frac{2EI}{L_e}$			$\frac{2EI}{H_1}$		
θ_3	$-\frac{6EI}{H_1^3}$	$\frac{6EI}{H_1^3}$		$\frac{2EI}{L_e}$	$4(\frac{EI}{H_1}+\frac{EI}{L_e}+\frac{EI}{L_r})$	$\frac{2EI}{L_r}$			$\frac{2EI}{H_1}$	
θ_4	$-\frac{6EI}{H_1^3}$	$\frac{6EI}{H_1^3}$			$\frac{2EI}{L_r}$	$4(\frac{EI}{H_1}+\frac{EI}{L_r})$				$\frac{2EI}{H_1}$
θ_5	$-\frac{6EI}{H_1^3}$	$\frac{6EI}{H_1^3}+\frac{6EI}{H_2^3}$	$\frac{2EI}{H_1}$				$4(\frac{EI}{H_1}+\frac{EI}{H_2}+\frac{EI}{L_e})$	$\frac{2EI}{L_e}$		
θ_6	$-\frac{6EI}{H_1^3}$	$\frac{6EI}{H_1^3}+\frac{6EI}{H_2^3}$		$\frac{2EI}{H_1}$			$\frac{2EI}{L_e}$	$4(\frac{EI}{H_1}+\frac{EI}{H_2}+2\frac{EI}{L_e})$	$\frac{2EI}{L_e}$	
θ_7	$-\frac{6EI}{H_1^3}$	$\frac{6EI}{H_1^3}+\frac{6EI}{H_2^3}$			$\frac{2EI}{H_1}$			$\frac{2EI}{L_e}$	$4(\frac{EI}{H_1}+\frac{EI}{H_2}+\frac{EI}{L_e}+\frac{EI}{L_r})$	$\frac{2EI}{L_r}$

Table 3-3 continued

θ_8	$-\dfrac{6EI}{H_1^3}$	$\dfrac{6EI}{H_1^3}+\dfrac{6EI}{H_2^3}$				$\dfrac{2EI}{H_1}$			$\dfrac{2EI}{L_r}$	$4(\dfrac{EI}{H_1}+\dfrac{EI}{H_2}+\dfrac{EI}{L_r})$

For all piers, the translational degree of freedom associated with the bent cap is the only degree of freedom associated with the superstructure mass. For this seismic assessment, the mass of the pier is neglected as it is considered insignificant in comparison to the overall mass of the superstructure. Using static condensation, the pier stiffness matrix is condensed to obtain the stiffness associated with u_1. The stiffness of all four piers is

$$K_{pier} = [3830 \quad 2259 \quad 2520 \quad 3661] \frac{kips}{in}. \tag{3-47}$$

The activated mass of the bridge in the transverse direction is calculated using superstructure geometry, barrier dimensions, and concrete stiffeners using the typical section of the bridge shown in Figure 3-23. The weight of the Bulb Tee (BT) 66 X 60 prestressed concrete beam is taken as $1028 \frac{lb}{lft}$ from INDOT's Design Manual Figure 406-14O (2013a). The mass attributed to each pier is calculated using the tributary length, or half of each span, adjacent to the pier. Using $150 \, pcf$ as the density of concrete, the mass of the primary structure system (SS), or the beams and deck, over each pier is

$$m_{SS} = \frac{l_{pier} * (w_{oto} * t_{deck} * \gamma_c + W_b * N_b)}{g}, \tag{3-48}$$

$$m_{SS} = \frac{93.9 \, ft * \left(72.1 \, ft * 9 \, in * 150 \, pcf + 1028 \frac{lb}{lft} * 7\right)}{386.4 \frac{in}{s^2}} = 3.78 \frac{kips}{g}.$$

The mass of the concrete bridge railing Type FT, calculated using INDOT standard drawing E 706-BRSF-02 (2012b), is

$$m_R = 2 * \frac{l_{pier} * (\gamma_c A_R + W_s)}{g}, \tag{3-49}$$

$$m_R = 2 * \frac{93.9 \, ft * \left(150 \, pcf * 2.58 \, ft^2 + 26.3 \frac{lb}{lft}\right)}{386.4 \frac{in}{s^2}} = 0.2 \frac{kips}{g}.$$

The presence of concrete diaphragms, shown in Figure 3-24, between the beams over each pier allows for the transfer of forces from the substructure to superstructures, but also contribute to the mass of the system. The total mass of the stiffener is a function of the beam spacing, beam height, and width of bent cap.
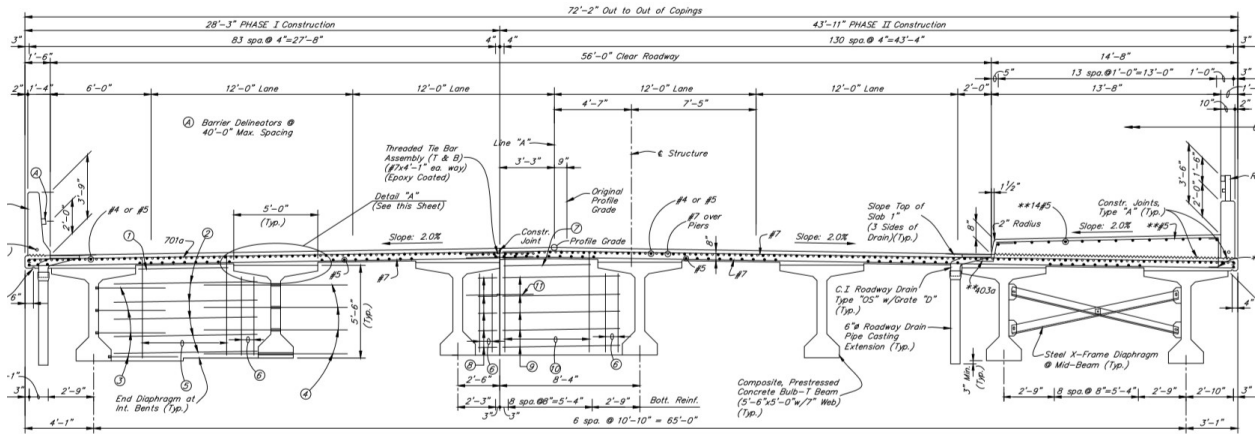
Figure 3-23. Transverse Elevation of Typical Diaphragms over Pier (NBI 18790) (2014)
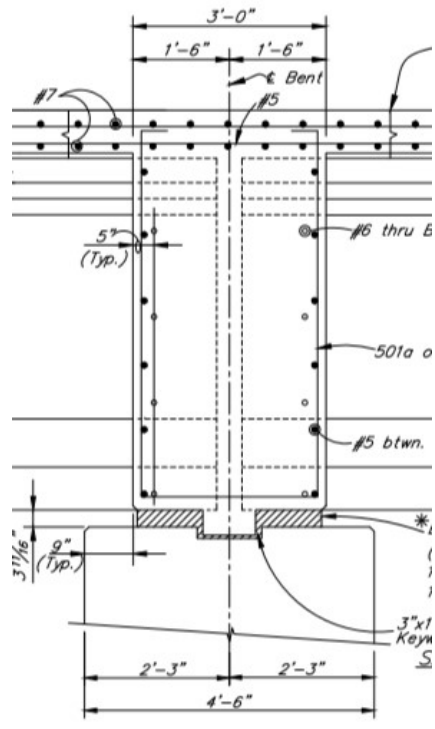
Figure 3-24. Elevation Detail of Typical Interior Diaphragm of Bridge (NBI 18790) (2014)

The mass of the diaphragm over each pier is

$$m_D = \gamma_c l_D (N_b - 1) \frac{(S_b - w_b)h_b + h_b w_b - A_b}{386.4}, \tag{3-50}$$

$$m_D = 6 * 150 \, pcf \, \frac{3 \, ft * 66 \, in((130 \, in - 60 \, in) - (60 \, in - \frac{1025}{60} \, in)}{386.4 \frac{in}{s^2}} = 0.37 \frac{kips}{g}.$$

Summing these components, the total mass of the superstructure over Pier 2 is

$$m_{pier} = m_{ss} + m_R + m_D = (3.78 + 0.2 + 0.37) \frac{kips}{g} = 4.36 \frac{kips}{g}. \tag{3-51}$$

Thus, the mass of the superstructure over each pier is computed as

$$m_{pier} = [4.36 \quad 5.03 \quad 5.03 \quad 4.35] \frac{kip}{g}. \tag{3-52}$$

Because the rigidity of the deck assumes a uniform displacement for all piers, the total stiffness and mass are calculated as the summation of all individual pier elements. The total stiffness in the transverse direction is

$$K_{sub} = \sum_{i=1}^{N_{piers}} K_{pier_i} = 12{,}270 \frac{kip}{in}. \tag{3-53}$$

The total activated mass in the transverse direction is

$$m_{sup} = \sum_{i=1}^{N_{piers}} m_{pier_i} = 18.8 \frac{kips}{g}. \tag{3-54}$$

Using an assumed damping ratio of 5% and Equation 3-5, the coefficient of damping is calculated as

$$c_{sub} = 0.1 \sqrt{12270 \frac{kip}{in} * 18.8 \frac{kips}{g}} = 48 \frac{kip * s}{in}. \tag{3-55}$$

Using Equation 3-8 and Equation 3-9, respectively, the circular natural frequency and period of the structure are calculated as

$$\omega_n = \sqrt{\frac{12270}{18.8} \frac{rads}{s}} = 25.5 \frac{rad}{s},$$ (3-56)

$$T = 0.25 \ s.$$ (3-57)

With the dynamic components of the structure well-defined the equation of motion is written as

$$\ddot{x}_s + 2.55\dot{x}_s + 652.7x_s = -\ddot{x}_g.$$ (3-58)

3.4.7 Non-Linear Pushover Analysis (NBI 18790)

An NLPA is required to better understand the redistribution of forces as the four piers progressively exhibit non-linear behavior and begin to soften. Piers 2 and 5 are nearly-identical piers, so their flexural response is very similar. While Piers 3 and 4 have the same collapse mechanism and moment capacity, the height varies slightly thus the response is slightly different, especially in the linear range, as Figure 3-25 shows below.
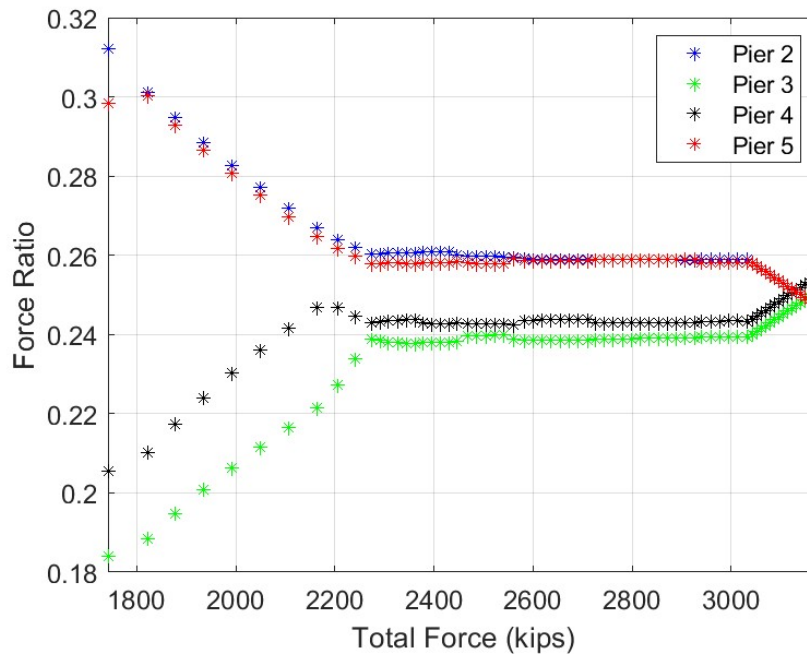
Figure 3-25. Non-Linear Pushover Analysis in Transverse Direction for Bridge (NBI 18790)

3.4.8 Apply Ground Motion (NBI 18790)

A sample analysis for one of the stochastically simulated earthquakes is shown. The earthquake, given in terms of ground acceleration versus time, is shown in Figure 3-26.
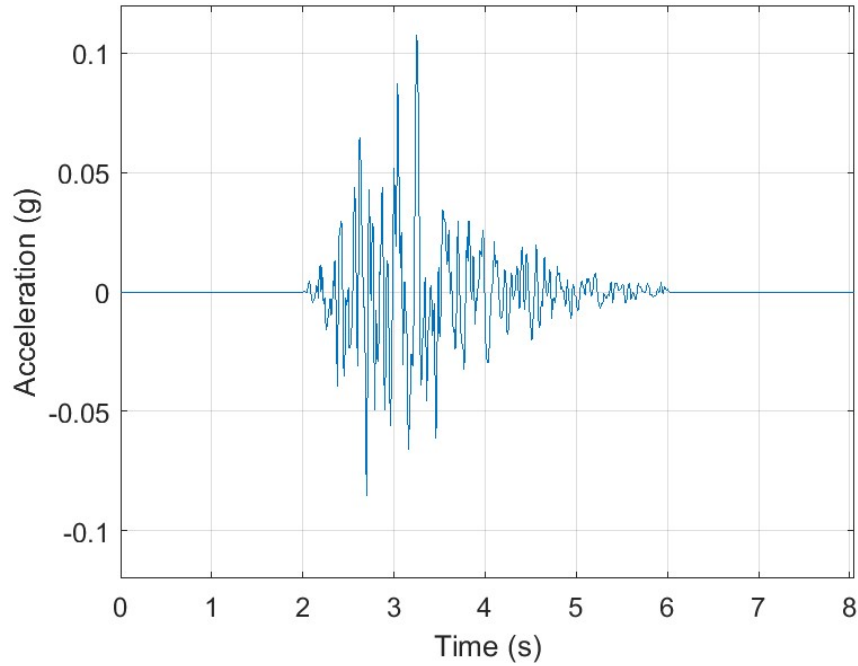
Figure 3-26. Stochastically Simulated Earthquake Specific to Bridge Site (NBI 18790)

By linearizing the equation of motion, the state space model is developed and solved using a 4th order Runge-Kutta solver. The state transition model is taken as

$$\begin{bmatrix} \dot{x}_s \\ \ddot{x}_s \end{bmatrix} = \begin{bmatrix} 0 & 1 \\ -\omega_n & -2\zeta_{sub}\omega_n \end{bmatrix} \begin{bmatrix} x_s \\ \dot{x}_s \end{bmatrix} + \begin{bmatrix} 0 \\ 1 \end{bmatrix}, \tag{3-59}$$

where the observation model, specifically for displacement and acceleration, is

$$\begin{bmatrix} x_s \\ \ddot{x}_s \end{bmatrix} = \begin{bmatrix} 1 & 0 \\ -\omega_n & -2\zeta_{sub}\omega_n \end{bmatrix} \begin{bmatrix} x_s \\ \dot{x}_s \end{bmatrix} + \begin{bmatrix} 0 \\ 1 \end{bmatrix}. \tag{3-60}$$

With the observation model defined, the displacement-response of the structure is directly recorded. The linear, time-dependent displacement response, before accounting for redistribution or non-linear response, is shown in Figure 3-27.
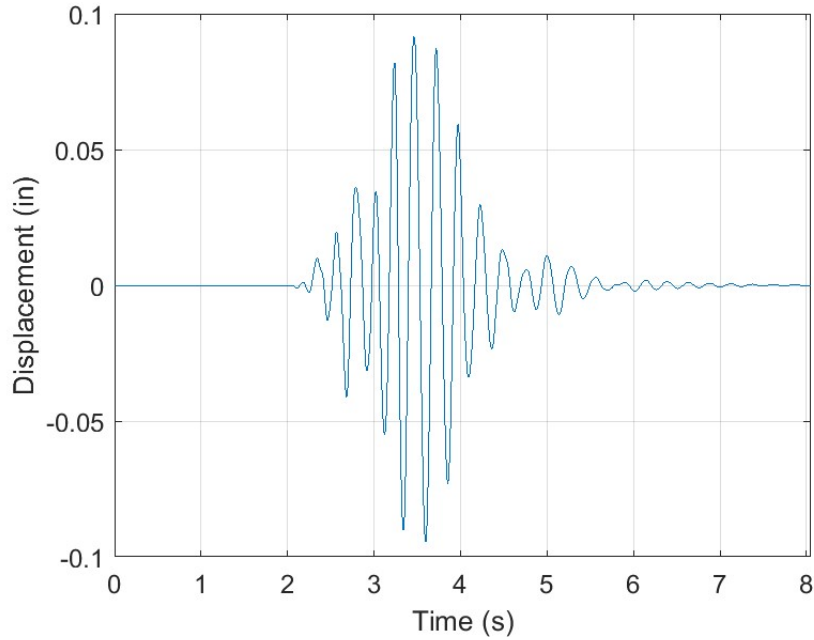
Figure 3-27. Displacement Response of Structure to Earthquake Excitation shown in Figure 3-26 (NBI 18790)

3.4.9 Maximum Force and Displacement (NBI 18790)

For the given earthquake, a maximum displacement of 0.108 inch is recorded. Using the linear spring relationship, the total force drawn to the structure is calculated as

$$F_{pier} = K_{pier}\Delta_1 = 12{,}270\frac{kip}{in} * 0.108\ in = 1{,}163.9\ kips. \tag{3-61}$$

The total load in the transverse direction is less than the force required to precipitate yielding of the longitudinal steel therefore no force redistribution is required. Additionally, no non-linear displacement occurs so leveraging the moment-area theorem presented in Section 3.3.8 is not required. Using the relative linear stiffness of each pier, the total force drawn to each pier is

$$F_{pier} = [363.3 \quad 214.2 \quad 239.0 \quad 347.3]\ kips. \tag{3-62}$$

3.4.10 Vulnerability Assessment of Detail (NBI 18790)

In the transverse direction, two-story frame bents are found to have the potential for low vulnerability since none of the 100 stochastically simulated earthquakes produced motions strong enough to develop the identified mechanism of hinge formation in the substructure. However,

68

given the uniqueness of the substructure, the vulnerability of every substructure labeled *other* must be evaluated on a case-by-case basis.

3.5   Summary of Seismic Assessment

3.5.1   Vulnerable Details

A seismic assessment of all 100 bridges reveals a variety of seismic vulnerabilities present in the bridge network throughout the entire state of Indiana. These vulnerabilities, classified as highly vulnerable if resulting in a brittle failure, and moderately vulnerable if resulting in a ductile failure, are summarized in Table 3-4 and can apply to all three superstructure types. As expected, the most critical vulnerabilities can be found in existing bridges designed prior to the implementation of seismic codes, where the primary design consideration was instability and resulting gravity load due to traffic loads and self-weight. Due to a lack of seismic detailing, the longitudinal reinforcement that is designed to support the axial demand in the columns and piers is often insufficient to resist the lateral demand associated with seismic excitation. The bridges considered in the sample, in particular the bridges supported by wall-type substructures built before the 1990's, were found to exhibit a moment-curvature response controlled by the cracking moment and are susceptible to experience a brittle mode of failure due to insufficient flexural reinforcement. Essentially, once the substructure has cracked due to flexure, the longitudinal steel is expected to undergo instantaneous strain hardening and possible rupture. For bridges with proper seismic detailing and adequate shear reinforcement, the expected response is more favorable. For these bridges, the ductile collapse mechanism is expected to form, and the collapse of the structure is controlled by the allowable rotation of the hinge. For the given level of seismic excitation in the state of Indiana, it is unexpected that this allowable rotation will be exceeded.

Table 3-4. Summary of Identified Vulnerabilities in INDOT's Bridge Network

Vulnerability Case	Substructure Type	Direction	Additional Comments/Criteria (When Applicable)	Level of Vulnerability	Reason for Classification
1	Walls	Longitudinal	Built Before 1990 (Grade 40 ksi steel)*	Highly Vulnerable	Low Flexural Reinforcement Ratio
2	Hammerhead Walls	Longitudinal	Built Before 1990 (Grade 40 ksi steel)*	Highly Vulnerable	Low Flexural Reinforcement Ratio
3	Hammerhead Walls	Longitudinal	Built After 1990 (Grade 60 ksi steel)	Moderately Vulnerable	Formation of Plastic Hinge
4	Hammerhead Walls	Transverse	Prestressed Concrete Superstructure Only	Moderately Vulnerable	Formation of Plastic Hinge
5	Frame Bents	Transverse	All types (H-Pile, CFT, Reinforced Concrete)	Moderately Vulnerable	Formation of Plastic Hinge
6	Frame Bents	Longitudinal	All types (H-Pile, CFT, Reinforced Concrete)	Moderately Vulnerable	Formation of Plastic Hinge
7	-	-	Rocker Bearings	Moderately Vulnerable	Unseating

*In accordance with the Manual for Bridge Evaluation (2018) Table 6A.5.2.2-1, bridges built after 1945 are assumed to have Grade 40 ksi steel. From the seismic assessment, it has been determined that bridges built after 1990 typically use Grade 60 ksi steel. Therefore, it is assumed, when structural drawings do not explicitly dictate, that bridges built between 1945 and 1990 use Grade 40 ksi steel. If a given bridge is identified as having Grade 60 ksi steel and was built before 1990, it may instead fall under vulnerability case 3.

3.5.2 Vulnerability Thresholds

The results from the seismic assessment are used to identify drift-based and displacement-based thresholds that are suitable for identifying different vulnerability levels using a more simplified modeling approach (Bonthron et al., 2020) or fragility functions (Chapter 4). These thresholds, originally taken from Ramirez et al. (2000), have been adapted to reflect the response seen in the sample set. The most applicable capacity thresholds, which apply very well to prestressed concrete and steel superstructure bridges supported by reinforced concrete substructures with adequate longitudinal reinforcement (plastic hinge) and insufficient longitudinal reinforcement (brittle failure), are shown in Table 3-5.

Table 3-5. Summary of Vulnerability Thresholds

	Drift-Based		Displacement-Based		
Level 2 Vulnerability	Formation of Plastic Hinge	Exceedance of Hinge Rotational Capacity	Formation of Plastic Hinge	Exceedance of Hinge Rotational Capacity	Brittle Failure
Level 1 Threshold	Drift > 0.5%	Drift > 1.5%	Displacement > 1 in.	Displacement > 6 in.	Displacement > 0.1 in.
Additional Identifiers	Substructure Built After 1990	Substructure Built After 1990	Substructure Built After 1990	Substructure Built After 1990	Substructure Built Before 1990*
Corresponding Vulnerability Classification	Moderate Vulnerability	High Vulnerability	Moderate Vulnerability	High Vulnerability	High Vulnerability

Note: See note for Table 3-4

4. PROBABILISTIC ASSESSMENT OF BRIDGE NETWORKS

4.1 Introduction

Networks, such as a state's bridge network, are essential for a community's prosperity. In the face of a natural disasters, like a seismic event, their disruption greatly impacts communities' safety, economic security, and social welfare. Typically, vulnerability assessments are focused on quantifying the expected damage of individual bridges in a bridge network. However, the fragility of a bridge network is far more complex, with the network's vulnerability derived as a function of multiple bridge's vulnerability rather than in isolation. This chapter focuses on developing a probabilistic methodology that has the capability to assess the joint performance of linked bridges in a bridge network. For DOTs, this methodology is powerful for the proactive designation of critical routes or prioritization of seismic retrofits. This chapter will also explore the uncertainty related to the numerical modeling technique and the method for deriving the analytical fragility function (FF). A Latin Hypercube sampling technique is leveraged to account for variations in the numerical model related to stiffness degradation, strength degradation, and the inherent uncertainty associated with viscous damping. While typical methods for generating FF assume a value for the capacity uncertainty, this methodology will utilize Bayesian inference coupled with a Monte Carlo approach to develop unique FF and corresponding credible intervals for various limit states. These FFs will be leveraged to calculate the overall probability of failure for the linked bridges. This simple yet powerful methodology for evaluating bridge networks can help DOT enhance the reliability of their bridge networks, in turn improving the safety and economic prosperity of communities.

4.2 Methodology

This methodology is designed to assist DOTs with the identification of the more vulnerable corridors within their bridge network. Proactively, the methodology can help prioritize retrofits or update critical routes. The applications of this methodology are discussed in more detail in Section 4.3. For clarity, four terms used throughout this chapter are defined here:

- Transportation system: The transportation infrastructure, both roadways and bridges, which the state DOT maintains.

- Node: An interchange between major routes in a state's transportation system.
- Link: A portion of a major route which occurs between nodes in a state's transportation system. A link may or may not contain bridges.
- Bridge network: All bridges which lie within a state's transportation system. This network is critical for the facilitation of undisturbed traffic flow.

4.2.1 Dynamic Modeling

The first step in robustly quantifying the vulnerability of a bridge network requires developing a methodology which characterizes the dynamic response of a single structure under uncertainty. This process is two-fold. First, a consistent procedure for developing each dynamic model is needed. This procedure is depicted in-detail in Section 3.3. However, to fully develop FF, the non-linearity of the structure must be calculated beyond the formation of the controlling collapse mechanism. The methodology discussed in Section 3.3.8 can calculate the displacement associated with the formation of the plastic hinge but cannot calculate the displacement after the collapse mechanism forms. For a vulnerability assessment of Indiana this is acceptable as the exceedance of the hinge's ultimate rotational capacity is not expected for the level of seismic hazard in Indiana. This assumption is further confirmed by the low probability of strong ground accelerations reflected in the hazard curve shown in Figure 4-2 for a small region of the Vincennes district. Thus, for the purpose of developing a probabilistic assessment methodology, the modeling approach in Section 3.3.8 is followed with slight adaptations. The non-linearity of the structure is incorporated by amplifying the linear displacement once the yielding in the substructure occurs. It is important to note that a typical approach for modeling non-linearity would come in the form of a more sophisticated finite-element model capable of calculating displacements after the formation of the collapse mechanism. However, since this chapter focuses solely on the development of the probabilistic methodology, the proposed approach for incorporating non-linearity is acceptable.

The second step in the two-fold process is to leverage a Latin Hypercube Sampling (LHS) technique to account for variations in the structural response due to physical uncertainties associated with stiffness, strength, and inherent viscous damping rate (Melchers & Beck, 2018). These uncertainties, or random variables, are modeled using the distributions shown in Table 4-1.

Table 4-1. Selected Distribution for Modeling Parameters

Parameter	Distribution	Mean	Variance (% of Mean)
Concrete compressive strength (f_c')*	Normal[1]	4,500 psi	900 psi (20 %)
Steel yield strength (f_y)	Lognormal[1]	48.8 ksi	5.22 ksi (10.6 %)
Steel modulus of elasticity (E_y)	Lognormal[2]	29000 ksi	960 ksi (3.3 %)
Nonlinear modifier (f_{nl})	Normal	0.7	0.05 (7%)
Viscous damping ratio (ζ_{sub})	Uniform[3]	3 %	0.5 % (16.7 %)

*Note: Concrete modulus of elasticity is calculated as a function of concrete compressive strength. Thus, this distribution is also normal. The equation used to model concrete's modulus of elasticity is: $E_c = 57000\sqrt{f_c'}$
References: 1. Shinozuka, Feng, Lee et al., 2000; 2. Barbato et al., 2010; 3. Hwang and Huo, 1994

These uncertainties help to develop a fragility function, and corresponding credible intervals, that encompass the performance of the structure throughout its lifetime. Stiffness and strength uncertainties are primarily associated with variations in material properties due to material imperfections, variation in expected fixity, uncertainty in non-linear response, and material degradation over time. Variations in inherent viscous damping are due to the complexities of using a linear effective damping value to model a highly non-linear element which is commonly derived as a function of structural softening (Khan et al., 2016).

While many sampling techniques exist, LHS is selected to efficiently vary the parameters across the entire domain (Peña, 2019). For each bridge, *10 models* are developed to accurately encompass the credible intervals associated with the modeling of FF. The impact the number of models has on reducing the epistemic uncertainty as well as the impact the overall wealth of data has on the development of an FF will also be explored.

This dynamic modeling procedure is applied to a link (in this case, three bridges) in the longitudinal direction. All three bridges are modeled as prestressed concrete superstructures supported by multi-column bents. For the purpose of demonstrating the methodology, all bridges are modeled as having expansion joints between the superstructure and adjacent abutments. The influential dynamic characteristics of each bridge, as a result of the LHS, are summarized in Table 4-2 with the period and linear displacement characterized by a normal distribution. The linear displacement calculated using Equation 3-13 corresponds to the displacement at the first yield of the extreme layer of longitudinal steel in tension.

Table 4-2. Dynamic Parameters of Each Bridge in a Link

Bridge	Mass (*kips/g*)	Period (*s*)		Linear Displacement (*in*)	
		Mean (μ)	Variance (σ)	Mean (μ)	Variance (σ)
A	6.94	0.81	$1.0 * 10^{-3}$	0.43	0.045
B	8.73	1.05	$1.4 * 10^{-3}$	0.53	0.056
C	7.35	0.35	$4.5 * 10^{-4}$	0.042	0.004

As mentioned previously, the non-linear displacement, solely for the purpose of demonstrating the methodology, is calculated as a function of the displacement received from the Simulink model (Δ_{sim}). This displacement is amplified as

$$\Delta_{sim} = \begin{cases} \Delta_{sim} & if \; \Delta_{sim} \leq \Delta_l \\ \Delta_l + \dfrac{\Delta_{sim} - \Delta_l}{f_{nl}} & else \end{cases} \tag{4-1}$$

While the stiffness of the substructure is calculated using gross-section properties, and thus only the stiffness of the concrete section is considered, the variation in steel properties (yield stress and modulus of elasticity) are considered in the calculations of the yield moment and resulting displacement. The variation in inherent viscous damping is incorporated directly into the Simulink model used to determine the displacement and resulting spectral velocity of the structure given the earthquake excitation.

4.2.2 Fragility Function

A fragility function is a probabilistic representation of a structure's likelihood to reach or exceed a certain level of vulnerability (hereafter referred to as limit state (LS)) for a given level of hazard, represented by an intensity measure (IM). The mathematical model for a FF, originally shown in Equation 2-1, is reintroduced in Equation 4-2 where the engineering demand parameter (EDP) is represented by Y, the LS by y_{LS}, and the IM by x_{IM}.

$$F_R(x_{IM}; y_{LS}) = P(Y \geq y_{LS} \,|\, X = x_{IM}) \tag{4-2}$$

While a variety of structure response parameters can be used to characterize the EDP and LS of a bridge (see Section 2.4.1), the parameter selected for this methodology is substructure drift. From the seismic assessment conducted in Section 3.3, a strong correlation between the substructure drift and the formation of the controlling collapse mechanism has been identified. The

drift-based thresholds for each limit state, as well as descriptions for each level of damage (slight, moderate, extensive) are shown in Table 4-3.

Table 4-3. Limit States and Metrics for Bridge Response

Limit State	Descriptor	Selected Metrics
Slight	Bridge sustains no significant structural damage. Small cracks in the substructure are present.	0.1% Drift
Moderate	Bridge sustains manageable damage while preserving the life of travelers. The plastic hinge mechanism has formed in the substructure.	0.5% Drift
Extensive	Bridge sustains significant structural damage. Substructure is barely capable of sustaining load from superstructure mass. The allowable rotation of the plastic hinge has likely been exceeded.	1.5% Drift

As discussed in Section 2.4.1, many approaches for developing fragility functions exist. This project leverages Bayesian inference to develop a map between the EDP and IM in log-space. This map characterizes the best-fit function ($\lambda_{Y|X}$) while allowing for the quantification of epistemic and aleatory uncertainty. The probabilistic derivation of this map is explained herein, but first a brief explanation on Bayes' theorem is provided.

Bayes' theorem is a conditional probability theorem that describes the probability of one event occurring given any previously known information about the probability of the event, $p(A)$, and the relationship between the event of interest and other events whose probability is easier to observe, $p(B|A)$. An event can signify an actual event with inherent randomness, such as the occurrence of an earthquake, or be used to represent data as a random variable which has some uncertainty. The latter is often the focus of Bayesian inference.

To describe the basis of Bayes' theorem more simply, two events are defined, with Event A representing a random variable over the model parameters and Event B representing a random variable over the observed data. The probability of the model parameters taking on a particular value conditioned on the observed data, otherwise known as the *posterior*, is calculated as

$$p(A|B) = \frac{p(A \cap B)}{p(B)} = \frac{p(B|A)p(A)}{p(B)} \tag{4-3}$$

where $p(B|A)$ represents the *likelihood* of the data given the modeling parameters, $p(A)$ is the *prior* information regarding the model parameters, and $p(B)$ represents the data. The *maximum a posteriori* parameter can then be extracted from the mode of the posterior distribution to form a point estimate of the inferred modeling parameters.

The principles behind Bayes' theorem are applied to identify the best-fit function between the EDP and IM in log-space by marginalizing the regression function hyperparameters $(\boldsymbol{\alpha}, \sigma)$ allowing for the inference of the regression weights $(\boldsymbol{w})$. The derivation of the regression weights is shown below by first assuming the most-probable hyperparameters. Then, the probabilistic process for marginalizing the hyperparameters is described.

First, a supervised learning technique is leveraged using a basis function to relate the drift of the substructure (θ) to the spectral velocity (s_v) as

$$\theta(s_v; \boldsymbol{w}) = \sum_{j=1}^{m} w_j \phi_j(s_v). \tag{4-4}$$

In Equation 4-4 $\boldsymbol{w}$ is a vector of length m which serve to characterize the most probable weights for the regression function and $\phi_j(\cdot)$ is the generalized notation for a basis function. The s_v of the structure is a deterministic function of the material properties, determined by the LHS, and resulting dynamic response parameters. The spectral velocity is characterized as

$$s_v = f(\omega_n, \zeta_{sub}, PGA). \tag{4-5}$$

Given the limited data, the prior beliefs regarding the positively-increasing relationship between spectral velocity and drift is represented by a first-degree polynomial, or linear, basis function. While the map is best represented by a linearly-increasing basis function, it is still referenced as a polynomial as other research has suggested using higher-order polynomial functions when considering more data (Peña, 2019).

The entire map in log-space can easily be written as

$$\log(\theta(s_v; \boldsymbol{w})) = w_1 + w_2 * \log(s_v). \tag{4-6}$$

for a value of s_v greater than 0. Thus, the basis function is represented by the vector

$$\phi_j(s_v) = [1 \log(s_v)]. \tag{4-7}$$

To infer the most-probable weights, we first assign a zero-mean Gaussian distribution with precision α_i as the *prior* for each weight. This is written as

$$p(w_i|\alpha_i) = \left(\frac{\alpha_i}{2\pi}\right)^{1/2} e^{-\alpha_i w_i^2}, \tag{4-8}$$

$$p(\boldsymbol{w}|\boldsymbol{\alpha}) = \prod_{i=1}^{m} p(w_i|\alpha_i), \tag{4-9}$$

where Equation 4-9 denotes the assumed independence of the weights. Combining the prior on the weights with the likelihood function, the posterior of the weights is approximated as

$$p(\boldsymbol{w}|\boldsymbol{s_v}, \boldsymbol{\theta}, \sigma_n, \boldsymbol{\alpha}) \propto p(\boldsymbol{\theta}|\boldsymbol{s_v}, \boldsymbol{w}, \sigma_n)p(\boldsymbol{w}|\boldsymbol{\alpha}) \tag{4-10}$$

Thus, the posterior is a probabilistic representation of the weights if the precision parameters (α_i) and noise parameter (σ_n) are known. With this derivation, the methodology for characterizing the hyperparameters is explored. For ease, we will represent these hyperparameters as a single variable, γ, such that

$$\boldsymbol{\gamma} = \{\boldsymbol{\alpha}, \sigma_n\} \tag{4-11}$$

The probability of these hyperparameters is maximized using an evidence approximation on the marginal posterior of the weights. The marginal posterior is written as

$$p(\boldsymbol{\gamma}|\boldsymbol{s_v}, \boldsymbol{\theta}) = \int p(\boldsymbol{\theta}, \boldsymbol{s_v}|\boldsymbol{w}, \boldsymbol{\gamma})p(\boldsymbol{w}|\boldsymbol{\gamma})p(\boldsymbol{\gamma}). \tag{4-12}$$

where the $p(\boldsymbol{\gamma})$ is assumed to be relatively flat (e.g. $p(\boldsymbol{\gamma}) = 1$). This evidence approximation is implemented using Automatic Relevance Determination in Python. Once marginalized, the hyperparameters are used to calculate the expected value of the weights using a Cholesky decomposition. For Gaussian likelihood and weights, the posterior, which is also Gaussian, is written as

$$p(\boldsymbol{w}|\boldsymbol{s}_v, \boldsymbol{\theta}, \sigma, \boldsymbol{\alpha}) = \mathcal{N}(\boldsymbol{w}|\boldsymbol{m}, \boldsymbol{S}).$$ (4-13)

The uncertainty ($\boldsymbol{S}$) and expected value of each weight ($\boldsymbol{m}$) are calculated as

$$\boldsymbol{S} = (\sigma_n^{-2}\boldsymbol{\Phi}^T\boldsymbol{\Phi} + \alpha\boldsymbol{I})^{-1}$$ (4-14)

$$\boldsymbol{m} = \sigma_n^{-2}\boldsymbol{S}\boldsymbol{\Phi}^T\boldsymbol{\theta}$$ (4-15)

where $\boldsymbol{\Phi}$ is the vectorized form of $\phi_j(s_v)$. For a first-order polynomial basis function, the shape of $\boldsymbol{\Phi}$ is $(k \; x \; d)$ where k corresponds to the desired number of data points to describe the function and d is the degree of the polynomial plus one. These values can be vectorized to form the posterior predictive distribution, or the best-fit function ($\lambda_{Y|X}$), for the data. The posterior predictive distribution, which replaces $\lambda_{Y|X}$ in Equation 2-2, is also Gaussian and written as

$$m(\boldsymbol{s}_v) = \boldsymbol{m}^T\phi(\boldsymbol{s}_v)$$ (4-16)

The predictive uncertainty, which forms the basis for the credible intervals, is written as

$$s^2(\boldsymbol{s}_v) = \phi(\boldsymbol{s}_v)^T\boldsymbol{S}\phi(\boldsymbol{s}_v) + \sigma_n^2$$ (4-17)

where σ_n^2 corresponds to the measurement noise and $\phi(\boldsymbol{s}_v)^T\boldsymbol{S}\phi(\boldsymbol{s}_v)$ is the epistemic uncertainty induced by limited data.

For each bridge in the link, all 10 models, generated through variations in the parameters thus allowing for the quantification of capacity uncertainty, are exposed to a suite of stochastically simulated ground motions representative of the expected seismic excitations for Indiana. These ground motions are generated in accordance with AASHTO (2017) and a 7% probability of exceedance in 75 years (Bonthron et al., 2020). These earthquakes consider the seismic source, attenuation, and soil conditions for each bridge. For the purpose of demonstrating the methodology, the 3 bridges in the link are assumed to be within an acceptable distance from each other such that the earthquake attenuation does not result in significant differences in the ground acceleration. Thus, the same set of 200 earthquakes are used as the demand input for all 3 bridges. For each bridge, the response of each model for all 200 earthquakes is recorded and the BI approach is applied to determine the posterior predictive distribution which best characterizes the response of each model. A sample regression, with epistemic and aleatory uncertainty bounds, is shown in Figure 4-1 for a single model of each bridge.
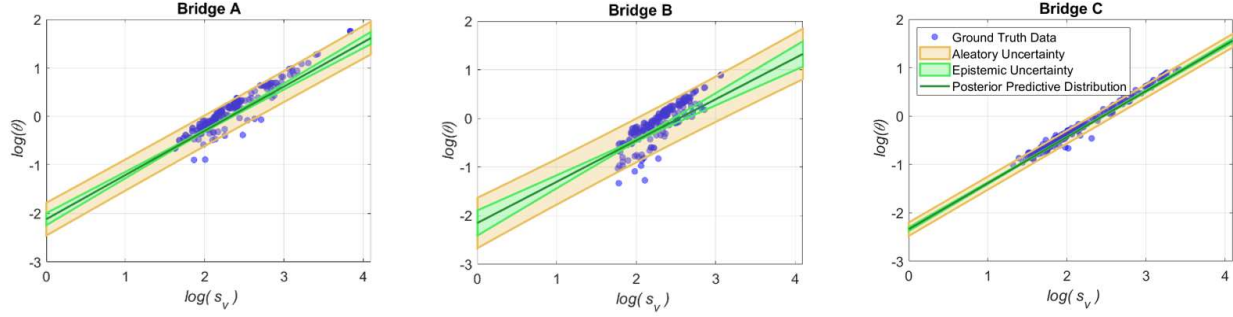
Figure 4-1. Bayesian inference Map Between EDP (Drift) and IM (Spectral Velocity)

Using the information ascertained through the BI approach, the original FF equation presented in Equation 2-2 is modified slightly to leverage the wealth of information gained using a probabilistic regression technique. The updated FF equation is written as

$$F_R(x_{IM}; y_{LS}) = P(Y \geq y_{LS} \mid X = x_{IM}) = 1 - \Phi\left(\frac{y_{LS} - m(s_v)}{\beta_T}\right), \qquad (4\text{-}18)$$

where $m(s_v)$ corresponds to the posterior predictive distribution, y_{LS} and Φ remain the same as previously defined in Section 2.4.1, and β_T represents the total uncertainty in the system. Slight modifications to the classical definition of β_T are applied to leverage the information gained through the LHS and BI approach. The uncertainty of the demand, $B_{D|s_v}$, which is characteristically represented by a single value calculated using a standard error formula, is replaced with the predictive uncertainty, $s^2(s_v)$. A value of 0.3 is assigned to β_m to account for modeling uncertainty, specifically the uncertainty in the ground motion. Rather than assigning a value to account for the uncertainty in the structure's capacity, a Monte Carlo (MC) approach is applied using the FF developed for each of the bridge's 10 models. This MC approach allows for the development of credible intervals and a visual interpretation of the uncertainty associated with the bridge's capacity.

4.2.3 Hazard Curve

The response of the bridge is simulated using 200 stochastically simulated ground motions generated in accordance with a deaggregation analysis of the uniform hazard curve from USGS. These uniform hazard curves are dependent on the soil class at the site, the fundamental frequency of the structure, and the return period (t). The basis of a uniform hazard curve is the annual

frequency of exceedance ($N(y_{max})$). This frequency, or rate, is the number of times for which an earthquake is expected to produce a certain spectral velocity, s_v. The annual frequency of exceedance is used to calculate the probability of exceedance, or the probability of occurrence, as

$$\lambda_X(x) = P(X = x_{IM}) = 1 - e^{-N(y_{max})t}. \qquad (4\text{-}19)$$

The probability of occurrence for this link is calculated using the same return period used to generate the stochastically simulated ground motion – 1000 years. The annual frequency of exceedance and the resulting probability of occurrence is shown in Figure 4-2.
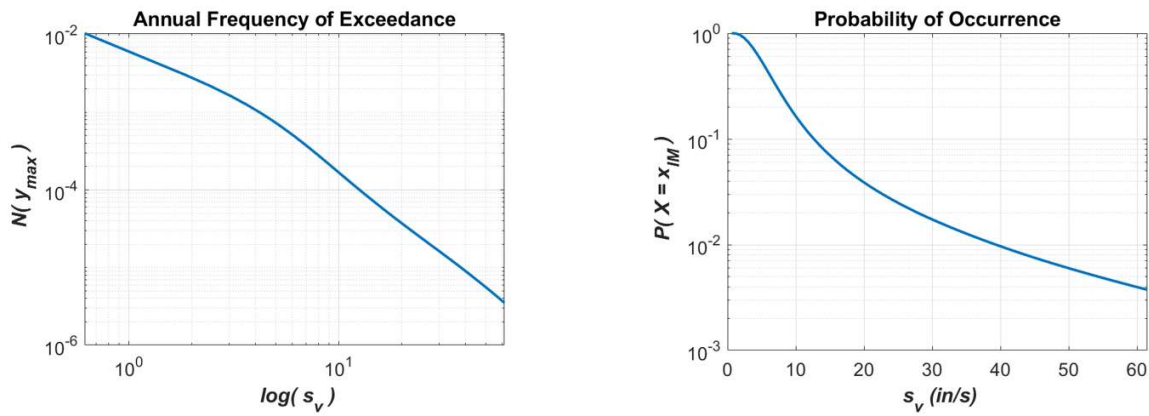
Figure 4-2. Annual Frequency of Exceedance (Left) with Corresponding Hazard Curve (Right) Representative of the Seismic Hazard at Link Location

4.2.4 Probability of Failure

The overall probability of failure of a bridge for a given LS, or the $P(Y \geq y_{LS})$, requires consideration for both the condition probability of damage for the structure and the probability of the hazard occurring. *This probability of failure doesn't represent the complete failure of the structure, rather it represents the likelihood of the bridge exceeding each LS, as defined in Table 4-3, in a determined return period.* The likelihood of damage, or capacity of the structure, is accounted for with the FF whereas the hazard is represented by the probability of occurrence shown in Figure 4-2. The bridge's probability of failure, $P_B(F)$, is calculated as

$$P_B(F) = P(Y \geq y_{LS}) = \int_0^{X_{max}} F_R(x_{IM}; y_{LS})\left(\frac{d\lambda_X(x)}{dx}\right)dx. \qquad (4\text{-}20)$$

With a single bridge's probability of failure calculated, the vulnerability of a link can be explored. The overall fragility of a bridge network is intrinsically more interdependent than the vulnerability of a single bridge in the network. Thus, the node and link model used to model the intricacy of various networks is adopted for this methodology. When the principles of a node and link model are applied to a transportation system, the node represent major interchanges whereas links represent the portion of the transportation system connecting the nodes. This concept is shown in Figure 4-3 for a section of INDOT's transportation system. It is important to note that in Figure 4-3, links correspond solely to critical routes designated by INDOT (2012a).
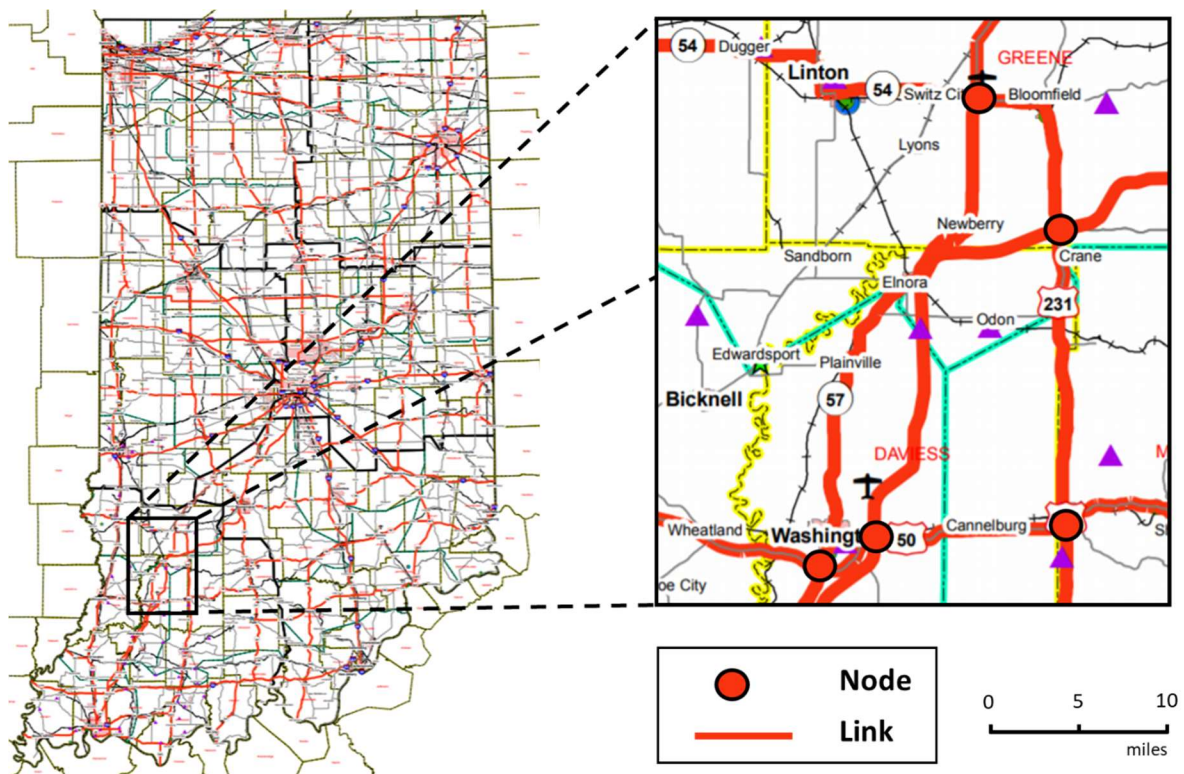
Figure 4-3. Node and Link Model for Section of INDOT's Critical Highway System

A single link in the transportation system is modeled as a series system or "weakest-link" system in that the failure of a single bridge in the link designates the failure of the entire link. Previous research has designated the vulnerability of the link as the vulnerability of the weakest bridge alone (Banerjee & Shinozuka, 2009), but this fails to account for the less-likely failure of other bridges in the link. This less-likely failure is related to uncertainties in the performance of the structure, the soil class at the site, or the actual attenuation of the seismic waves. With the

calculated probability of failure for each bridge for each LS, this methodology models the likelihood of each bridge failure using a Bernoulli random variable to account for the less-likely failure of the more reliable structures. Using this approach, the overall probability of failure for the link, both empirically using a Monte Carlo Simulation and theoretically, is calculated.

To calculate the theoretical probability of link failure ($P_L(F)$), the failure of each bridge in the link is modeled as a Bernoulli random variable (B_i) with their corresponding $P_{B_i}(F)$. The $P_{B_i}(F)$ represents the likelihood of bridge damage for each LS. This probability distribution is represented as

$$B_i \sim Bern\left(P_{B_i}(F)\right)$$ (4-21)

We can define the probability a bridge does not fail, or the probability of success, as

$$P_{B_i}(S) = 1 - P_{B_i}(F).$$ (4-22)

Given the weakest-link condition for the series system, the only time the link does not fail is when all bridges succeed. Thus, the theoretical $P_L(F)$ for a series of n bridges in a link is calculated as

$$P_L(F) = 1 - \left[P_{B_1}(S) \cap P_{B_2}(S) \cap ... \cap P_{B_n}(S)\right].$$ (4-23)

4.3   Application of Methodology

The methodology developed in Section 4.2 is applied to the series of three bridges to determine the overall vulnerability of the link for each LS. This methodology can easily be applied to links of varying sizes while also allowing for DOT to assess sub-sections of larger links, if desired. Similarly, it can be used to assess the vulnerability of nodes thus allowing for the complete probabilistic assessment of the network.

4.3.1   Fragility Functions (Application)

The FF for each bridge detailed in Table 4-2 are developed using the dynamic modeling methodology and the three limit states defined in Table 4-3. With the use of a BI approach, the epistemic and aleatory uncertainty associated with the modeling technique can also be quantified. Epistemic uncertainty is associated with a lack of knowledge which is typically reduced at the cost of additional modeling time whereas aleatory uncertainty is not reduceable. Both types of

uncertainty are briefly explored for a single bridge with the primary goal of validating the use of 10 models to represent the fragility of each bridge accurately and efficiently. As Figure 4-1 shows, it is clear that increased epistemic uncertainty corresponds to a lack of data in certain regions of the simulation whereas aleatory uncertainty corresponds to the data's deviation from a perfectly linear response. The number of models necessary for reducing the epistemic uncertainty in the response of Bridge B is explored with the results shown in Figure 4-4.
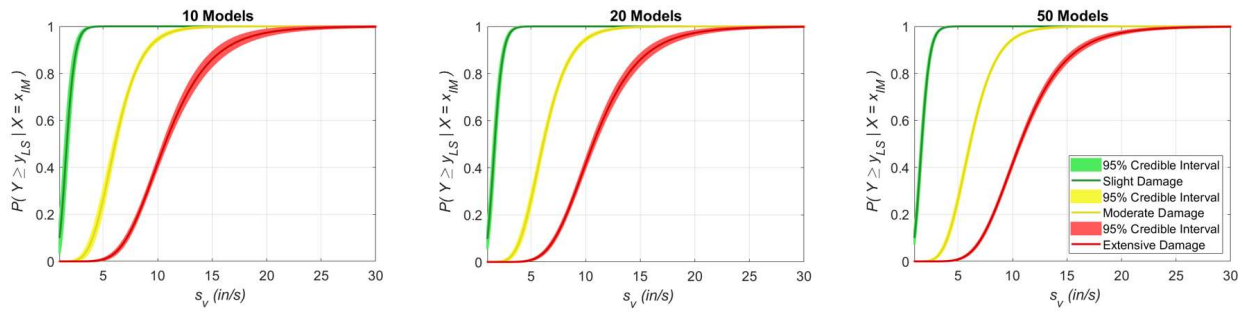
Figure 4-4. Epistemic Uncertainty in FF for Various Number of Models

While 50 models are suitable for significantly reducing the epistemic uncertainty in the modeling, the time required to run a dynamic simulation of this size for multiple bridges within a link is costly. The impact the number of models has on the overall credible intervals is also explored with the results shown in Figure 4-5.
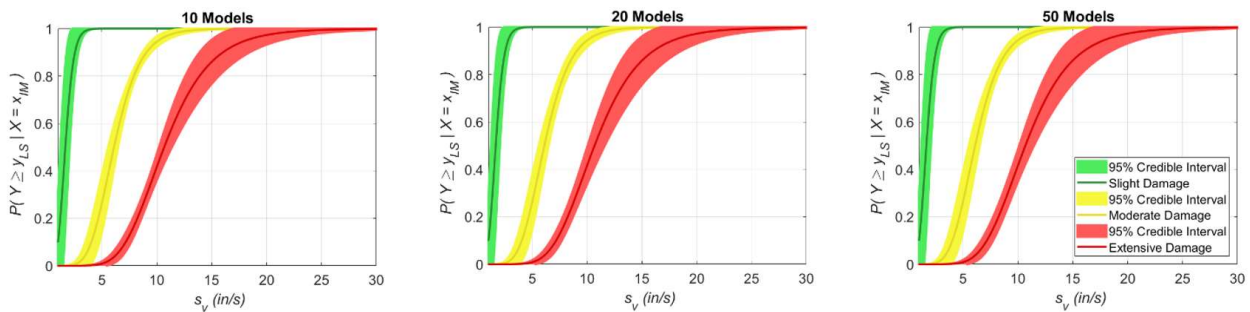
Figure 4-5. FF with 95% Credible Interval for Various Number of Models

In Figure 4-5, a noticeable similarity is apparent between the expected FF and corresponding credible interval for each damage state across all number of models. Thus, the use of 10 models is validated for the purpose of accurately and efficiently accounting for the capacity

uncertainty in the structure. Furthermore, 10 models are selected for simulation purposes due to the drastic cost-saving capabilities. The difference in simulation time between 50 models and 10 models is calculated as 1 minute per model which corresponds to a difference of 40 minutes per bridge or approximately 160 days for INDOT's entire bridge network.

With 10 models for each bridge, the FFs and corresponding credible intervals are developed for the three bridges in the link. The FFs for each bridge are shown in Figure 4-6.
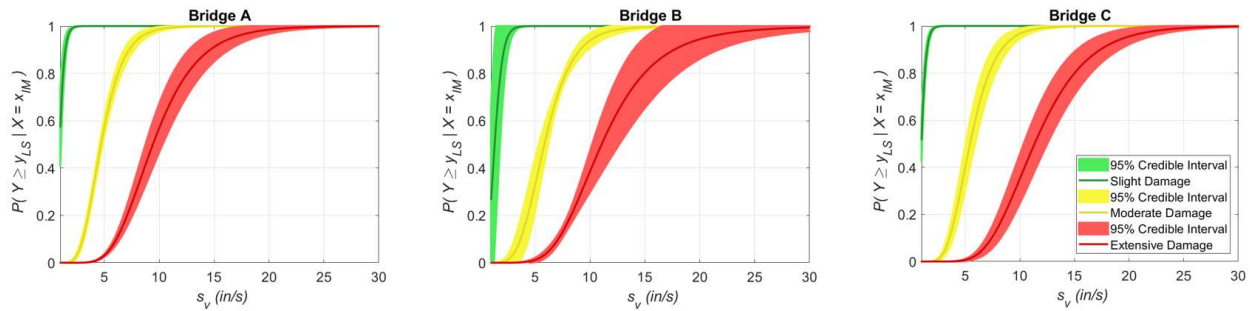
Figure 4-6. FF with 95% Credible Interval for Three Bridges in Link

4.3.2 Probability of Failure (Application)

For each model, the conditional damage response for the structure (FF) is coupled with the hazard curve that corresponds to the simulated earthquakes. The probability of failure for each of the 10 bridge models for each LS is calculated using Equation 4-20 with the mean probability of failure and variance for each bridge and LS summarized in Table 4-4.

The next step in the methodology is to calculate the overall probability of failure for the link. In this case, the link corresponds to the series of three bridges, but the approach can as easily be applied to links with more bridges or smaller subsets of larger links. Applying a Bernoulli distribution to each bridge with a $P_B(F)$ corresponding to Table 4-4, the number of simulations necessary to accurately calculate the link's probability of failure for each LS is explored. Since the link is modeled using a weakest-link approach, the failure of just one bridge (or multiple) denotes the failure of the entire link. The $P_L(F)$ as a function of MC simulations is shown in Figure 4-7 for each damage state with the mean expectation for the link failure using 25,000 simulations recorded in Table 4-4.
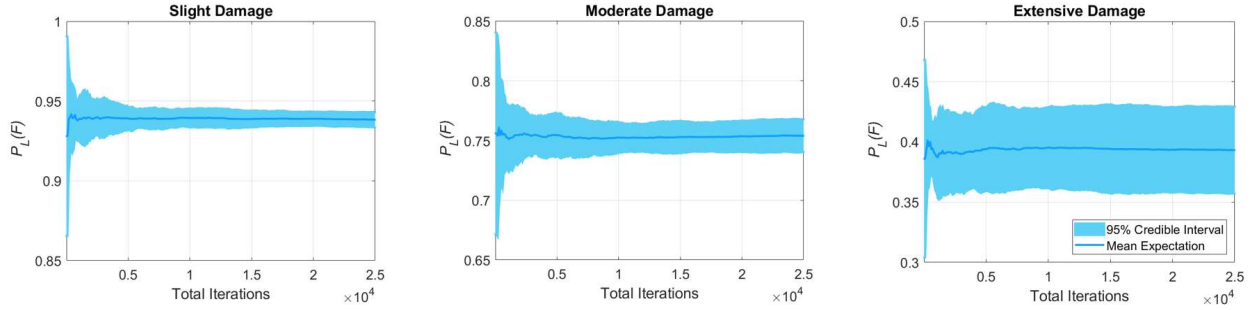
Figure 4-7. Link Probability of Failure as a Function of MC Simulations

The empirical prediction for the link's probability of failure, notated as Network – E in Table 4-4, is compared to the theoretical value using the approach outlined in Equation 4-23. As an example, the $P_L(F)$ for moderate damage using the $P_{B_i}(F)$ from Table 4-4 is calculated as

$$P_L(F) = 1 - (0.41)(0.34)(0.36) = 0.75. \tag{4-24}$$

This theoretical value, notated as *Network – T*, compares well to the probability of link failure calculated using the empirical approach with the only shortcoming of the theoretical approach being the inability to account for the uncertainty in the model.

Table 4-4. Probability of Failure $P_B(F)$ for Each Bridge and the Link $P_L(F)$

Structure(s)	Slight Damage		Moderate Damage		Extensive Damage	
	Mean (μ)	Variance	Mean (μ)	Variance	Mean (μ)	Variance
Bridge A	0.61	$3 * 10^{-4}$	0.41	$9 * 10^{-3}$	0.18	$12 * 10^{-3}$
Bridge B	0.60	$5 * 10^{-3}$	0.34	$12 * 10^{-3}$	0.14	$9 * 10^{-3}$
Bridge C	0.61	$4 * 10^{-4}$	0.36	$13 * 10^{-3}$	0.13	$9 * 10^{-3}$
Network - E	0.94	$4 * 10^{-3}$	0.76	$16 * 10^{-3}$	0.39	$3 * 10^{-2}$
Network - T	0.94	--	0.75	--	0.39	--

4.4 Pre-Assessment Filters for Reduction of Modeling Time

This methodology, while demonstrated on a link of 3 bridges, has the potential to apply to large links (20+ bridges) or sub-sections of links in a local, state, or even national transportation systems. While this methodology may be costly when applied to larger links, additional pre-assessment filters can be leveraged to identify bridges that have negligible probability of failure and can be eliminated from the link when estimating its overall vulnerability. From the seismic

assessment in Chapter 3, these filters, further explained in Bonthron et al. (2020), in the longitudinal direction include:

- Buried structures, like culverts, as they do not maintain a surface separate from the ground and thus are expected to move entirely with the ground
- Bridges with integral or semi-integral abutments as these details eliminate the inertial effects of the mass thus allowing for the structure to move entirely with the ground
- All single span bridges not supported by rocker bearings
- Short span single span steel bridges supported by rocker bearings (less than 60 *ft.*)

4.5   Summary for Probabilistic Assessment of Bridge Networks

As expected, the vulnerability of the bridge network is intrinsically more complex than the vulnerability of individual bridges alone. This methodology, coupled with additional information readily available to DOT, can be used to improve the reliability of their transportation systems (see Section 6.2: Future Work). While this approach is demonstrated for a link of 3 bridges, it can readily be applied to links of various sizes in a local, state or even national transportation system. Additional pre-assessment filters, derived from trends identified using the seismic assessment procedure in Chapter 3, can decrease the amount of computational time required for assessing links with a higher number of bridges. Overall, this methodology allows DOTs to robustly understand the current resiliency of their infrastructure thus allowing for decisive improvements to corridors resulting in increased public safety.

5. MODELING OF SEISMIC RETROFITS

5.1 Introduction

A seismic assessment of 100 bridges in Indiana's bridge inventory has identified specific vulnerabilities throughout the state, as summarized in Table 3-4. With the identification of these vulnerabilities comes the need to identify retrofit strategies that can reduce the damage associated with the expected level of hazard in Indiana. The proposed retrofits will serve to decrease damage by either reducing the seismic demand or increasing the substructure capacity. Each of the recommended retrofit options is demonstrated using a model of its application to a representative bridge from INDOT's bridge network. This chapter demonstrates the necessary changes to the modeling procedure discussed in Chapter 3 and the assumptions that should be adopted to successfully demonstrate the impact each retrofit has on the seismic performance of the bridge.

5.2 Synopsis of Retrofits

Table 5-1 maps seismic retrofits identified in Section 2.3.1 and Section 2.3.2 to each of the vulnerability cases shown in Table 3-4. As shown by Table 5-1, it is possible that the vulnerability of each bridge detail can be improved by more than one retrofit. Additionally, it is possible that more than one vulnerability case applies to the bridge, such as a combination of a vulnerability from case 1-6 and vulnerability case 7. This is the case for steel girder bridges (both continuous and non-continuous) with deficient substructure (vulnerability case 1-6 may apply) and rocker bearings (vulnerability case 7). As a note, the vulnerability cases for which isolation is identified as a potential retrofit only apply to bridges having a superstructure that is not rigidly connected to the substructure. From the sample set of bridges in Indiana, this has been identified as including primarily steel and prestressed concrete superstructures. It can therefore be assumed that seismic isolation will not typically be a viable retrofit option for bridges having a reinforced concrete slab deck superstructure due to the presence of longitudinal reinforcement extending from the substructure's bent cap into the superstructure.

Table 5-1. Summary of Recommended Retrofits for Identified Vulnerabilities

Vulnerability Case (Table 3-4)	Potential Retrofits					
	Integral Abutments	Restrainers	Isolation Device	Additional Confinement	Post-Tension	Jacketing
1	x	x	x			x
2	x	x	x			x
3	x	x	x	x		
4	x	x	x	x		
5	x	x	x	x	x	
6	x	x	x	x		
7	x		x			
Pros	Eliminate longitudinal vulnerability entirely	1. Simple design 2. Simple construction 3. Common design detail for INDOT bridges	1. Common retrofit 2. Reduce substructure demand significantly	1. Increases ductility 2. Simple design 3. Simple application	Changes to preferred failure mechanism (strong column – weak beam)*	1. Increases ductility and capacity 2. Identified as most beneficial for highly vulnerable bridges
Cons	1. Transverse direction check still requires vulnerability assessment 2. Extensive construction	May require another substructure retrofit (based on design constraints)	Potential for pounding unless appropriately designed or additional retrofit exist	1. Negligible increase in structural capacity 2. Not applicable post-damage (per INDOT)	1. Moderate design difficulty 2. May require additional retrofits	Jacketing options (steel, reinforced concrete) vary in implementation difficulty

Note: The post-tensioning is applied to the beam element of the frame bent to change the mechanism of hinge formation from strong column – weak beam (less favorable for rehabilitation) to weak column – strong beam (more favorable for rehabilitation).

A flowchart that maps each of the vulnerabilities in Table 3-4 to the recommended retrofits summarized in Table 5-1 is shown in Figure 5-1. This flowchart, in addition to a flowchart depicting a modified seismic assessment procedure, is shown in Appendix B as a recommended design aid. Together they serve as a comprehensive guide for conducting a seismic assessment and identifying retrofit options that can improve the seismic response of the bridge. This final selection of a retrofit from the "Select One" section requires additional design considerations usually at the discretion of the business owner, such as: design-level earthquake, acceptable level of vulnerability given the structure's local risk, and cost-benefit aspects associated with each retrofit type.
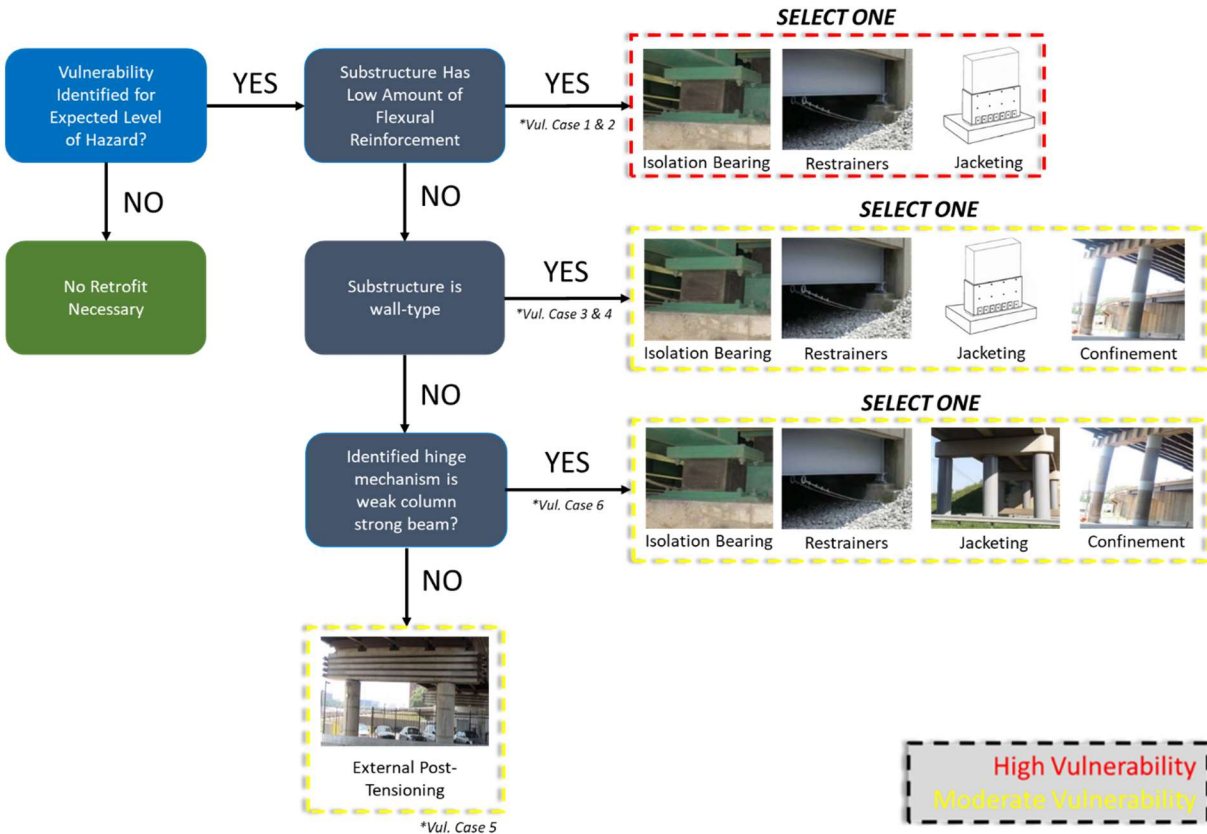
Figure 5-1. Retrofit Selection Procedure

The implementation of integral abutment, additional confinement, and post-tensioning do not require modifications to the modeling technique, and thus are only briefly discussed. These retrofit methods have the potential to eliminate the vulnerability entirely (as is the case for integral abutments in the longitudinal direction) or to maintain the same level of vulnerability but facilitate a more desirable response (as is the case for additional confinement and post-tensioning). The implementation of restrainers, isolation device, and jacketing do require slightly modification to the modeling technique. The degree of impact these retrofit methods have on a bridge's vulnerability is dependent on the design of the retrofit. These retrofit methods are discussed more extensively, with the impact of each approach demonstrated by assessing the updated seismic response of an as-built, highly vulnerable bridge in the longitudinal direction.

Structure number 067-18-05459 D (NBI 24210) is a two-span continuous steel girder bridge with 8 beams and a hammerhead wall substructure. The structure was originally constructed in 1973 with rehabilitations in 1996, 1999, 2008, and 2014 focused on the straightening and eventual

replacement of an exterior beam. The substructure has a reinforcement ratio (ρ) of 0.22% and 40 ksi yield stress steel – an assumed yield stress based on the year of construction (AASHTO, 2018). The bridge has been identified as highly vulnerable due to a low longitudinal reinforcement ratio resulting in the potential for brittle failure. Because of the brittle mode of failure, the non-linear displacement associated with structural softening is ignored (see Section 3.3.8). The moment-curvature and displacement response of the as-built structure is shown in Figure 5-2.
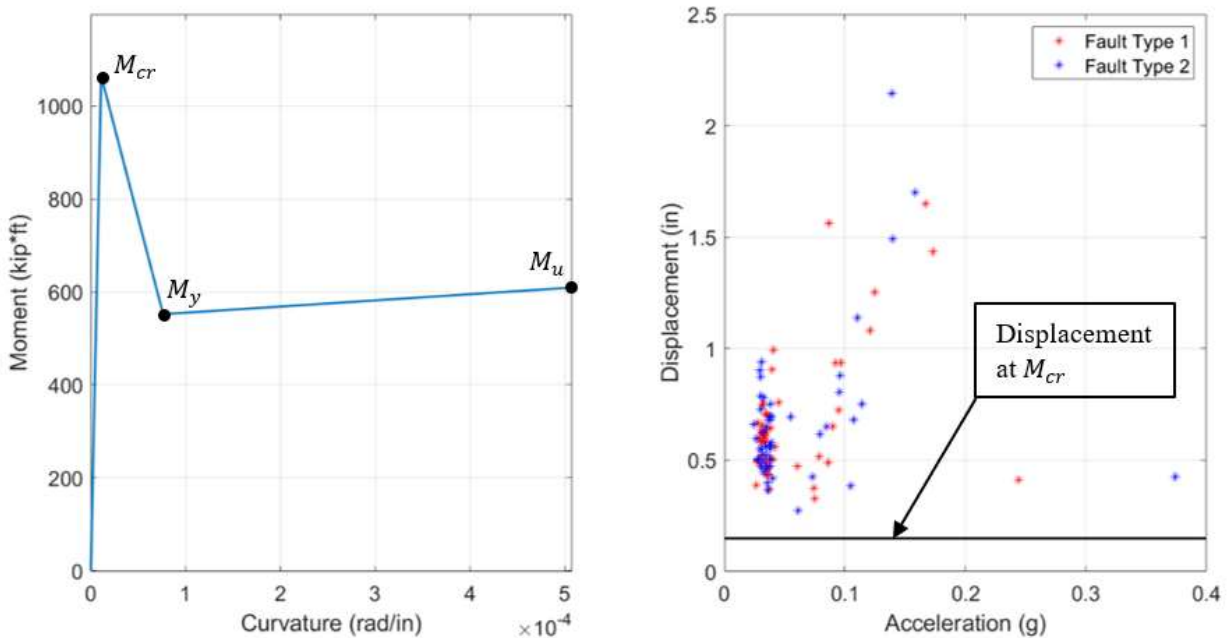
Figure 5-2. Moment-Curvature (Left) and Displacement Response (Right) of As-Built Structure (NBI 24210)

As Figure 5-2 shows, the cracking moment of the structure exceeds the yield moment and ultimate moment. This design flaw is likely to result in the rupturing of longitudinal steel once cracking of the concrete occurs. This sudden, instantaneous failure mode is considered brittle.

5.3   Application of Seismic Restrainer

The installation of restrainers between the continuous superstructure and adjacent abutment when an expansion joint is present allows for the development of a stiffer system leading to decreased displacement and substructure restoring force. These restrainers, either a bar-type or cable-type, is assumed to function as a tension-only element (DesRoches et al., 2004a). The design

of the restrainer system is based on determining the amount of stiffness needed to decrease the overall vulnerability to an acceptable threshold. As is the case for bridges with a brittle mode of failure, this corresponds to the displacement associated with the cracking moment.

The overall stiffness of the system is the total stiffness of the restrainer plus the stiffness of the substructure modeled as springs in parallel. The restrainer stiffness (K_{rest}) value corresponds to the stiffness associated with one restrainer placed on a single side of one beam. Thus, the overall stiffness of the system is taken as

$$K_{sys} = K_{pier} + K_{rest} * N_b \qquad (5\text{-}1)$$

where the total stiffness of the restrainers ($K_{rest} * N_b$) must be added at both ends of the superstructure because it is expected that only one end of the bridge will experience tension at a time under normal earthquake excitations. The necessary amount of restrainer stiffness is determined by incrementally increasing the restrainer stiffness and studying the dynamic response of the retrofitted bridge, shown in Figure 5-3.
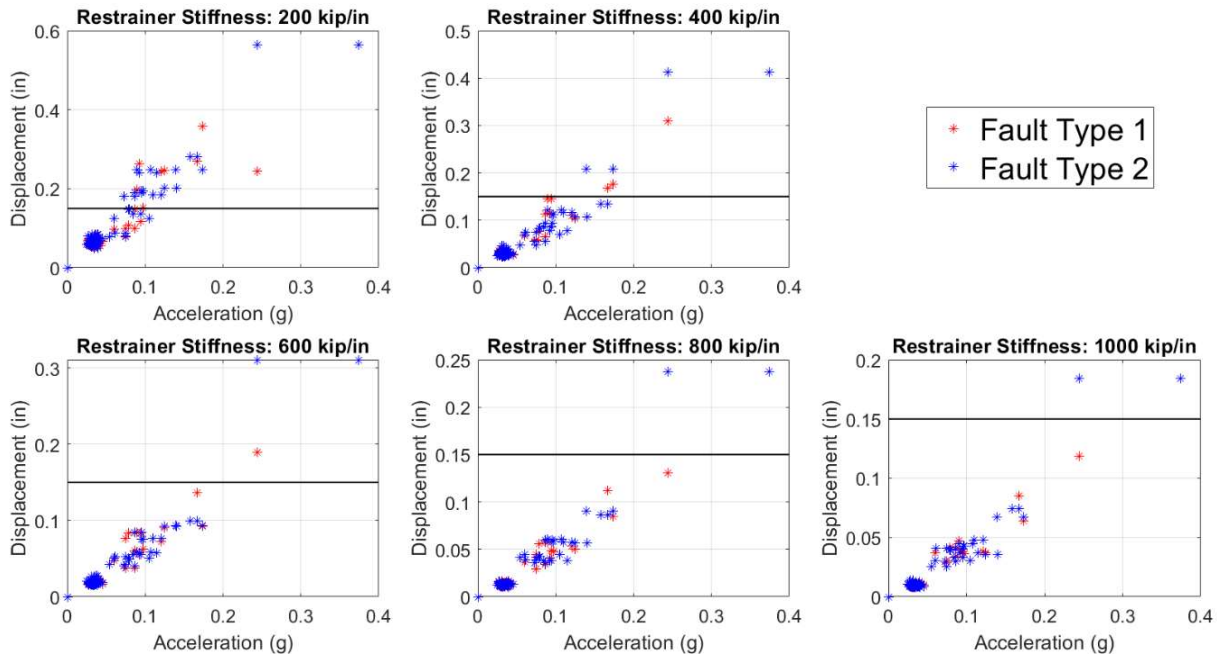
Figure 5-3. Displacement Response of Retrofitted Bridge for Several Restrainer Stiffness Values (NBI 24210)

The appropriate amount of stiffness should be selected based on the desired level of performance. Figure 5-3 shows the displacement response as a function of base excitation. The impact each restrainer system has on decreasing the overall vulnerability of the as-built structure is summarized in Table 5-2, as determined using the suite of site-specific earthquakes for NBI 24210. In this table, the percent exceedance corresponds to the percentage of the total number of earthquakes that result in a displacement greater than the cracking displacement of the substructure ($\Delta_{cr}= 0.15\ in$).

With a desired level of performance identified, the restrainer area required to achieve the level of stiffness is calculated using a standard approach (Trochalakis et al., 1996). Like most tension-only elements, the stiffness of the restrainer derives primarily from axial stiffness. Even for the case of bar-type restrainers, where the thickness of the bar means a potential for transferring force via shear and moment, the effects of this are low. Thus, the shear stiffness and flexural stiffness are considered negligible in comparison to axial stiffness. The cross-section area required to achieve a specific axial stiffness is calculated as

$$N_{bars} * A_{rest} = \frac{K_{rest} * N_b * L_{rest}}{E_{rest}} \tag{5-2}$$

Assuming values for length ($L_{rest} = 24\ in$), yield stress of high-strength steel ($f_{y_{rest}} = 150\ ksi$), modulus of elasticity ($E_{rest} = 29000\ ksi$), and a single bar per restrainer ($N_{bars} = 1$), the minimum area to achieve each restrainer stiffness is calculated. The tensile stress of the restrainer at the design displacement should also be checked to confirm that yielding of the restrainer does not occur. A conservative estimate of the stress in the restrainer is calculated using the maximum allowable displacement of the substructure ($\Delta_{cr}= 0.15\ in$). In practice, the actual displacement corresponding to the level of seismic excitation would be used in this calculation.

Table 5-2. Dynamic Parameters and Vulnerability for Various Restrainer Stiffnesses

Restrainer Stiffness (kips/in)	Period (s)	Percent Exceedance (%)	Minimum Area per Restrainer (in²)	Stress (ksi) at $\Delta_{cr} = 0.15\ in$
200	0.28	18	0.17	30
400	0.2	5	0.33	60
600	0.17	2	0.50	90
800	0.15	1	0.66	120
1000	0.13	1	0.83	150

As shown in Table 5-2, most of these restrainers can physically and realistically be applied. However, choosing a restrainer stiffness of $1000\ kips/in$ stiffness is not recommended, as the minimum area invokes yielding of the steel. An alternative in this case would be to use multiple restrainer bars ($N_{bars} = 2$) or ensure a lower maximum displacement of the structure ($\Delta_{cr} < 0.15\ in$).

5.4 Application of Isolation Bearings

The decoupling of the superstructure mass from the substructure via an isolation device has been shown to reduce the displacement and corresponding restoring force of the substructure without significantly impacting the displacement of the superstructure (when compared to a non-isolated model). The implementation of seismic isolation requires three modifications to the modeling technique developed in Chapter 3. The modifications and their resulting implications are:

- Changing the single-degree-of-freedom (SDOF) model to a multi-degree-of-freedom (MDOF) system to account for differential displacement between the superstructure and substructure.
- Incorporating the stiffness of the isolation system allowing for the effective decoupling of the superstructure mass from the substructure.
- Incorporating non-classical damping to account for the large difference in the inherent damping ratio between the substructure and isolator device.

The original modeling technique presented in Chapter 3 assumes a uniform displacement between the substructure and superstructure. For steel superstructures, this is precipitated by the fixed-bearing connection present over one or multiple piers. With the introduction of a seismic isolator, this assumption is no longer valid. To account for the differential displacement of the isolator, the structure is modeled as a MDOF, as shown in Figure 5-4.
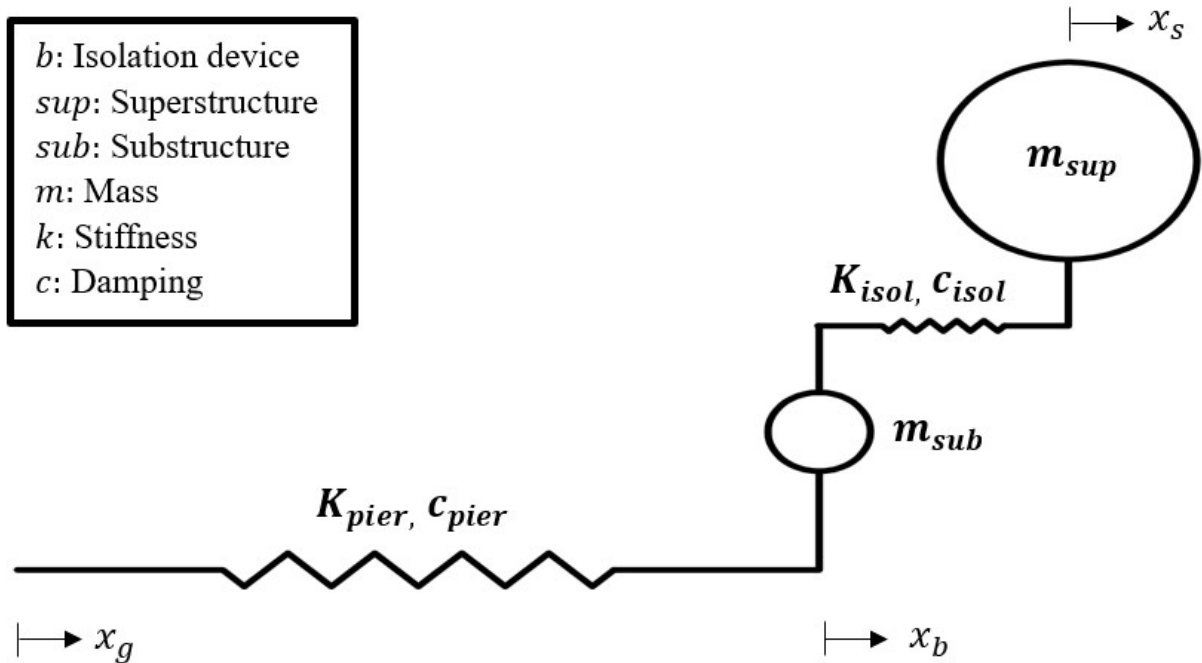
Figure 5-4. MDOF Model of Bridge with Isolator Device

While the uniform displacement assumption between the superstructure and substructure is no longer valid, the rigidity of the deck assumption presented in Section 3.3.5 still ensures that the superstructure will displace equally. Thus, the total stiffness for both the substructure and isolators is modeled as the sum of individual components. For a two-span bridge, the substructure stiffness (K_{sub}) is equivalent to the pier stiffness (K_{pier}). For a bridge with more than two spans, the total stiffness for each component is the sum of individual piers and isolator stiffnesses.

With this in mind, and replacing absolute displacement parameters (x_s, x_b, x_g) for relative displacement parameters $(u_s = x_s - x_g; \ u_b = x_b - x_g)$, the equation of motion considering only mass and stiffness is written as

$$\begin{bmatrix} m_{sub} & 0 \\ 0 & m_{sup} \end{bmatrix}\begin{bmatrix} \ddot{u}_b \\ \ddot{u}_s \end{bmatrix} + \begin{bmatrix} K_{sub} + K_{isol} & -K_{isol} \\ -K_{isol} & K_{isol} \end{bmatrix}\begin{bmatrix} u_b \\ u_s \end{bmatrix} = -\begin{bmatrix} m_{sub} & 0 \\ 0 & m_{sup} \end{bmatrix}\begin{bmatrix} \ddot{x}_g \\ \ddot{x}_g \end{bmatrix}. \tag{5-3}$$

Isolation devices such as elastomeric bearings are highly non-linear elements, as shown in Figure 5-5. However, in most modeling cases the response of the isolator can be sufficiently represented by an effective linear stiffness (Buckle et al., 2006). Significant experimental research has been conducted to characterize the fundmanetal properties of elastomeric bearings, such as the shear modulus (AASHTO; Roeder et al., 1987). This research also shows the impact that the stiffness of the elastomeric bearing is primarily developed as

Figure 5-5. Force-Displacement Response of Typical Elastomeric Isolator (Buckle et al., 2011)

shear stiffness, thus the dimensions of the pad are highly influential. Using a common elastomeric bearing pad that has dimensions 20 *in* x 13 *in* x 3 *in* (INDOT, 2012c), the stiffness of the elastomeric bearing pad can be calculated as

$$k_{isol} = \frac{G_{isol}A_{isol}}{h_{isol}} = \frac{(100 \ psi) * (20in * 13 \ in)}{3in} = 8.6ksi. \tag{5-4}$$

The total stiffness of all the isolators in the system, assuming an elastomeric bearing pad is used to support beams over every interior pier, is calculated as

$$K_{isol} = N_b * N_{piers} * k_{isol}. \tag{5-5}$$

The modeling technique proposed in Chapter 3 leverages modal damping to incorporate the assumed inherent viscous damping coefficient for the substructure into the dynamic models. However, for a system where various DOFs maintain differenet viscous damping coefficients, another method must be used. Non-classical damping is leveraged to account for the difference between the damping coefficients introduced by the substructure ($\zeta_{pier} = 0.05$) and the isolator (Chopra, 2012). The presence of the elastomeric bearing pad is captured using a damping ratio of 0.10 (Choi, 2002). Using a force-equilibrium technique (like the one used to write Equation 5-3), the damping portion of the equation of motion is constructed as

$$\begin{bmatrix} c_{sub} + c_{isol} & -c_{isol} \\ -c_{isol} & c_{isol} \end{bmatrix} \begin{bmatrix} \dot{u}_b \\ \dot{u}_s \end{bmatrix}. \tag{5-6}$$

Thus, the viscous damping rate for the pier and isolator, respectively, are calculated as

$$c_{sub} = 2\zeta_{sub}\sqrt{K_{sub} * m_{sub}}, \tag{5-7}$$

$$c_{isol} = 2\zeta_{isol}\sqrt{K_{isol} * m_{sup}}. \tag{5-8}$$

With the updated modeling assumptions defined, the impact the retrofit has on the response of the structure for the same set of site-specific earthquakes is shown in Figure 5-6. This response can be compared to the response of the as-built, non-isolated structure shown in Figure 5-2. While the capacity of the substructure does not change with the introduction of the isolation device, the substructure displacement is significantly reduced. Furthermore, the superstructure displacement response has the same magnitude as the non-isolated structure which is ideal. In addition to the cracking displacement of the substructure, the allowable displacement of the superstructure must be checked. In this case, the allowable displacement of the superstructure is controlled by the size of the expansion joint.
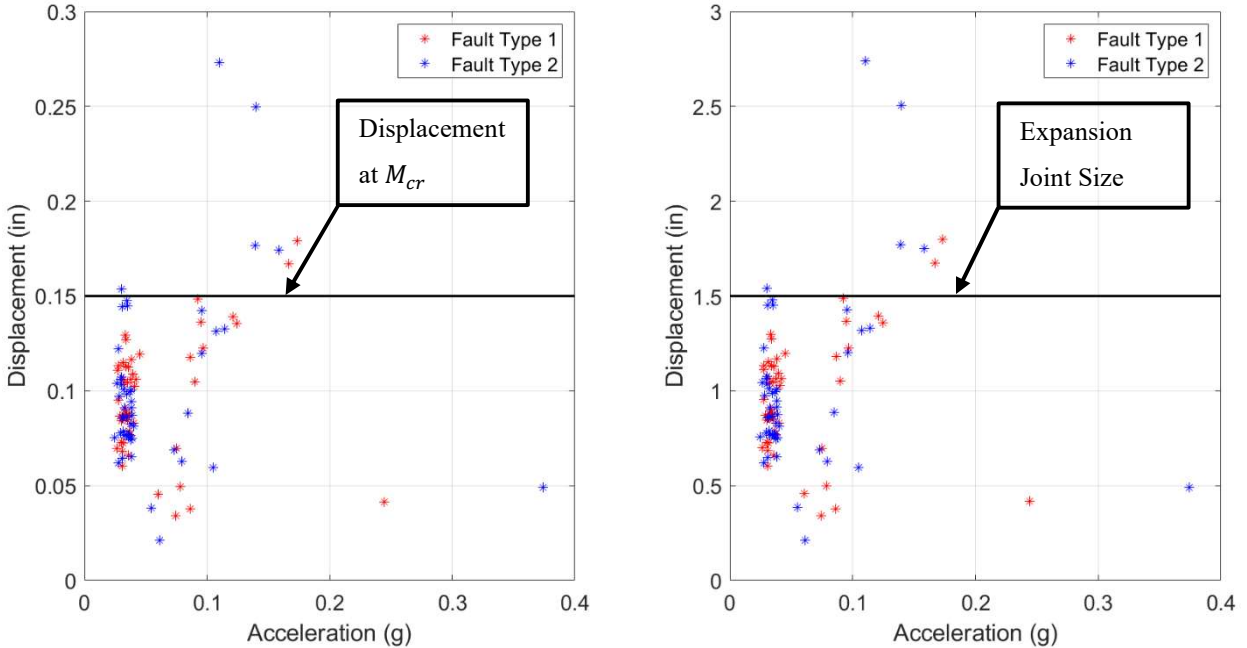
Figure 5-6. Displacement Response of Substructure (Left) and Superstructure (Right) of Isolated Bridge (NBI 24210)

As shown in Figure 5-6, introducing the isolator reduces the displacement response for more than 90% of the simulated earthquakes to an acceptable level. This moves the structure from high vulnerability to low vulnerability for those earthquakes. Seismic isolators for this bridge could feasibly be designed for an identified level of base excitation such that it is guaranteed that the bridge would achieve a low level of seismic vulnerability.

5.5   Application of Jacketing

An alternate approach to improving the seismic performance of the structure is to increase the overall capacity of the vulnerable detail. For vulnerable substructures, either with high or moderate vulnerability, the addition of a steel jacket to the outside of the substructure can significantly improve the base shear of the substructure. The base shear is the shear capacity which corresponds to the identified mechanism of hinge formation (see Section 3.3.1). To capture the increased capacity in the model, the implementation of steel jacketing requires a small update to the assumptions made for the moment-curvature calculations presented in Section 3.3.1. Specifically, the assumptions for the cracking moment are updated to reflect the addition of the steel jacket. The cracking stress of the concrete remains the same ($7.5\sqrt{f_c'}$) and the cracking

moment is achieved when this stress occurs at the interface between the original concrete section and the steel jacket. Using a linear strain profile, the corresponding strain is calculated in the steel jacket and the total cracking moment is calculated using the defined stress-strain profiles for concrete (Equation 3-22) and steel (Equation 3-24). The updated moment-curvature response for NBI 24210 and a steel plate thickness (t_{steel}) of 0.25 in is shown in Figure 5-7.
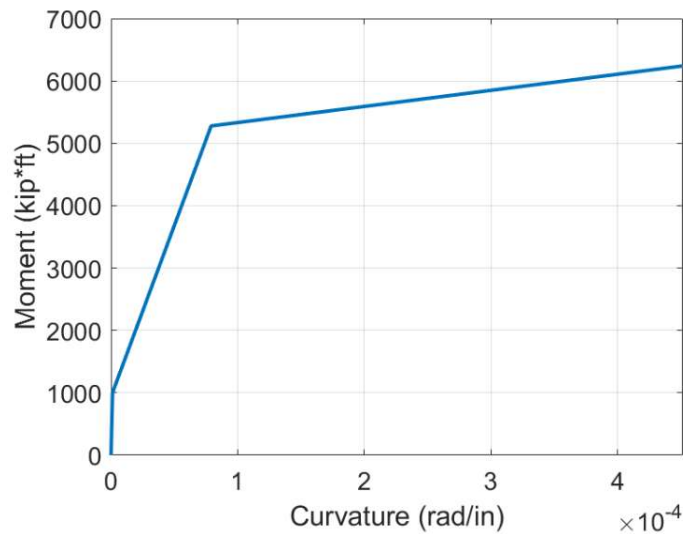
Figure 5-7. Moment-Curvature Response for Retrofitted Bridge with Steel Jacketing (NBI 24210)

Table 5-3 shows the impact the thickness of the jacket has on the overall vulnerability of the structure when subjected to the site-specific earthquakes for the bridge. This optimization approach allows for the appropriate plate thickness to be selected based on the desired level of performance. Like before, the percent exceedance corresponds to the total number of simulated earthquakes resulting in a displacement greater than the allowable substructure displacement.

Table 5-3. Likelihood of Earthquake Displacement Exceeding Retrofit Capacity for Corresponding Plate Thickness

Plate Thickness (in)	Percent Exceedance (%)
0.25	48
0.38	10
0.50	6
0.63	4
0.75	1
1.00	0
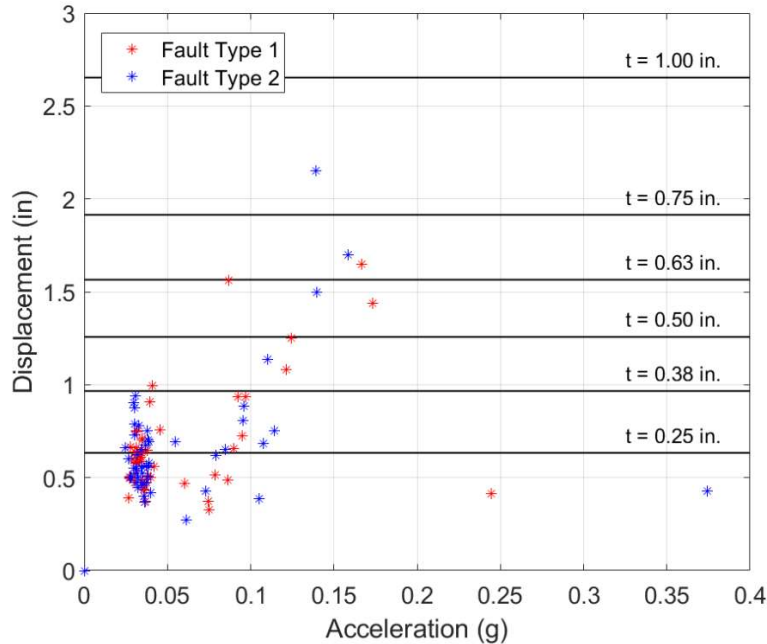
Figure 5-8. Impact of Steel Plate Thickness for Retrofitted Bridge Response (NBI 24210)

As shown in Figure 5-8, the response of NBI 24210 improves as the thickness of the steel is increased. While the additional steel allows for a more ductile response too, it is still recommended to design the retrofit such that the structure remains linear. This recommendation is carried out in the modeling approach and shown in the corresponding results. Because the base shear capacity of the substructure has increased, the mechanism of shear failure must be checked to determine the controlling mechanism of failure. It is recommended that the retrofit be designed so that the base shear of the structure controls rather than the shear capacity.

5.6   Additional Retrofits

5.6.1   Integral Abutments

The use of integral abutments for continuous superstructures eliminates the inertial effects of the structure and any differential displacement between the abutment and superstructure via a monolithic connection. However, these bridges may still be vulnerable in the transverse direction and must be checked. The use of integral abutments eliminates substructure vulnerabilities but results in increased demand on the abutment and foundation. Frosch et al. (2009) showed, using field data and laboratory tests, that INDOT standard details for integral abutments have enough

capacity to resist the forces transferred to the abutments and foundation by earthquakes. The major conclusion of the project is that bridges with a structural length less than 500 ft. have enough capacity to provide seismic resistance. Thus, it is recommended to continue with the implementation of integral abutments using INDOT's standard drawing.

5.6.2   Added Confinement

Additional confinement is recommended to increase the rotational capacity of the identified mechanism of hinge formation once it has formed in the structure (Alkhrdaji & Silva, 2008). This retrofit does not significantly increase the flexural capacity of the substructure or reduce the overall vulnerability of the structure. Rather, additional confinement only ensures more rotational capacity and thus a more ductile response of the structure. It is recommended that any additional capacity that might be added to the substructure due to the added confinement, e.g. a fiber-reinforced polymer wrap, be considered negligible. As Table 5-1 shows, this retrofit has the potential to apply to every case in which the identified level of vulnerability is moderate. However, a couple other factors must also be considered when determining whether the retrofit is necessary for the given vulnerability. For the vulnerability cases in which the development of the identified mechanism of hinge formation is expected, the primary concern is the occurrence of bar buckling in the longitudinal bars after the formation of the hinge and the corresponding concrete spalling.

To determine whether the section will experience buckling of the longitudinal bars after the formation of the identified mechanism of hinge formation requires assessing the transverse reinforcement spacing. In accordance with AASTO Section 5.10.11.4 (2017), the transverse reinforcement ratio must meet specific criteria depending on the type of substructure. These thresholds are based on work by the Applied Technology Council with additional research and more stringent thresholds influenced by CalTrans and the Loma Prieta earthquake (AASHTO, 2017). Table 5-4 shows a summary of these design requirements.

Table 5-4. Transverse Reinforcement Criteria in Region(s) of Plastic Hinge

Substructure Type	Code Requirement	Code Reference
Wall-Type	Weak direction (primary direction of concern) designed using column requirements	5.10.11.4.2
Circular Column	$\rho_s \geq 0.12 \dfrac{f_c'}{f_y}$	5.10.11.4.1d-1
Rectangular Column	$A_{sh} \geq 0.30 s h_c \dfrac{f_c'}{f_y}(\dfrac{A_g}{A_c} - 1)$	5.10.11.4.1d-2
	$A_{sh} \geq 0.12 s h_c \dfrac{f_c'}{f_y}$	5.10.11.4.1d-3

For substructure with an adequate transverse reinforcement ratio, additional confinement is not necessary as the plastic hinge has adequate confinement and stability to prevent the buckling of longitudinal reinforcing bars. For substructures with an inadequate reinforcement ratio, additional confinement is recommended to achieve adequate ductility and improved energy dissipation. Fiber-reinforced polymer (FRP), such as carbon reinforced polymer (Alkhrdaji & Silva, 2008) is typically recommended for wrapping vulnerable details. Currently, INDOT does not permit the use of external FRP jacketing to restore the structural ductility of the substructure once damage has occurred (INDOT, 2013c). In such a case where the retrofit is applied retroactively to a seismic event on a bridge that experienced damage, jacketing can be implemented to provide the required confinement. Though the purpose of jacketing in this case is not to increase the capacity, but rather improve ductility, the section will also gain capacity from the jacketing. This will result not in just increase ductility and rotational capacity, but also improved flexural strength and overall structural response. Of the vulnerability cases identified in Table 3-4, the requirements in Table 5-4 apply to wall-type substructures and reinforced-concrete frame bents. For pile-type substructures, specifically H-Piles with an outer cage of reinforcement such as typical RC columns, the parameters shown in Table 5-4 do apply. For H-Pile columns without an outer cage of reinforcement, additional confinement is recommended. Bridges with concrete-filled tubes (CFT) do not require additional confinement as this substructure type is rather ductile due to the presence of the steel jacket and is not prone to local buckling failure as the column is braced along its entire length with the in-fill concrete.

The criteria shown in Table 5-4 is specific to bridges in Seismic Zone 3 and 4 where adequate ductility must be ensured. Some of the identified vulnerable bridges in Indiana may not meet the criteria to be classified in these seismic zones, thus the criteria may be considered conservative. Regardless, it is at the discretion of the business owner to ultimately determine the acceptable thresholds given a cost-benefit analysis.

5.6.3 Post-Tensioning

Using the seismic assessment procedure developed in Chapter 3, a small percentage of the frame bents in the sample set exhibited a strong column – weak beam failure mechanism. This means that under strong ground motions plastic hinges will form as the base of each column and the ends of every beam element as shown in Figure 5-9 for a single-story frame bent. This mechanism is not ideal for rehabilitation as it requires extensive effort to lift the entire superstructure and make repairs to the concrete and steel in the hinge region. Therefore, it is recommended to use post-tensioning to change the failure mechanism from strong column – weak beam to weak column – strong beam. This more favorable collapse mechanism is shown in Figure 5-10. The required amount of added post-tensioning should be calculated by first determining the amount of additional energy required for the weak column – strong beam mechanism of hinge formation to develop. Alternatively, this analysis can be incrementally conducted using a moment curvature analysis (like the one demonstrated for steel plate encasement in Section 5.5) where the compression force added by the post-tensioning is increased until the energy necessary to form the strong column – weak beam mechanism is less than the energy necessary to form the weak column – strong beam. A calculation of the energy associated with each mechanism follows the procedure outlines in Section 3.3.4.
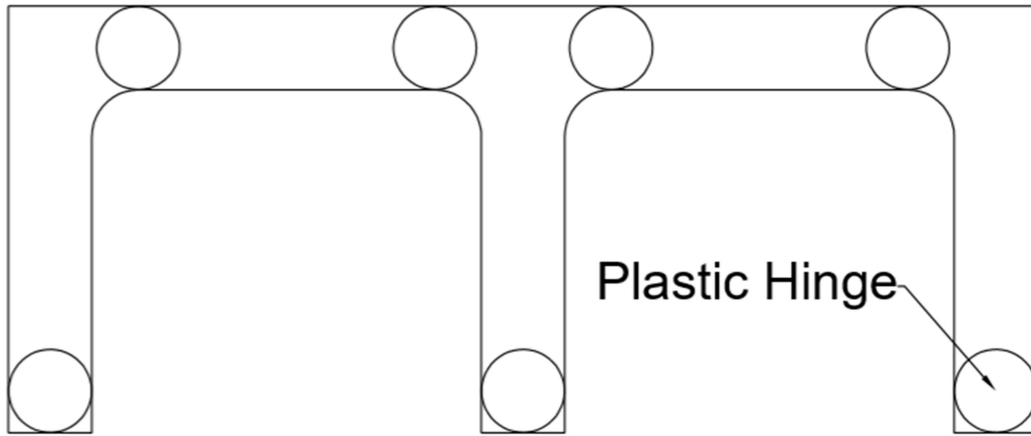
Figure 5-9. Strong Column - Weak Beam Collapse Mechanism for Single-Story Frame Bents
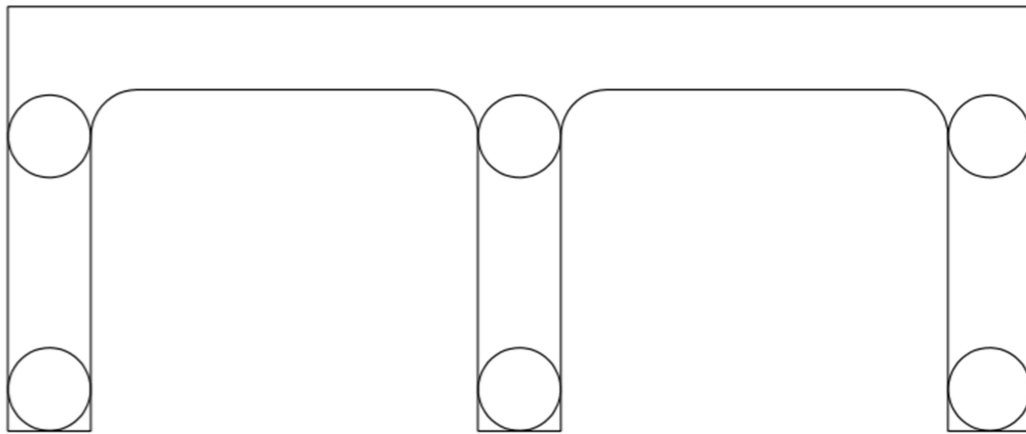
Figure 5-10. Weak Column - Strong Beam Collapse Mechanism for Single-Story Frame Bents

5.6.4 Replacement of Rocker Bearings

For older steel bridges throughout the state of Indiana, the allowable displacement of the rocker bearing is a concern. An exceedance of this allowable displacement would result in the overturning of the rocker bearing and result in unseating of the superstructure. This displacement, calculated as a function of the bearing's dimensions and ability to rotate, is

$$\Delta_{rb} = \frac{w_{rb} * 2 * \sin^{-1}\left(\frac{0.5 * w_{rb}}{r_{rb}}\right)}{2}. \tag{5-9}$$

While the allowable displacement of the rocker bearing often exceeds the displacement associated with the substructure vulnerability or the displacement that would cause abutment pounding, the replacement of the rocker bearings is still recommended. The allowable displacement of the rocker bearing calculated in Equation 5-9 assumes a perfect, upright initial position with the ability to freely rotate. Therefore, it is recommended that any rocker bearings having either an initial angle greater than 30 degrees or a significant amount of corrosion that would limit rotation, be replaced. In addition, rocker bearings should be replaced whenever a bridge is scheduled for rehabilitation. It is recommended to convert bridges with rocker bearings and expansion joints to semi-integral abutments, which behave similar to integral abutments to earthquake excitation.

5.7   Summary for Seismic Retrofit

The application of seismic retrofits has the potential to significantly improve the seismic performance of bridges throughout Indiana that are found to be vulnerable. As shown in this chapter, a variety of retrofit methods are available for the level of hazard and bridge vulnerabilities in Indiana. These retrofit methods, aimed at reducing damage either by increasing capacity or decreasing demand, are capable of decreasing vulnerability or guaranteeing the adequate performance of the structure at the same level of vulnerability. These methods, when coupled with additional design considerations such as a cost-benefit analysis, can help DOTs improve the reliability of their bridge network.

6. CONCLUSION AND FUTURE WORK

With the increased seismic risk due to the identification of the Wabash Valley Seismic Zone comes the need for a network-wide vulnerability assessment of INDOT's bridge inventory. However, the development of a seismic assessment procedure applied independently to bridges within the network is insufficient for capturing the overall vulnerability of a complex network. Thus, the development of a probabilistic assessment procedures (Chapter 3) which leverages the seismic assessment procedure (Chapter 4) allows DOTs like INDOT to robustly assess the vulnerability of their entire bridge network and identify corridors and interchanges which are most susceptible to damage in a given time period. Proactively, this insight allows for the effective prioritization of retrofits even more so than the independent approach since key access corridors function as weakest-link systems. This means that while bridges may independently be highly vulnerable, a corridor containing a single highly vulnerable structure and many non-vulnerable structures may not be as vulnerable as a corridor containing multiple moderately vulnerable structures. The use of just the seismic assessment procedure would conclude the bridge in the former corridor should be retrofitted first, when in actuality this may not be the most strategic decision to ensure network functionality and resiliency. Of course, additional considerations outside the scope of this thesis such as network redundancies and rehabilitation cost must also be considered throughout the decision-making process.

The implementation of this probabilistic assessment procedure would require the development of dynamic models for all bridges throughout the state. As discussed in Section 4.4, certain pre-assessment filters can be leveraged to reduce the number of bridges in the bridge network that must be assessed. Additionally, certain sections of the bridge network could be prioritized for assessment, such as critical routes maintained by the DOT, corridors with bridges predominantly supported by poor soil class, or corridors in areas of higher seismic risk.

6.1   Conclusions

In summary, the major take-aways from each chapter are summarized in this section. While many methods exist for implementing the robust seismic vulnerability procedure, the lessons highlighted herein are important for business owners, like DOT, to remember.

6.1.1   Conclusions for Seismic Assessment Procedure

The major conclusions from the seismic assessment (Chapter 3) are as follows:

- The sample set used to develop the seismic assessment is representative of INDOT's bridge network. Thus, the seismic assessment should be applicable to all substructure-superstructure combinations in Indiana's bridge network.
- A linear dynamic modeling procedure is inadequate for a seismic assessment as this approach does not:
    - encompass major deficiencies in INDOT's bridge network
    - identify accurate limit state thresholds.
- A non-linear dynamic modeling procedure, encompassing a moment curvature analysis, is necessary for:
    - identifying substructures maintaining a low flexural reinforcement ratio and resulting brittle mode of failure
    - conducting a pushover analysis for bridges with a substructure maintaining an adequate flexural reinforcement ratio
- Bridges with wall-type substructures built before 1990 tend to exhibit a brittle mode of failure due to an inadequate flexural reinforcement ratio whereas bridges built after 1990 tend to have adequate flexural reinforcement ratio and exhibit a ductile mode of failure.
- Bridges controlled by a brittle mode of failure are highly vulnerable to the level of seismic risk regardless of their location or soil class due to the small displacement required to initiate concrete cracking (M_{cr}).

6.1.2 Conclusions for Probabilistic Assessment of Bridge Networks

The major conclusions from the development of a probabilistic methodology leveraged to assess the vulnerability of linked bridges along a key-access corridor (Chapter 4) are as follows:

- The use of a probabilistic regression method, such as Bayesian inference coupled with a polynomial basis function, allows for the accurate identification of best-fit capacity functions and corresponding credible intervals. This allows for the identification of epistemic and aleatory uncertainty.

- This methodology can be leveraged to estimate the probability of link failure for any given return period. It is important to stochastically generate earthquakes using the same return period as is used to calculate the probability of occurrence for the seismic hazard.

- The overall probability of failure for a link of bridges is higher than the probability of failure of the most vulnerable bridge in the link alone.

- The costs (e.g. time) associated with implementing the probabilistic assessment procedure can be significantly reduced via the application of pre-assessment filters which identify bridges expected to have a negligible probability of failure due to key design elements.

6.1.3 Conclusions for Modeling of Seismic Retrofits

The major conclusions from the modeling of seismic retrofits (Chapter 5) are as follows:

- As expected, retrofits identified for the CSUS are also applicable to the vulnerabilities identified for the CEUS.

- Retrofits, either focused on increasing capacity or decreasing demand, have the ability to significantly improve the seismic performance of bridges throughout Indiana as demonstrated for a single bridge expected to have a brittle mode of failure.

- Additional considerations such as a cost-benefit analysis must be considered when fully deciding which retrofit is most suitable since, as shown, many of the identified retrofits can be leveraged to improve the seismic performance of bridges in INDOT's bridge network.

6.2   Future Work

With the development of this robust seismic vulnerability assessment procedure comes the ability to evaluate the vulnerability of structures independently, but also interconnectedly. From an independent approach, a more comprehensive seismic assessment procedure which considers liquefaction potential can be conducted with the addition of sufficient geotechnical information. Currently, a majority of boring data throughout INDOT's bridge network does not extend to a sufficient depth. Thus, it is recommended that borings extend to greater depths to reach harder rocks (e.g. those with shear-wave velocity greater than 1000 *m/s*) (Bonthron et al., 2020).

By taking an interconnected approach, DOTs can leverage the information to probabilistically assess the vulnerability of their infrastructure network. This methodology can be coupled with additional information readily available to DOT to effectively prioritize retrofits or update critical routes. For example, the information presented in this thesis can be coupled with a loss function to monetarily quantify the impact a seismic event would have on the state. This loss function can take many forms such as a loss function which is concerned with post-event construction costs necessary to repair various degrees of expected damage or a loss function which accounts for costs accrued by residents due to road closure and increased commute time. This wealth of information can allow DOT to effectively prioritize retrofits so as to minimize such losses thereby guaranteeing the improved functionality of corridors post-earthquake. Alternatively, this methodology can be coupled with traffic flow information which would allow DOT to effectively identify the intersection between the most vulnerable and most traveled key-access corridors. This approach would allow for the designated of updated critical routes or the strategic prioritization of seismic retrofits. With the procedures developed in this thesis and the additional improvements, DOT will have the powerful capability to strategically improve the seismic performance of their complex bridge network.

APPENDIX A. BRIDGES IN SAMPLE SET

The 100 bridges referenced throughout the thesis are summarized in this appendix. The rationale for selecting these bridges is provided in Section 3.2. As a note, the SS used in District column corresponds to bridges which site-specific amplification factors were used to generate the ground motions. More information regarding the simulation process is provided in Section 3.2.

Table A-1. Bridges in Sample Set

Asset Name	NBI Number	District	Material
024-56-00899 B	5880*	La Porte	Concrete
064-63-03590 A	22950	Vincennes	Concrete
067-28-00938 A	23770	Vincennes	Concrete
I69-030-09187 NB	80114	Vincennes SS	Concrete
018-05-06573 B	4880	Fort Wayne	Concrete Continuous
028-79-07672	7640	Crawfordsville	Concrete Continuous
(35)22-27-04724 B	11170	Fort Wayne	Concrete Continuous
(237)37-13-07277	11840	Vincennes	Concrete Continuous
041-42-05080 BNBL	14650	Vincennes	Concrete Continuous
041-56-03828 BSBL	15440*	La Porte	Concrete Continuous
044-55-06793	16310	Seymour	Concrete Continuous
055-45-07366	19880	La Porte	Concrete Continuous
056-63-07286	19933	Vincennes	Concrete Continuous
057-14-06739	20690	Vincennes	Concrete Continuous
063-86-05970 BNBL	22810	Crawfordsville	Concrete Continuous
064-19-03723 A	22960	Vincennes	Concrete Continuous
066-13-05443 A	23670	Vincennes	Concrete Continuous
067-42-07298	23760	Vincennes	Concrete Continuous
067-55-03831 ANBL	24100	Crawfordsville	Concrete Continuous
075-06-04958 A	24860	Crawfordsville	Concrete Continuous
252-55-08713	30721	Seymour	Concrete Continuous
252-24-06934 A	30780	Seymour	Concrete Continuous
327-17-06419 A	31350	Fort Wayne	Concrete Continuous

I69-334-04590 BNB	40720	Fort Wayne	Concrete Continuous
I70-112-05137 DEBL	42960	Greenfield	Concrete Continuous
018-04-09861	4591	Crawfordsville	Prestressed Concrete
064-26-06591	22850	Vincennes	Prestressed Concrete
006-20-09858	51480	Fort Wayne	Prestressed Concrete
(37)145-13-08531	76728	Vincennes	Prestressed Concrete
031-50-09771 SB	79822	La Porte	Prestressed Concrete
031-50-02753 SB	79834	La Porte	Prestressed Concrete
I69-029-09183 SB	80106	Vincennes SS	Prestressed Concrete
I69-037-09460 SB	80136	Vincennes	Prestressed Concrete
I69-038-09462 NB	80140	Vincennes SS	Prestressed Concrete
I69-049-09492 NB	80175	Vincennes SS	Prestressed Concrete
I69-061-09527 DRN	80242	Vincennes SS	Prestressed Concrete
I69-062-02793 DR	80246	Vincennes SS	Prestressed Concrete
I69-064-09401 NB	80266	Vincennes SS	Prestressed Concrete
I69-069-09531 NB	80306	Vincennes SS	Prestressed Concrete
I69-077-02797 NB	80316	Vincennes SS	Prestressed Concrete
I69-083-09446 NB	80338	Vincennes SS	Prestressed Concrete
231-28-09532	80380	Vincennes SS	Prestressed Concrete
(50)750-40-02771	80488	Seymour	Prestressed Concrete
024-91-08973	5941	La Porte	Prestressed Concrete Continuous
231-19-08231	16711	Vincennes	Prestressed Concrete Continuous
050-15-00210 BEBL	18790	Seymour	Prestressed Concrete Continuous
105-35-05447 A	25280	Fort Wayne	Prestressed Concrete Continuous
152-45-02730	27661	La Porte	Prestressed Concrete Continuous
I69-317-09800	40441	Fort Wayne	Prestressed Concrete Continuous
I70-004-04612 BEBL	41070	Crawfordsville	Prestressed Concrete Continuous
I465-149-08854 JSBL	50795	Greenfield	Prestressed Concrete Continuous
I69-112-09708 SB	51350	Seymour	Prestressed Concrete Continuous
I69-106-09739 SB	51385	Seymour	Prestressed Concrete Continuous
I69-095-09674 SB	60622	Vincennes	Prestressed Concrete Continuous
(52)231-79-07531 AEBL	76430	Crawfordsville	Prestressed Concrete Continuous
I465-129-08708	76442	Greenfield	Prestressed Concrete Continuous
I465-128-09119 EBL	76636	Greenfield	Prestressed Concrete Continuous

024-02-09089 A	76840	Fort Wayne	Prestressed Concrete Continuous
031-71-08917	79844	La Porte	Prestressed Concrete Continuous
031-71-08916	79846	La Porte	Prestressed Concrete Continuous
I69-100-09683 SB	79944	Vincennes	Prestressed Concrete Continuous
I69-040-09473 NB	80150	Vincennes SS	Prestressed Concrete Continuous
(56)61-63-09488	80168	Vincennes SS	Prestressed Concrete Continuous
I69-050-09496	80180	Vincennes	Prestressed Concrete Continuous
I69-051-09504	80186	Vincennes SS	Prestressed Concrete Continuous
I69-065-09405 NB	80274	Vincennes SS	Prestressed Concrete Continuous
I69-066-09409 NB	80278	Vincennes SS	Prestressed Concrete Continuous
I69-074-09423 NB	80302	Vincennes SS	Prestressed Concrete Continuous
I69-079-09437 NB	80326	Vincennes SS	Prestressed Concrete Continuous
I69-087-09551 NB	80356	Vincennes SS	Prestressed Concrete Continuous
064-26-09191	80372	Vincennes SS	Prestressed Concrete Continuous
356-63-09491	80374	Vincennes SS	Prestressed Concrete Continuous
058-14-09425	80376	Vincennes SS	Prestressed Concrete Continuous
045-28-09679	80438	Vincennes	Prestressed Concrete Continuous
(265)I265-11-09604	80482	Seymour	Prestressed Concrete Continuous
031-34-09790 SBL	80602	Greenfield	Prestressed Concrete Continuous
038-89-04111 B	13000	Greenfield	Steel Continuous
052-24-06649	19430	Seymour	Steel Continuous
062-74-06621	22190	Vincennes	Steel Continuous
067-18-05459 D	24210	Greenfield	Steel Continuous
I64-05-05201 CEBL	33240	Vincennes	Steel Continuous
041-82-05415 CSBL	14280	Vincennes SS	Steel Continuous
062-82-02589 WBL	21985	Vincennes	Steel Continuous
062-13-07329	22240	Vincennes	Steel Continuous
I469-12-06947 AEB	32841	Fort Wayne	Steel Continuous
I64-07-02367 BEBL	33280	Vincennes	Steel Continuous
I69-309-04548 B	40300	Fort Wayne	Steel Continuous
037-55-03632 JASBL	12250	Seymour	Steel
057-26-03322 A	20530	Vincennes	Steel
154-77-01976 B	27720	Vincennes	Steel
(421)39-12-01792 B	32200	Crawfordsville	Steel
041-77-03864 JBNB	14840	Vincennes	Steel Continuous

I65-118-02313 JCSB	36890	Greenfield	Steel Continuous
I70-006-04712 BEBL	41130	Crawfordsville	Steel Continuous
I70-008-02344 BEBL	41230	Crawfordsville	Steel Continuous
I70-074-05231 A	42020	Greenfield	Steel Continuous
I94-29-04469 CEB	49120	La Porte	Steel Continuous
I465-127-05274 DEBL	50340	Greenfield	Steel Continuous
I69-050-09497 NB	80182	Vincennes	Steel Continuous
I69-057-09506	80226	Vincennes SS	Steel Continuous

Note: Bridges have been replaced during the duration of the project. The notated NBI no longer exists within BIAS.

APPENDIX B. COMPREHENSIVE RETROFIT DESIGN PROCEDURE FOR IMPROVED SEISMIC PERFORMANCE OF A BRIDGE

With the identification of vulnerable structure(s) either using the procedure for a single structure outlined in Chapter 3 or a series of bridges using the procedure outlined in Chapter 4, the design of a retrofit for these vulnerable structure(s) can proceed. First, from the seismic assessment of the bridge(s), one can identify specific vulnerabilities for the structure(s). This vulnerability most likely is, but is not limited to, one of the vulnerabilities identified in Table B-2.
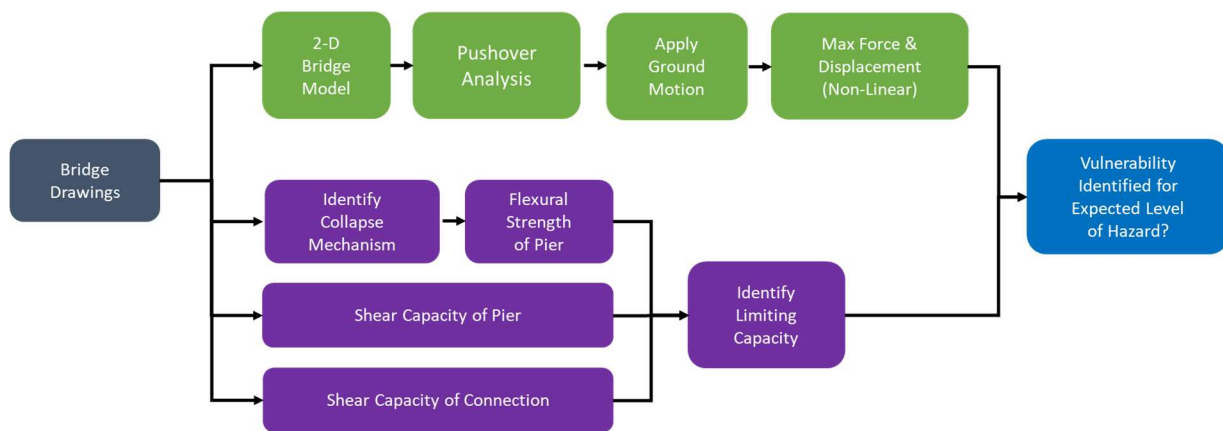
Figure B-6-1. Modified Seismic Assessment Procedure

With the vulnerability identified, retrofits that have the potential for improving the seismic performance of each structure can be determined. In addition to the approaches of increasing the seat length to accommodate the calculated length of need, or making the abutments integral or semi-integral (INDOT, 2013c), the strategies in Figure B-6-2 for vulnerabilities identified during the seismic assessment of the sample of 100-bridge sample set have been identified.
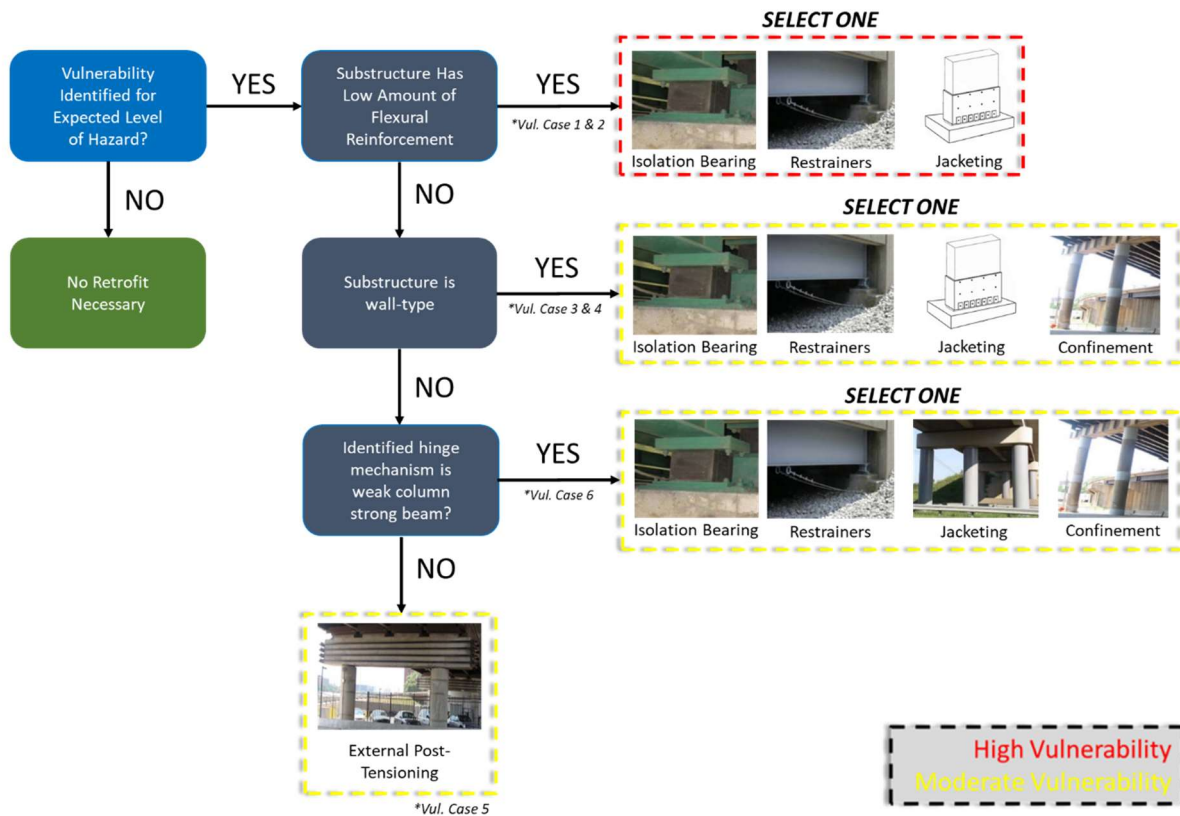
Figure B-6-2. Retrofit Selection Procedure

Notes:

1. *The actual retrofit from the 'Select One' section used to improve the seismic performance of the structure should be determined by an engineer who considers all applicable design aspects.*

2. *While not depicted, the use of integral abutments has the potential to be a suitable retrofit for all vulnerability cases*

3. *An important note to* Figure B-6-2*, is that presently according to INDOT's Design Manual (Sec. 412-3.05(05)) (2013c), improvement in structural capacity and/or confinement is only guaranteed with a jacketing system (concrete or steel) in addition to the fiber wrap.*

4. *The purpose of external post-tensioning is to eliminate the unfavorable development of strong column – weak beam hinge mechanism (see Section 5.6.3 for schematics). The development of weak column – strong beam hinge mechanism may also require additional retrofits.*

5. **Vul. Case 'X' corresponds to vulnerability cases identified in Table B-2 below.*

Vulnerability Case	Substructure Type	Direction	Additional Comments/Criteria (When Applicable)	Level of Vulnerability	Reason for Classification
1	Walls	Longitudinal	Built Before 1990 (Grade 40 ksi steel)*	Highly Vulnerable	Low Flexural Reinforcement Ratio
2	Hammerhead Walls	Longitudinal	Built Before 1990 (Grade 40 ksi steel)*	Highly Vulnerable	Low Flexural Reinforcement Ratio
3	Hammerhead Walls	Longitudinal	Built After 1990 (Grade 60 ksi steel)	Moderately Vulnerable	Formation of Plastic Hinge
4	Hammerhead Walls	Transverse	Prestressed Concrete Superstructure Only	Moderately Vulnerable	Formation of Plastic Hinge
5	Frame Bents	Transverse	All types (H-Pile, CFT, Reinforced Concrete)	Moderately Vulnerable	Formation of Plastic Hinge
6	Frame Bents	Longitudinal	All types (H-Pile, CFT, Reinforced Concrete)	Moderately Vulnerable	Formation of Plastic Hinge
7	-	-	Rocker Bearings	Moderately Vulnerable	Unseating

In accordance with the Manual for Bridge Evaluation (2018) Table 6A.5.2.2-1, bridges built after 1945 are assumed to have Grade 40 ksi steel. From the detailed assessment, it has been determined that bridges built after 1990 typically use Grade 60 ksi steel. Therefore, it is assumed, when structural drawings do not explicitly dictate, that bridges built between 1945 and 1990 use Grade 40 ksi steel. If a given bridge is identified as having Grade 60 ksi steel and was built before 1990, it may instead fall under vulnerability case 3.

REFERENCES

AASHTO. (2017). *AASHTO LRFD Bridge Design Specifications*, 8th Edition. Washington, D.C.: American Association of State Highway and Transportation Officials.

AASHTO. (2018). *The Manual for Bridge Evaluation*, 3rd Edition. Washington, DC: American Association of State Highway and Transportation Officials

Atkinson, G. M., & Boore, D. M. (2006). *Earthquake ground-motion prediction equations for eastern North America.* Bulletin of the Seismological Society of America, 96(6), 2181-2205.

Avossa, A. M., Di Giacinto, D., Malangone, P., & Rizzo, F. (2018). Seismic Retrofit of a Multi-Span Prestressed Concrete Girder Bridge with Friction Pendulum Devices. *Shock and Vibration*.

Banerjee, S., & Shinozuka, M. (2009). Uncertainties in Seismic Risk Assessment of Highway Transportation Systems. Proceedings of the 2009 Technical Council on Lifeline Earthquake Engineering, Oakland, CA.

Barbato, M., Gu, Q., & Conte, J. P. (2010). *Probabilistic push-over analysis of structural and soil-structure systems.* Journal of Structural Engineering, 10, 1330-1341.

Bonthron, L., Beck, C., Lund, A., Zhang, X., Orellana Montano, R., Dyke, S., & Ramirez, J. (In Press) (2020). Empowering the Indiana Bridge Inventory Database Toward Rapid Seismic Vulnerability Assessment. Rep. JTRP No. 4222, Purdue University, IN.

Boore, D. M. (1983). *Stochastic simulation of high-frequency ground motions based on seismological models of the radiated spectra.* Bulletin of the Seismological Society of America, 73(6A), 1865-1894.

Boore, D. M., & Campbell, K. W. (2016). Adjusting central and eastern North America ground-motion intensity measures between sites with different reference-rock site conditions. Bulletin of Seismological Society of America, 107(1), 132-148.

Buckle, I. G., Consantinou, M. C., Dicleli, M, & Ghasemi, H. (2006). *Seismic Isolation of Highway Bridges* (Special Report MCEER-06-SP07). Buffalo, NY: MCEER.

Buckle, I. G., Al-Ani, M., & Monzon, E. (2011). Seismic Isolation Design Examples of Highway Bridges (Final Report NCHRP 20-7 / Task 262(M2)). Washington, D.C.: Transportation Research Board, National Research Council.

Calvi, P. M., & Calvi, G. M. (2016). Historical development of friction-based seismic isolation systems. *Soil Dynamics and Earthquake Engineering, 106,* 14-30.

Choi, E. (2002). Seismic Analysis and Retrofit of Mid-America Bridges (Doctoral dissertation). Retrieved from Georgia Tech Library.

Choi, E., DesRoches, R., Nielson, B. (2004). Seismic fragility of typical bridges in moderate seismic zones. *Engineering Structures,* 26, 187-199.

Chopra, A. K. (2012). *Dynamics of Structures: Theory and Applications to Earthquake Engineering* (4th ed). Upper Saddle River, NJ: Prentice Hall.

De Biasio, M., Grange, S., Dufour, F., Allain, F., Petre-Lazar, I. (2014). A simple and efficient intensity measure to account for nonlinear structural behavior. *Earthquake Spectra,* 30(4), 1403-1426.

DesRoches, R., Choi, E., Leon, R. T., Dyke, S. J., & Aschheim, M. (2004a). Seismic Response of Multiple Span Steel Bridges in Central and Southeastern United States. I: As Built. *Journal of Bridge Engineering,* 9(5), 464-472.

DesRoches, R., Choi, E., Leon, R. T., & Pfeifer, T. A. (2004b). Seismic Response of Multiple Span Steel Bridges in Central and Southeastern United States. II: Retrofitted. *Journal of Bridge Engineering,* 9(5), 473-479.

Ealangi, I. (2010). *Earthquake Protection of Buildings by Seismic Isolation, Design and Concepts.* Technical University of Civil Engineering Bucharest.

Escolano-Margarit, D., Klenke, A., Pujol, S., & Benavent-Climent, A. (2012). *Failure Mechanism of Reinforced Concrete Structural Walls with and without Confinement.* 15th World Conference on Earthquake Engineering, Lisbon, Portugal.

Fares, A. (2018). Simplified Equations for Rigidity and Lateral Deflection for Reinforced Concrete Cantilever Shear Walls. *International Journal of Civil and Environmental Engineering,* 12(10), 1051 - 1055.

Federal Highway Administration (FHWA). (2006). Seismic retrofitting manual for highway structures: Part 1—Bridges (Publication No. FHWA-HRT-06-032). McLean, VA: Research, Development, and Technology Turner-Fairbank Highway Research Center.

Frosch, R., Kreger, M., & Talbott, A. (2009). Earthquake Resistance of Integral Abutment Bridges. Rep. JTRP No. 2867, Purdue University, IN.

Garcia, L. E. (1998). *Dinámica Estructural Aplicada al Diseño Sísmico.* Bogotá: Universidad de los Andes, Departamento de Ingeniería Civil.

Gillich, G. R., Iancu, V., Gillich, N., Korka, Z. I., Chioncel, C. P., & Hatiegan, C. (2018). Decoupling the structure from the ground motion during earthquakes by employing friction pendulums. *Materials Science and Engineering*, 294.

Guikema, S., & Gardoni, P. (2009). Reliability Estimation for Networks of Reinforced Concrete Bridges. *Journal of Infrastructure Systems*, 15(2), 61-69

Halldorsson, B., & Papageorgiou, A. S. (2005). *Calibration of the specific barrier model to earthquakes of different tectonic regions.* Bulletin of the Seismological Society of America, 95(4), 1276-1300.

Hermann, R. B., Withers, M., & Benz, H. (2008). The April 18, 2008 Illinois earthquake: an ANSS monitoring success. *Seismological Research Letters, 79(6),* 830-843.

Hill, 2008. Map of Indiana showing predicted responses of geologic materials to seismically induced ground shaking. *Indiana Geological Survey Report of Progress 35, Plate 1.*

Hwang, H. H., & Huo, J. R. (1994). Generation of hazard-consistent fragility curves. *Soil Dynamics and Earthquake Engineering,* 13(50), 345-354.

INDOT (2012a). CETRP Attachment No. 4: INDOT Primary Disaster Routes. Indianapolis, IN.

INDOT (2012b). *INDOT Standard Drawing No. E 706-BRSF-02: Bridge Railing Type FT.* Indianapolis, IN.

INDOT (2012c). *Standard Drawing No. E 726-BEBP-05: Elastomeric Bearing Pads Type S.* Indianapolis, IN.

INDOT (2013a). *INDOT Design Manual Chapter 406.* Indianapolis, IN. Last Updated: May 2020.

INDOT (2013b). *INDOT Design Manual Chapter 409*. Indianapolis, IN. Last Updated: May 2020.

INDOT (2013c). *INDOT Design Manual Chapter 412.* Indianapolis, IN. Last Updated: April 2020.

Johnston, A. C., & Schweig, E. S. The enigma of the New Madrid earthquakes of 1811-1812. *Annual Review of Earth and Planetary Sciences,* 24, 339-384.

Karim, K. R., & Yamazaki, F. (2001). Effect of earthquake ground motions on fragility curves of highway bridge piers based on numerical simulation. Earthquake Engineering and Structural Dynamics, 30, 1839-1856.

Khan, E. Kowalsky, M. J., Nau, J. M. (2016). Equivalent Viscous Damping Model for Short-Period Reinforced Concrete Bridges. *Journal of Bridge Engineering,* 21(2).

Melchers, R. E., & Beck, A. T. (2018). Structural Reliability Analysis and Prediction (3rd ed.). Hoboken, NJ: Wiley.

Metzger, L. E. (2004). *Vulnerability of Bridges in Southern Indiana to Earthquakes.* Master's Thesis, Purdue University, IN.

Nateghi-A, F., & Shahsava, V. L. (2004). Development of Fragility and Reliability Curves for Seismic Evaluation of a Major Prestressed Concrete Bridge. 13th World Conference on Earthquake Engineering, Vancouver, Canada.

Nielson, B. G., & DesRoches, R. (2007a). Analytical Seismic Fragility Curves for Typical Bridges in the Central and Southeastern United States. *Earthquake Spectra*, 23, 615-633.

Nielson, B. G., & DesRoches, R. (2007b). Seismic fragility methodology for highway bridges using a component level approach. *Earthquake Engineering & Structural Dynamics*, 36(6), 823-839.

Padgett, J. E., DesRoches, R., & Nilsson, E. (2010). Regional Seismic Risk Assessment of Bridge Network in Charleston, South Carolina. *Journal of Earthquake Engineering*, 14(6), 918-933.

Papageorgiou, A. S., & Aki, K. (1983). *A specific barrier model for the quantitative description of inhomogeneous faulting and the prediction of strong ground motion. I. Description of the model.* Bulletin of the Seismological Society of America, 73(3), 693-722.

Peña, F. (2019). Efficient Computation of Accurate Seismic Fragility Functions Through Strategic Statistical Selection. Doctoral Dissertation, Purdue University, IN.

Peña, F., Bilionis, I., & Dyke, S. (2019). Model Selection and Uncertainty Quantification of Seismic Fragility Functions. *Journal of Risk and Uncertainty in Engineering Systems, Part A: Civil Engineering,* 5(3).

Petersen, M. D., Moschetti, M. P., Powers, P. M., Mueller, C. S., Haller, K. M., & Olsen, A. H. (2014). *Documentation for the 2014 update of the United States national seismic hazard maps.* USGS Open-File Report 2014-1091, U.S. Geological Survey

Pitilakis, K., Argyroudis, S., Kakderi, K. & Selva, J. (2016). Systemic vulnerability and risk assessment of transportation systems under natural hazards towards more resilient and robust infrastucture. *Transportation Research Procedia,* 14, 1335-1334.

Ramirez, J., Peeta, S., Sozen, M., Garcia, L., & Viswanath, K. (2005). *Emergency Earthquake Routes; Part I, Criteria for Selection of Primary Routes; and Part II: Route Seismic Vulnerability Aspects*. Rep. JTRP No. 2480, Purdue University, IN. https://doi.org/10.5703/1288284313203

Ramirez, J., Frosch, R., Sozen, M., & Turk, M. (2000). Handbook for the Post-Earthquake Safety Evaluation of Bridges and Roads. Rep. JTRP No. 2377, Purdue University, IN. https://doi.org/10.5703/1288284315557

Roeder, C.W., Stanton, J.F., & Taylor, A.W. (1987). Performance of Elastomeric Bearings (NCHRP Report 298). Washington, D.C.: Transportation Research Board, National Research Council.

Shinozuka, M., Feng, M. Q., Kim, H. K., & Kim, S. H. (2000). Nonlinear Static Procedure for Fragility Curve Development. *Journal of Engineering Mechanics, 126(12),* 1287-1295.

Shinozuka, M., Feng, M. Q., Lee, J., & Naganuma, T. (2000). Statistical analysis of fragility curves. *Journal of Engineering Mechanics,* 126(12), 124-1231.

Silva, W. J., Darragh, R. B., Gregor, G., Martin, N., Abrahamson, A., & Kircher, C. (2000). *Reassessment of site coefficients and near-fault factors for building code provisions*. Final report to USGS, Award No. 98HQGR1010, United States Geological Survey.

Siqueira, G. H., Tavares, D. H., Paultre, P., & Padgett, J. E. (2014). Performance evaluation of natural rubber seismic isolators as a retrofit measure for typical multi-span concrete bridges in eastern Canada. *Engineering Structures, 74,* 300–310.

Taylor, E. (2007). *The Development of Fragility Relationships for Controlled Structures.* Master's Thesis, Washington University, MO.

Timothy, W., DesRoches, R., & Padgett, J. E. (2011). Bridge Seismic Retrofitting Practices in the Central and Southeastern United States. *Journal of Bridge* Engineering, 16(1), 82–92.

Trochalakis, P., Eberhard, M. O., & Stanton, J. F. (1996). *Design of Seismic Restrainers for In-Span Hinges* (Technical Report T9903, Task 41). Seattle, WA: Washington State Transportation Center (TRAC).

U.S. Nuclear Regulatory Commission. (1975). Reactor Safety Study: An Assessment of Accident Risk in U.S. Commercial Nuclear Power Plants (NUREG-75/104). Rockville, MD.

Werner, S. D., Taylor, C. E., Moore III, J. E., Walton, J. S., & Cho, S. (2000). *A Risk-Based Methodology for Assessing the Seismic Performance of Highway Systems* (Technical Report MCEER-00-0014). Buffalo, NY: MCEER.

Zayas, V. A., Low, S., Mokha, A. S., & Imbsen, R. A. (2001). Seismic Isolation of Benicia-Martinez Bridges. Proceedings of the 2001 Structures Congress and Exposition, Washington, D.C.